ISSN 0169-6548

Communications on hydraulic and geotechnical engineering

Notes on the mathematical modelling of alluvial mountain rivers

May 1994

A. Sieben

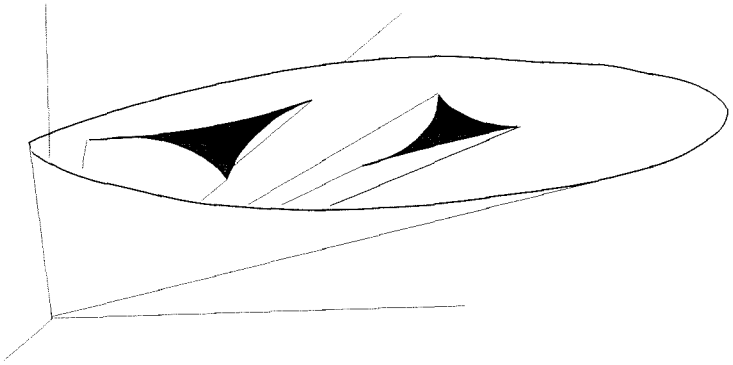

TU Delft
Delft University of Technology

Faculty of Civil Engineering

NOTES ON THE MATHEMATICAL MODELLING OF ALLUVIAL MOUNTAIN RIVERS WITH GRADED SEDIMENT

by

A. Sieben

May 1994

Communications on Hydraulic and
Geotechnical Engineering

Report No. 94-3

Faculty of Civil Engineering
Delft University of Technology

Abstract.

The ability of describing and predicting hydraulic and morphological phenomena in mountain rivers is limited, partially due to the limits of deterministic approaches where stochastic effects in sediment supply and water inflow are extremely significant, and partially due to the very specific conditions that can be observed in mountain rivers, that complicate the modelling.

The dynamics of morphology and hydraulics of mountain rivers must be known when applying numerical modelling procedures to mountain rivers. Simplifying a complex, non-uniform geometry significantly affects the behaviour of the model at high values of the *Froude* number. The number and type of boundary conditions to be prescribed at a boundary can change with flow regime. Hydraulic and morphological changes in supercritical flows are coupled and transversal effects are significant.

The mathematical models discussed are a single-layer model and a double layer model conform Ribberink (1987). With the help of the characteristics, the models are analysed and compared. Analysing the characteristic surface yields indispensible insight in the two-dimensional behaviour of the mathematical models. To prevent the mathematical model from being elliptical, the thickness of the mixing layer has a maximum. This value is investigated, approximated and evaluated.

It appears that the behaviour of the model can be significantly affected by the model parameters (hydraulic as well as morphological). Regarding the selection between one-dimensional and two-dimensional modelling, it can be concluded that transverse effects have a significant influcence on the behaviour of the model for *Froude* near unity.

Conclusions in this report stress the need for research on the modelling of complex geometry for flow with higher values of *Froude* and the prediction of the model parameters used (such as mixing-layer thickness and sediment fluxes) at varying flow conditions.

Acknowledgements.

The scrutinizing reviews and the very stimulating and constructive comments by Prof. Dr. M. de Vries and Dr. Z.B. Wang are considered of great benefit to the report. Also, the pleasant discussions on characteristics and related subjects with Mr. C.J. Sloff are acknowledged. Finally, thanks are to Ariëtte for supportively sharing interest in "balloons" and "stars".

Contents.

1. Introduction.

Hazards of erosion or flooding due to excessive sediment deposition in mountainous regions have increased the interest in hydraulic and morphological phenomena in mountain rivers. However, due to the erratic character of sediment inflow and flood hydrographs, the planning, construction and managing of river projects and subsequent infrastructure in mountainous regions is extremely complex. To perform river engineering that involves the dynamics of alluvial mountain rivers, the impact of rather specific conditions relative to low-land rivers should be known.

When applying mathematical models, knowledge on the effects of high velocities, small depths (large and varying values of the *Froude* number) and graded sediment with wide ranges in diameter and composition is required to select a numerical solution procedure, to simplify complex geometries, to prescribe the proper boundary conditions and to interpretate the behaviour of the model.

In this report a general, two-dimensional, depth-averaged (2-DH) mathematical model for alluvial rivers is analysed. The effect of graded material is investigated conform the layer model of Ribberink (1987). The number of size fractions analysed in the model is restricted to two. The behaviour of a single-layer and a double-layer model is compared. A simple description for the vertical fluxes in the river bed is proposed.

Sediment transport in the model is described with a power law that approximates the Meyer-Peter and Müller sediment-transport formula (Meyer-Peter and Müller, 1948). The performance of the Meyer-Peter and Müller sediment-transport formula is compared with the formula proposed by Parker et al. (1982) and modified by Diplas (1987). Horizontal-hiding effects are accounted for by correction with a hiding coefficient suggested by Egiazaroff (1965).

Relaxation effects by the suspended sediment are included conform Galapatti (1983).

The behaviour of the model is analysed with the help of the characteristic equations; the bicharacteristic surfaces and the compatibility equations.

The bicharacteristic surfaces are equivalent to characteristics in one-dimensional models, and represent the two-dimensional propagation of physical information through the mathematical model. The *magnitude* of propagation indicates the possibility of decoupling hydraulic and morphological processes (De Vries, 1965) and the *direction* of propagation determines the number of boundary conditions to be prescribed at the up- and downstream boundaries.

The compatibility equations are composed of gradients in variables along the bicharacteristics, which enables relating the more or less coupled variables to the bicharacteristics at varying conditions. Also, the two-dimensional behaviour can be

analysed and compared to one-dimensional models, and conditions can be found that promotes and checks initial growth of disturbances in bed level and composition.

With the help of the characteristics, the behaviour of single- and multiple-layer models are analysed. A criterion is derived to ensure the hyderbolicity of the mathematical model and the sensitivity of dynamic phenomena to the model parameters is investigated.

Fixed-bed models show that the transition from subcritical to supercritical flow marks a significant change in flow behaviour. In analogy, the hydraulic and morphological behaviour of mobile bed models with transitions from sub- to supercritical flows (and vice versa) differs significantly from that in low-land rivers where, relative to mountain rivers, velocities are low and depths are large.

Algebraic manipulations have been carried out with the *Mathematica* package (Wolfram, 1991).

Chapter 2

Mathematical 2DH-model.

2.1. Introduction.

In this chapter, equations are derived based on the general balances of mass and momentum, averaged over the depth. Based on analogy with mobile bed models for uniform sediment, the mathematical modelling of alluvial rivers with sediment mixtures is described. The resulting systems of equations in non-conservative form are described in Appendix A.

To account for alluvial rivers at steep slopes variables are defined in a system of coordinates that is tilted relative to a horizontal reference plane (Section 2.2.2). As a result, slope effects on gravity forces, bed shear-stresses and sediment transport are introduced. Because the sediment mass balances includes gradients in sediment transport, the latter effect yields the introduction of a diffusive term which will be neglected in the analysis.

To describe the gradients in transport in a non-conservative form, a power-law approximation is used (e.g. Jansen et al, 1978) based on the Meyer-Peter and Müller transport formula (Appendix B). Because this formula refers to a bed-material load situation, the effects of bed load and suspended-load transport that are seperated in the mathematical model are not distinguished in the numerical experiments in Chapter 4 and 5.

The composition of the river bed is described with the help of a horizontal-layer concept. Naturally, with an increasing number of layers, the "discretized" river bed approaches the proto type. However, distinction of a layer implies the introduction of vertical sediment fluxes from the layer. At present, the description of this sediment exchange between layers is a topic of research.

Two alternatives are discussed; a single-layer model (Section 2.3) and a double-layer model (Section 2.4). For the double layer model, an additional expression for the vertical flux is suggested to describe a net exchange of sediment from the subpavement layer. These two types of models are considered sufficient to discuss the main features such as significance and physical background of the layer-thickness and the vertical fluxes.

2.2 General model.

2.2.1. Balances of flow-mass and momentum.

The flow-mass balance can be written as

$$\frac{\partial \rho a}{\partial t} + \frac{\partial \rho u a}{\partial x} + \frac{\partial \rho v a}{\partial y} = 0 \qquad 2.1$$

Witout any diffusion terms describing effects of turbulence, the balance of x-directed momentum in a depth-averaged system with hydrostatic pressure is

$$\frac{\partial \rho u a}{\partial t} + \frac{\partial \rho u^2 a}{\partial x} + \frac{\partial \rho v u a}{\partial y} - \rho g_x a - \frac{\partial \rho g_z a^2}{2\partial x} + \tau_{bx} - \rho g_z a \frac{\partial z_b}{\partial x} = 0 \qquad 2.2$$

The balance of y-directed momentum is

$$\frac{\partial \rho v a}{\partial t} + \frac{\partial \rho v u a}{\partial x} + \frac{\partial \rho v^2 a}{\partial y} - \rho g_y a - \frac{\partial \rho g_z a^2}{2\partial y} + \tau_{by} - \rho g_z a \frac{\partial z_b}{\partial y} = 0 \qquad 2.3$$

where

ρ = density of water
u = velocity component in x-direction
v = velocity component in y-direction
ρg_j = gravity force component in j-direction due to orientation of the space-averaged level of the river bed Z_b relative to a reference plane
τ_{bj} = bed shear-stress in j-direction

2.2.2. Slope effects.

Because slopes in mountain rivers can be steep, the following definitions are introduced. The bed level z_b is defined relative to Z_b that represents the spatially-averaged, constant equilibrium slope of the bed. In Figure 2.1, the defined z- and x-axes are shown relative to Z_b.

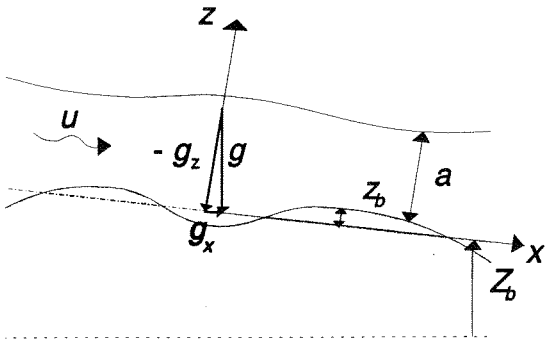

Figure 2.1

The components of gravity forces can be described as

$$\begin{pmatrix} g_x \\ g_y \\ g_z \end{pmatrix} = \frac{-g}{\sqrt{\cos^2\theta_x + \sin^2\theta_x \cos^2\theta_y}} \begin{pmatrix} \sin\theta_x \cos\theta_y \\ \cos\theta_x \sin\theta_y \\ \cos\theta_x \cos\theta_y \end{pmatrix} \qquad \textbf{2.4}$$

where

$$\begin{bmatrix} \tan\theta_x \\ \tan\theta_y \end{bmatrix} = \begin{bmatrix} \dfrac{\partial Z_b}{\partial x} \\ \dfrac{\partial Z_b}{\partial y} \end{bmatrix}$$

Analogeously, the shear-stress components at the bed are defined as

$$\begin{bmatrix} \tau_{bx} \\ \tau_{by} \\ \tau_{bz} \end{bmatrix} = \frac{\tau_b}{\sqrt{\cos^2\alpha \cos^2\theta_y + \sin^2\alpha \cos^2\theta_x}} \begin{bmatrix} \cos\alpha \cos\theta_x \cos\theta_y \\ \sin\alpha \cos\theta_x \cos\theta_y \\ \sqrt{\cos^2\alpha \cos^2\theta_y + \sin^2\alpha \cos^2\theta_x - \cos^2\theta_x \cos^2\theta_y} \end{bmatrix}$$

where τ_b represents the bed shear stress and α is the direction of velocity **2.5**

$$\tan\alpha = \frac{v(z_b)}{u(z_b)} \qquad \textbf{2.6}$$

The shear-stress component in z-direction induces deviations from the hydrostatic pressure at the bed level. If deviations from the spatial-averaged bed level Z_b are small,

the shear stress can be reduced to

$$\begin{bmatrix} \tau_{bx} \\ \tau_{by} \\ \tau_{bz} \end{bmatrix} = \tau_b \begin{bmatrix} \cos\alpha \\ \sin\alpha \\ 0 \end{bmatrix} \qquad 2.7$$

The space-averaged level of the river bed Z_b is constant in time and equals the space-averaged equilibrium slope of the bed level. This implies that changes in relatively small slope-effects on gravity components ρg_j, bed shear-stress components τ_{bj} and sediment transport are not taken into account.

2.2.3. Mass balances of uniform sediment.

In the analysis, two transport layers are defined to distinguish bed load and suspended load transport (Figure 2.2).

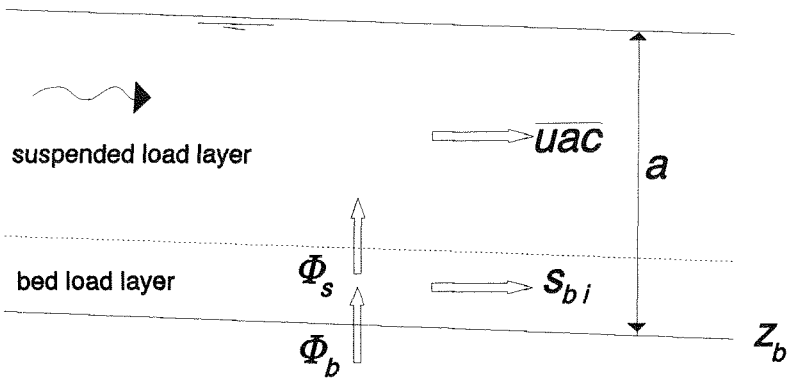

Figure 2.2

The mass balance of sediment in suspension integrated over the depth is

$$\frac{\partial \int_{z_b}^{z_s} c\,dz}{\partial t} + \frac{\partial \int_{z_b}^{z_s} uc\,dz}{\partial x} + \frac{\partial \epsilon_s \partial \int_{z_b}^{z_s} c\,dz}{\partial x^2} + \frac{\partial \int_{z_b}^{z_s} vc\,dz}{\partial y} + \frac{\partial \epsilon_s \partial \int_{z_b}^{z_s} c\,dz}{\partial y^2} - \Phi_s = 0 \qquad 2.8$$

where ϵ_s is the sediment mixing-coefficient. However, contributions to the horizontal transport of suspended sediment by diffusion are neglected in this analysis.
The sediment flux at the bed level is composed of a convective and diffusive part

$$\Phi_s = (w(z_b) - w_s)c(z_b) - \epsilon_s \frac{\partial c}{\partial z}\Big|_{z_b} \qquad 2.9$$

The first-order approximation (without second-order diffusion terms) of the depth-integrated mass balance of sediment in suspension can be described with

$$T_A \frac{\partial c}{\partial t} + L_x \frac{\partial c}{\partial x} + L_y \frac{\partial c}{\partial y} + c - c_e = 0 \qquad \textbf{2.10}$$

where T_A a relaxation period and L_x and L_y the components in x- and y-direction of a relaxation length to take into account the relatively slow adaptation of the vertical concentration-profile to local changes (e.g. Galapatti, 1983).

The mass balance of sediment moving as bed load is

$$\frac{\partial (1-p) z_b}{\partial t} + \frac{\partial c_b \delta_b}{\partial t} + \frac{\partial u_b c_b \delta_b}{\partial x} + \frac{\partial v_b c_b \delta_b}{\partial y} + \Phi_s = 0 \qquad \textbf{2.11}$$

where c_b is the sediment concentration in the bed-load transport-layer δ_b, and u_b the average grain-velocity in the bed-load transport-layer. The bed-load storage term is usually very small (e.g. Armanini and Di Silvio, 1989) and is neglected by assuming instantaneous adjustment.

Consequently, the mass balance of bed load and suspended load is

$$\frac{\partial (ca + z_b)}{\partial t} + \frac{\partial (uca + S_{bx})}{\partial x} + \frac{\partial (vca + S_{by})}{\partial y} = 0 \qquad \textbf{2.12}$$

with the effect of porosity p included in the definitions of sediment transport.

If the bedload transport is described as

$$c_b u_b \delta_b = S_{bx} = \frac{u}{u_{tot}} S_b \quad ; \quad c_b v_b \delta_b = S_{by} = \frac{v}{u_{tot}} S_b \qquad \textbf{2.13}$$

(De Vriend, 1987), and if the transport of bed load is approximated with $S_b = f(u_{tot})$ (e.g. Jansen et al. 1978), this can be rewritten as

$$\frac{\partial (ca + z_b)}{\partial t} + \frac{\partial uca}{\partial x} + T_1 \frac{\partial u}{\partial x} + T_3 \frac{\partial v}{\partial x} + \frac{\partial vca}{\partial y} + T_2 \frac{\partial v}{\partial y} + T_3 \frac{\partial u}{\partial y} = 0 \qquad \textbf{2.14}$$

with

$$T_1 = \frac{u^2}{u_{tot}^2} \frac{dS_b}{du_{tot}} + \frac{v^2 S_{bi}}{u_{tot}^3} \; ; \; T_2 = \frac{v^2}{u_{tot}} \frac{dS_b}{du_{tot}} + \frac{u^2 S_b}{u_{tot}^3} \; ; \; T_3 = \frac{uv}{u_{tot}^2} \left(\frac{dS_b}{du_{tot}} - \frac{S_b}{u_{tot}} \right) \qquad \textbf{2.15}$$

The resulting system of equations is described in Appendix A.1.

2.3. Single-layer model for non-uniform material.

2.3.1. Sediment-mass balances.

Again, two layers for horizontal transport are defined (Figure 2.3) to distinguish bed-load and suspended-load transport.

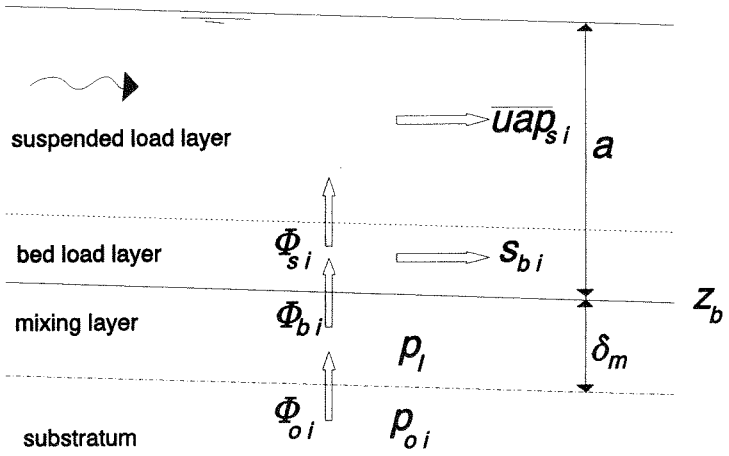

Figure 2.3

Depth integration of the mass balance for p_{si} (fraction i in suspension) yields

$$\frac{\partial \int_{z_b+\delta_b}^{z_s} p_{si}\,dz}{\partial t} + \frac{\partial \int_{z_b+\delta_b}^{z_s} up_{si}\,dz}{\partial x} + \frac{\partial \epsilon_{si}\partial \int_{z_b+\delta_b}^{z_s} p_{si}\,dz}{\partial x^2} + \frac{\partial \int_{z_b+\delta_b}^{z_s} vp_{si}\,dz}{\partial y} + \frac{\partial \epsilon_{si}\partial \int_{z_b+\delta_b}^{z_s} p_{si}\,dz}{\partial y^2} - \Phi_{si} = 0 \qquad \textbf{2.16}$$

where ϵ_{si} is the sediment mixing-coefficient for fraction i, which will be considered negligible in the analysis. The thickness of the bedload layer δ_b is considered constant in time and space.
Without diffusive transport-terms, Eq.2.16 can be written as

$$\frac{\partial p_{si}a}{\partial t} + \frac{\partial up_{si}a}{\partial x} + \frac{\partial vp_{si}a}{\partial y} - \Phi_{si} = 0 \qquad \textbf{2.17}$$

The vertical sediment-flux of a fraction at the bed level is composed of a convective

and diffusive part, in analogy with fluxes of uniform material

$$\Phi_{si} = \left(w(z_b+\delta_b) - w_{si}\right) p_{si}(z_b+\delta_b) - \epsilon_{si}\frac{\partial p_{si}}{\partial z}\Big|_{z_b+\delta_b} \qquad \textbf{2.18}$$

The first-order approximation (without second-order diffusion terms) of the depth-integrated balance of suspended sediment is described with

$$T_{Ai}\frac{\partial p_{si}a}{\partial t} + L_{xi}\frac{\partial p_{si}a}{\partial x} + L_{yi}\frac{\partial p_{si}a}{\partial y} + \left(p_{si} - p_{ei}\right)a = 0 \qquad \textbf{2.19}$$

(Armanini and Di Silvio, 1988).

The transport of a size fraction i is approximated with $S_i = f(u_{tot}, p_{mi}, D_m)$.

The mass balance over the bedload layer is

$$\frac{\partial s_{bxi}}{\partial x} + \frac{\partial s_{byi}}{\partial y} + \Phi_{si} - \Phi_{bi} = 0 \qquad \textbf{2.20}$$

The mass balance over the underlying mixing-layer is

$$\frac{\partial \int_{z_b-\delta_m}^{z_b} p_{mi}\mathrm{d}z}{\partial t} + \Phi_{bi} - \Phi_{oi} = 0 \qquad \textbf{2.21}$$

The net flux Φ_{oi} at $z = z_b - \delta_m$ is

$$\Phi_{oi} = -\beta_i\frac{\partial(z_b-\delta_m)}{\partial t} \qquad \textbf{2.22}$$

where β_i equals p_{mi} when $z = z_b - \delta_m$ moves upwards (deposition) and β_i equals p_{oi}, the fraction in the substratum when $z = z_b - \delta_m$ moves downwards (erosion). However, even if the average value of $z = z_b - \delta_m$ is constant during a time interval, still a vertical transport of size fractions can exist due to zero-averaged fluctuations around $z = z_b - \delta_m$.

After elimination of Φ_{oi}, the mass balance can be written as

$$\frac{\partial \int_{z_b-\delta_m}^{z_b} p_{mi}\mathrm{d}z}{\partial t} + \Phi_{bi} + \beta_i\frac{\partial(z_b-\delta_m)}{\partial t} = 0 \qquad \textbf{2.23}$$

The mixing-layer thickness δ_m is taken constant. The total mass balance for suspended and bed load per fraction i is

$$a\frac{\partial \overline{p_{si}}}{\partial t} + ua\frac{\partial \overline{p_{si}}}{\partial x} + \frac{\partial s_{bxi}}{\partial x} + va\frac{\partial \overline{p_{si}}}{\partial y} + \frac{\partial s_{byi}}{\partial y} - \Phi_{bi} = 0 \qquad \textbf{2.23}$$

or

$$\delta_m\frac{\partial p_{mi}}{\partial t} + \beta_i\frac{\partial z_b}{\partial t} + a\frac{\partial \overline{p_{si}}}{\partial t} + ua\frac{\partial \overline{p_{si}}}{\partial x} + va\frac{\partial \overline{p_{si}}}{\partial y} +$$

$$+ K_{1i}\frac{\partial u}{\partial x} + K_{2i}\frac{\partial u}{\partial y} + K_{2i}\frac{\partial v}{\partial x} + K_{3i}\frac{\partial v}{\partial y} + \qquad \textbf{2.25}$$

$$+ uK_{4i}\frac{\partial p_{mi}}{\partial x} + vK_{4i}\frac{\partial p_{mi}}{\partial y} + uK_{5i}\sum_{j=1}^{N} D_j\frac{\partial p_{mj}}{\partial x} + vK_{5i}\sum_{j=1}^{N} D_j\frac{\partial p_{mj}}{\partial y} = 0$$

The coefficients K_{ij} are described in Appendix B.5.

In the case of N size fractions, the number of variables becomes 4 + 2*N. The system consists of three equations describing conservation of fluid mass and momentum (Eqs 2.1, 2.2 and 2.3), N equations describing relaxation effects per size fraction in suspension (Eq.2.16), and N mass balances per sediment size fraction (Eq.2.22). To complete the set of equations it can be stated

$$\sum_{i=1}^{N} p_{mi} = 1 \qquad \textbf{2.26}$$

which is used to eliminate p_{mN} from the system of equations. The resulting system of equations is described in Appendix A.2.

2.3.2. Mixing-layer thickness.

In the mixing layer, a direct and complete mixing of the fractions is assumed to take place due to fluctuations in the bed level. This implies that the mixing phenomena are assumed to be fast compared to changes in bed level and composition and because the development of the mixing layer is assumed instantaneous, δ_m is taken constant. As a result, the type of mixing mechanism and subsequently the thickness of the mixing layer is related to the scale of morphological changes that are simulated (Rahuel, et al. 1988).

If the time scale considered is instantaneous, the mixing layer only contains sediment particles at the surface of the bed. If in the time scale considered bed forms can develop and travel through the area of interest, the mixing layer is related to the height

of the bedforms. If during the period considered alternating deposition and erosion occurs, the extend of the mixing is related to those changes in bed level.

In conditions where the bed level and composition are in or near an equilibrium state (and when changes in morphology are supposed to be "slow" and "small"), the mixing process can be considered decoupled.

By definition, the mixing layer differs from an armour layer. In single-layer models where armouring is simulated, the thickness of the predicted armour layer approaches the selected mixing layer-thickness if no motion occurs under the armour layer. If the armour layer is destroyed, interrupted or covered with finer material, the extend of vertical mixing will be larger than the thickness of the armour layer. Then, the mixing layer is larger and finer than the armour layer.

Consequently, the application of single-layer models with a constant δ_m for simulating dynamic armouring phenomena is restricted; during the armouring process the bed-level fluctuations, and subsequently the extend of the vertical mixing decreases. In that case a δ_m-predictor should be used, or contributions by fluxes from deeper layers should be allowed.

As reviewed for instance in Sieben (1993) and Laguzzi (1994), many expressions for δ_m have been used. The mixing layer has been related to bed forms (Borah et al. 1982; Ribberink,1987), flow depth (Karim et al. (1981), grain size (Di Silvio and Peviani, 1991) or thickness of the armour layer by prediction of the mobile and immobile particles.

2.3.3. Scale of changes in mixing-layer composition.

To analyse the scale of changes in composition, it can be found with the mass balance of the mixing layer

$$\frac{\partial p_{mi}\delta_m}{\partial t} = \left(\frac{\Phi_{bi}}{\sum_{i=1}^{N} \Phi_{bi}} - \beta_{oi} \right) \frac{\partial z_b}{\partial t} = (p_{Ti} - \beta_{oi}) \frac{\partial z_b}{\partial t} \qquad \textbf{2.27}$$

or

$$\int_t^{t+\Delta t} \frac{\partial p_{mi}}{\partial t} dt = \int_t^{t+\Delta t} (p_{Ti} - \beta_{oi}) \frac{1}{\delta_m} \frac{\partial z_b}{\partial t} dt \approx (p_{Ti} - \beta_{oi}) \frac{1}{\delta_m} \int_t^{t+\Delta t} \frac{\partial z_b}{\partial t} dt \qquad \textbf{2.28}$$

Consequently, changes in composition are determined by two effects

- the difference in composition of pick-up and substratum in the case of erosion or with the difference in composition of deposition and mixing layer in the case of sedimentation.

- changes in bed level relative to the thickness of the mixing layer

Because the response of the bed level is related to the composition of the river bed, the changes in bed level and composition can be considered to be coupled. The fraction i in horizontal transport p_{Ti} is defined as

$$p_{Ti} = \frac{s_{bi}}{\sum_{i=1}^{N} s_{bi}} = \frac{s_{bi}}{s_b} \qquad \textbf{2.29}$$

The composition of the sediment transport p_{T1} is described in Appendix B.3.

For sediment composed of two fractions with $D_1 = 0.001$ mm and $D_2 = 0.004$ mm, the changes in mixing layer composition relative to changes in bed level are shown. Figure 2.4 represents sedimentation, Figure 2.5 represents erosion of an armoured bed.

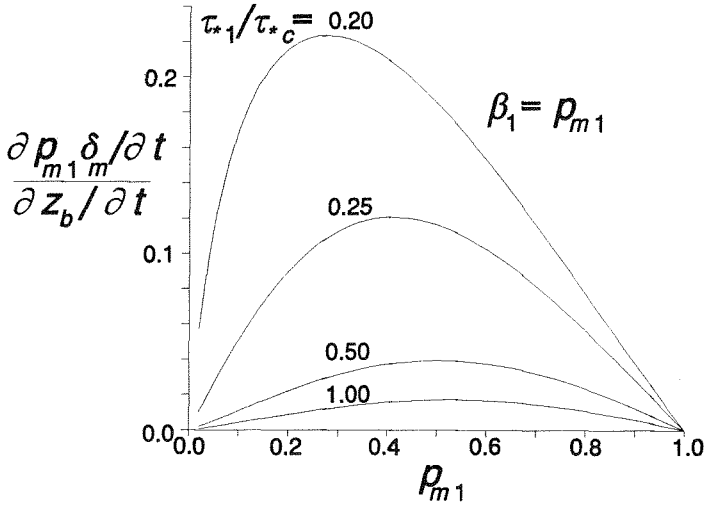

Figure 2.4

In case of sedimentation at higher shear-stresses, the changes in composition are small at significantly fine or coarse beds.

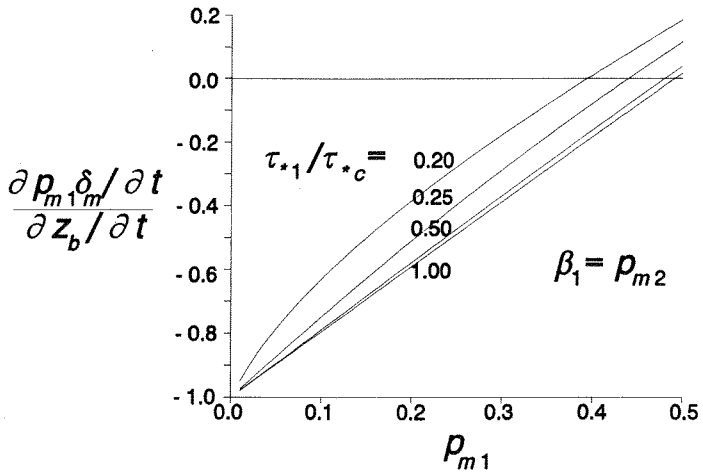

Figure 2.5.

In case of erosion of an armoured bed, the mixing layer refines if the availability of fine material in this layer is low relative to the fine fraction in the substratum. Mainly the coarse fraction is picked up, whereas mainly fine material is supplied by the substratum. Consequently, the armour layer is destroyed.

If the composition of the mixing layer becomes less coarse relative to that of the substratum, the layer coarsens and the armour layer stabilizes. The stability of an armour layer reduces at high shear-stresses.

2.3.4. Coarsening criteria.

Based on Section 2.3.3, a simple armouring criterion for the single-layer model is

$$p_{T1} < p_{m1} \quad (sedimentation) \quad ; \quad p_{T1} > p_{o1} \quad (erosion) \qquad \textbf{2.30}$$

Because the composition of the transported sediment is finer than that of the bed, only the second criterion can be satisfied. At high shear-stresses, the composition of the transported sediment approaches that of the mixing layer, which subsequently approaches that of the substratum. Consequently, no armour layer can be stable at high shear stress.

2.4. Double-layer model for non-uniform material.

2.4.1. Background.

The layer-concept is based on the following assumptions (Ribberink 1983):

- no sediment motion occurs beneath the mixing layer
- intantane mixing of size fractions in the mixing layer

However, due to large fluctuations in the bed level, the undisturbed material under the mixing layer can be exposed to the flow without affecting the sediment-transport conditions. Therefore, to refine the modelling of vertical fluxes, Ribberink (1983) suggest the distinction of a transitional exchange layer (pavement and subpavement layer) within the mixing layer.

Distinction of a transition layer (Figure 2.6) enables a better description of the vertical bed-composition in the presence of active armour-layers, or if armour layers are distributed in an interrupted, non-uniform manner ("patches") over the river bed.

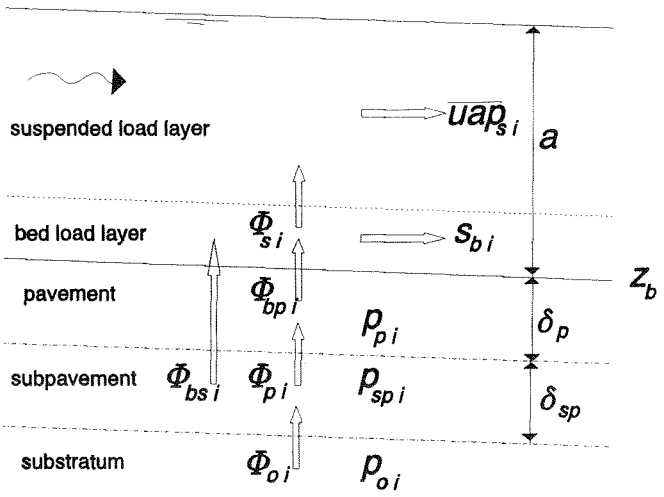

Figure 2.6

The sediment transport is assumed to be mainly affected by the composition of the mixing layer conform Ribberink (1987). The exchange of sediment from the subpavement is reduced by vertical-hiding effects by the material in the pavement layer.

If bed forms are present, the subpavement is exposed to the flow and can contribute to the sediment transport, due to the bed-level fluctuations. If at higher flow regimes bed forms are washed out, fluctuations in the bed level and consequently, the thickness of the layers reduce to the order of the grain sizes. The mechanism of vertical sediment exchange is no longer related to well-developed bed forms, and a constant relative-exposure coefficient should be applied.

It is stated that the contribution of the pavement layer is proportional with the probability of exposure g of this layer. The constant κ is a reduction factor for the mutual sediment exchange between the layers, and is introduced in the mass balances to distinguish the situation with a net contribution from the subpavement layer ($\kappa = g$) from the situation without a net contribution from the subpavement layer ($\kappa = 1$).

2.4.2. Sediment-mass balances.

The mass balance per size fraction i of the bed-load layer is

$$\frac{\partial s_{bxi}}{\partial x} + \frac{\partial s_{byi}}{\partial y} + \Phi_{si} - \Phi_{pbi} - \Phi_{psi} = 0 \qquad \textbf{2.31}$$

The mass balance per size fraction i of the pavement layer is

$$\frac{\partial \int_{z_b-\delta_p}^{z_b} p_{pi}\mathrm{d}z}{\partial t} + \Phi_{bpi} - \kappa\,\Phi_{pi} = \frac{\partial \delta_p p_{pi}}{\partial t} + \Phi_{bpi} - \kappa\,\Phi_{pi} = 0 \qquad \textbf{2.32}$$

The mass balance per size fraction i of the subpavement layer is

$$\frac{\partial \int_{z_b-\delta_p-\delta_{sp}}^{z_b-\delta_p} p_{spi}\mathrm{d}z}{\partial t} + \kappa\,\Phi_{pi} + \Phi_{bsi} - \Phi_{oi} = \qquad \textbf{2.33}$$

$$= \frac{\partial \delta_{sp} p_{spi}}{\partial t} + \kappa\,\Phi_{pi} + \Phi_{bsi} - \Phi_{oi} = 0$$

The flux Φ_{pi} at $z = z_b - \delta_p$ is

$$\Phi_{pi} = -\beta_{pi}\frac{\partial(z_b-\delta_p)}{\partial t} = -\beta_{pi}\frac{\partial z_b}{\partial t} \qquad \textbf{2.34}$$

where β_{pi} equals p_{pi} when $z = z_b - \delta_p$ moves upwards (deposition) and β_{pi} equals p_{spi}, the fraction in the subpavement when $z = z_b - \delta_p$ moves downwards (erosion).

Similarly the flux Φ_{oi} at $z = z_b - \delta_p - \delta_{sp}$ is

$$\Phi_{oi} = -\beta_{oi}\frac{\partial(z_b-\delta_p-\delta_{sp})}{\partial t} = -\beta_{oi}\frac{\partial z_b}{\partial t} \qquad \textbf{2.35}$$

where β_{oi} equals p_{spi} when $z = z_b - \delta_p - \delta_{sp}$ moves upwards (deposition) and β_{oi} equals p_{oi}, the fraction in the substratum under the pavement when $z = z_b - \delta_p - \delta_{sp}$ moves downwards (erosion).
Consequently, the mass balance of the subpavement can be written as

$$\frac{\partial \delta_{sp} p_{spi}}{\partial t} + (\beta_{oi} - \kappa\,\beta_{pi})\frac{\partial z_b}{\partial t} + \Phi_{bsi} = 0 \qquad \textbf{2.36}$$

If no sediment contribution to the horizontal transport exists, changes in the subpavement are directly related to changes in bed level.

Ribberink (1987) and Di Silvio (1991) use for the thickness of the subpavement

$$\delta_{sp} = 0.50\ \delta_p \qquad \textbf{2.37}$$

2.4.3. Subpavement flux conform Ribberink (1987).

Ribberink (1987) considers subpavement fluxes during deep troughs of bed forms and suggests the subpavement-fluxes to be independent from sediment fluxes in the pavement. The net flux of a size fraction i can be described as

$$\Phi_{bsi} = \xi\ (1-g)\ \frac{\delta_{sp}}{H_c}\ \frac{s_b}{L}\ (p_{spi} - p_{Ti}) \qquad \textbf{2.38}$$

with ξ = 1.8 - 2.0, representing the ratio of local transport over the crest of the bed form and the average transport-rate, 1-g is the probability of exposure of the subpavement layer to the flow, L and H_c are the average bed-form length and height.

The net, fraction-integrated flux is

$$\sum_{i=1}^{N} \Phi_{bsi} = \xi\ (1-g)\ \frac{\delta_{sp}}{H_c}\ \frac{s_b}{L} \sum_{i=1}^{N} (p_{spi} - p_{Ti}) = 0 \qquad \textbf{2.39}$$

which implies that even in non-equilibrium conditions, the total sediment contribution from the subpavement to the horizontal transport-layers is zero. Consequently, κ = 1 in the sediment-mass balances (Section 2.4.2). As a result, subpavement fluxes as described by Eq.2.38 only affect the morphological behaviour *indirectly*, via changes in composition in subpavement and the transported sediment. The rate of sediment transport is not affected.

If a sediment contribution to the sediment transport is considered, the exchange with the pavement layer is formulated as

$$\Phi_{bsi} = \xi\ (1-g)\ \frac{\delta_{sp}}{H_c}\ \frac{s_b}{L}\ p_{bi} \qquad \textbf{2.40}$$

with p_{bi} equals p_{bsi} in case of upward fluxes (erosion), and $-p_{Ti}$ in case of downward fluxes (deposition).

It can be defined

$$\gamma = \xi\,(1-g)\,\frac{\delta_{sp}}{H_c} \quad \rightarrow \quad 1 - g = \frac{\gamma H_c}{\xi \delta_{sp}} \qquad \textbf{2.41}$$

Experimentally, Ribberink found $0.07 < \gamma < 0.093$, which yields

$$0.035 < (1 - g)\frac{\delta_{sp}}{H_c} < 0.052 \qquad \textbf{2.42}$$

With $\delta_{sp} = H_c/4$, it can be found that $0.14 < 1\text{-}g < 0.21$. This is in agreement with $1\text{-}g = 0.16$ used by Di Silvio (1991).

2.4.4. Simplified subpavement sediment-contribution.

When simulating armouring phenomena, a different interpretation of the layer-model can be applied. Stating the net subpavement flux to be zero implies that the time scale of the mixing phenomena in the pavement equals the time scale of vertical subpavement fluxes. In other words, mixing of the pavement and fluxes from the subpavement are assumed to be caused by the same instantaneuous mechanism; fluctuations in the bed level.

However, in case of a non-uniformly armoured river bed, or in case of local destruction of an armour layer, fine material from the subpavement can be eroded without any refill of the subpavement. In this case, the local fluxes from the subpavement can occur at a time scale similar to that of the changes in bed level that are slow relative to the "instantaneous" mixing.

Distinction of a contributing subpavement layer enables a closer relation between the thickness and composition of the pavement layer and that of the actual armour layer. Di Silvio (1991) allows a net sediment flux between the subpavement and transport layer, taking into account the size composition in both layers but neglecting hiding effects. In the following, the fluxes from and to the subpavement and the pavement layer are defined with the help of the power law.

Because the composition of the pavement layer is assumed to affect the sediment transport, the power-law coefficients m_i, l_i and n_i (Appendix B) are based on the properties of the pavement layer only. With the sediment transport approximated with a power-law, the ratio of both contributions can be written as

$$\frac{\Phi_{bsi}}{\Phi_{bpi}} = \frac{(1-g)p_{spi}}{gp_{pi}} \left(\frac{D_{mp}}{D_{ms}}\right)^{l_i} = \alpha_i \qquad \textbf{2.43}$$

Di Silvio and Brunelli (1991) find the hiding effects on the exchange coefficient

negligible, and suggest $l_i = 0$, resulting in a constant for varying shear-stress. The effect of hiding on α_i is shown in Figure 2.7.

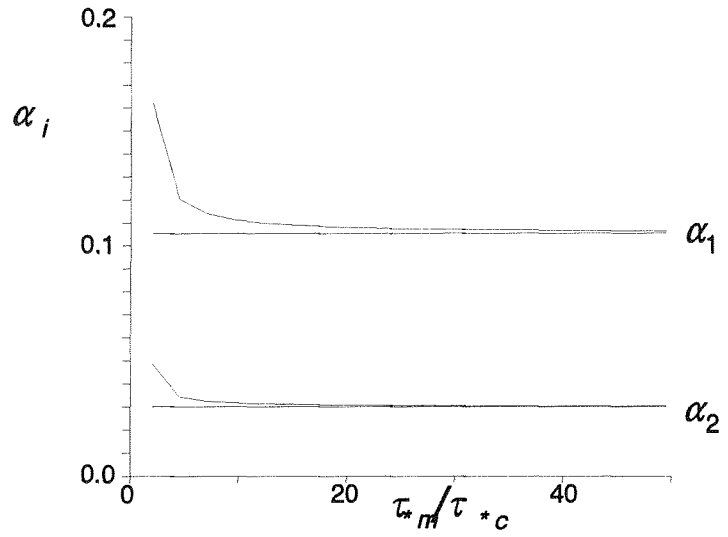

Figure 2.7

Due to the hiding correction, the pick-up of the fine material is favoured relative to the coarse fraction. For large shear-stresses the α_i found by use of the power-law approximation converges to the expression suggested by Di Silvio and Brunelli (1991).

The mass balance over the bedload layer is

$$\frac{\partial(s_{pbxi} + s_{sbxi})}{\partial x} + \frac{\partial(s_{pbyi} + s_{sbyi})}{\partial y} + \Phi_{si} - \Phi_{pbi} - \Phi_{psi} = 0 \qquad \textbf{2.44}$$

or

$$\frac{\partial g s_{bxi}(1 + \alpha_i)}{\partial x} + \frac{\partial g s_{byi}(1 + \alpha_i)}{\partial y} + \Phi_{si} - \Phi_{pbi} - \Phi_{psi} = 0 \qquad \textbf{2.45}$$

which can be rewritten with the pavement and subpavement mass balances as

$$\frac{\partial g s_{bxi}(1+\alpha_i)}{\partial x} + \frac{\partial g s_{byi}(1+\alpha_i)}{\partial y} + \Phi_{si} + \delta_p \frac{\partial p_{pi}}{\partial t} + \delta_s \frac{\partial p_{spi}}{\partial t} + \beta_{oi} \frac{\partial z_b}{\partial t} = 0 \qquad \textbf{2.46}$$

Apparently, the transport of a fraction i is multiplied by $g(1+\alpha_i)$. If the subpavement is finer than the pavement, the transport of the fine material is enhanced, whereas the transport of the coarser material is reduced by contributions from the subpavement.

This is illustrated in Figure 2.8, where the effect of subpavement fluxes on the fine and coarse fraction and the total rate for $g = 0.80$ relative to $g = 1$ is presented. At low shear-stresses, the contributions from the fine subpavement increase the rate of

sediment transport and subsequently directly affect the morphological changes in bed level. At higher shear-stresses this effect diminishes.

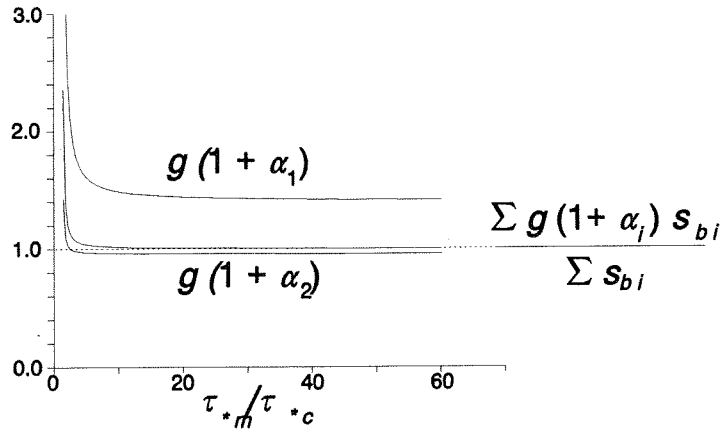

Figure 4.8

Due to the introduction of p_{spi}, an additional equation should be formulated to close the system of equations. This additional equation can be found by combination of the sediment mass balances of the subpavement and the pavement layer (Eqs 2.33 and 2.37)

$$-\alpha_i \delta_p \frac{\partial p_{pi}}{\partial t} + \delta_{sp} \frac{\partial p_{spi}}{\partial t} + \left(\beta_{oi} - \kappa\,(1+\alpha_i)\,\beta_{pi}\right)\frac{\partial z_b}{\partial t} = 0 \qquad \textbf{2.47}$$

The resulting set of Eqs 2.1, 2.2, 2.3, 2.17, 2.46 and 2.47 in non-conservative form is described in Appendix A.3.

2.4.5. Scale of changes in pavement and subpavement composition.

Again, with the help of the mass balance of the pavement it can be found

$$\frac{\partial p_{pi}\delta_p}{\partial t} = \left(\frac{\Phi_{bpi}}{\sum_{i=1}^{N} (1+\alpha_i)\Phi_{bpi}} - \kappa\,\beta_{pi} \right) \frac{\partial z_b}{\partial t} \qquad \textbf{2.48}$$

where α_i the ratio of contributions from sub- and pavement layer (see subpavement sediment contribution). Similarly for the subpavement

$$\frac{\partial p_{spi}\delta_s}{\partial t} = \left(\frac{\alpha_i\,\Phi_{bpi}}{\sum_{i=1}^{N} (1+\alpha_i)\Phi_{bpi}} + \kappa\,\beta_{pi} - \beta_{oi} \right) \frac{\partial z_b}{\partial t} \qquad \textbf{2.49}$$

The effect of the additional layer at the time-derivatives in the pavement composition relative to changes in bed level is shown in Figure 2.9 at different shear-stresses. For the composition of the subpavement, the constant average between pavement and substratum is taken.

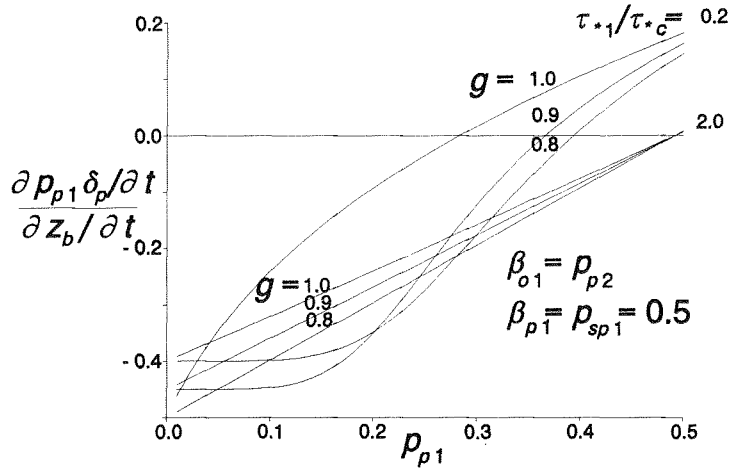

Figure 2.9

The probability of exposure of the pavement to the flow is represented by g. As can be concluded from Figure 2.9, armouring can occur if differences in subpavement and pavement composition are small and shear-stresses are low. If the pavement layer is coarse relative to the subpavement, the armour layer is not stable. The effect of g on changes in pavement is significant at low shear-stresses and decreases if the compositions of pavement and subpavement approach each other.

The corresponding changes in the subpavement are presented in Figure 2.10.

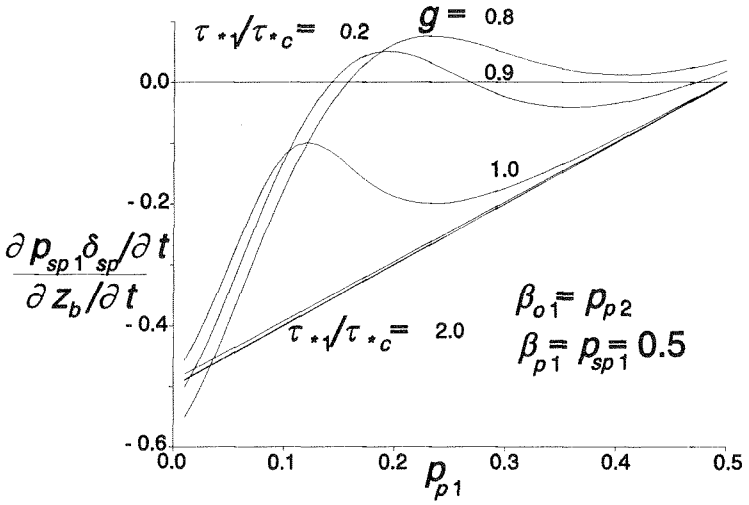

Figure 2.10

It can be concluded from Figure 2.10 that at low shear-stresses, the subpavement can transfer from refining to coarsening, with increasing exposure of the subpavement. At high shear-stresses, the subpavement refines and the effect of g on the changes in

composition is relatively small.

2.4.6. Coarsening criteria.

Based on Section 2.4.5, a simple coarsening criterion for both layers can be derived. A similar armouring criterion for the pavement layer in the double-layer model is (Section 2.4.5)

$$\frac{\Phi_{bp1}}{\sum_{i=1}^{2}(1+\alpha_i)\Phi_{bpi}} < \kappa\, p_{p1} \quad (sedimentation)$$

$$\frac{\Phi_{bp1}}{\sum_{i=1}^{2}(1+\alpha_i)\Phi_{bpi}} > \kappa\, p_{sp1} \quad (erosion) \qquad 2.50$$

For high shear-stresses, no armouring can occur in case of sedimentation, whereas the armouring criterion in case of erosion can be written as

$$p_{p1} > \frac{\kappa}{g}\, p_{sp1} = p_{sp1} \qquad 2.51$$

Equation 2.51 states that the underlying subpavement layer should be coarser than the pavement layer which contradicts the definition of armoured river beds.

For the subpavement layer, the armouring (coarsening) criterion is

$$\frac{\alpha_1\Phi_{bp1}}{\sum_{i=1}^{2}(1+\alpha_i)\Phi_{bpi}} + \kappa\, p_{p1} - p_{sp1} < 0 \quad (sedimentation)$$

$$\frac{\alpha_1\Phi_{bp1}}{\sum_{i=1}^{2}(1+\alpha_i)\Phi_{bpi}} + \kappa\, p_{sp1} - p_{o1} > 0 \quad (erosion) \qquad 2.52$$

For high shear-stresses, the coarsening criteria for the subpavement layer are

$$p_{p1} < \frac{g\, p_{sp1}}{\kappa + g} = \frac{p_{sp1}}{2} \quad (sedimentation)$$

$$p_{p1} > \frac{p_{o1} - (1 + \kappa - g)p_{sp1}}{g} = \frac{p_{o1} - p_{sp1}}{g} \quad (erosion) \qquad 2.53$$

Chapter 3

Derivation of characteristic surfaces.

3.1. Introduction.

In this Chapter, the system of partial-differential equations is analysed, using the method of characteristics. This theory has been applied extensively to analyse one-dimensional models with and without mobile bed (e.g. De Vries, 1959) and 2DH-models with a fixed bed (Daubert and Graffe, 1967; Katopodes and Strelkoff, 1978; Abbott, 1979) and a mobile bed (Lin and Shen, 1984; Lai, 1986; De Vriend, 1987a,b and Sloff 1992). These analyses are continued with the help of some numerical experiments.

In the first part of Chapter Three, a description of methods and derivation of the characteristic condition is given. An extensive use of the Huyghens' method has been made to construct and analyse the characteristic surfaces. This method is described in Section 3.2. In Section 3.2.2, 3.2.3 and 3.2.4 respectively, the characteristic conditions are determined for mobile bed models with uniform material and with a mixture with a one and two horizontal layers in the bed.

The analysis of characteristic surfaces starts in Chapter 4.

The characteristics of 1-DH models are described in Chapter 6.

3.2. Derivation of characteristic conditions.

3.2.1 Mathematical background.

Characteristic surfaces in two-dimensional models are the equivalent of characteristics in one-dimensional models. The mathematical background is described here very briefly. Interested readers are refered to Courant and Hilbert (1962), Fletcher (1988) or Hirsch (1990) among others, where the method of characteristics applied to a system of partial-differential equations is decribed extensively.

The characteristic condition states that along characteristic surfaces described with a normal vector $\vec{n} = \vec{n}(x,y,t)$, the partial derivatives of the variables in x-, y- and t-direction are undetermined. Consequently, along a characteristic surface, the determinant of the system of equations is zero (see section 3.2.2). This will be worked out in Section 3.2.2.

The normal vector $\vec{n}$ of the characteristic surface is defined as

$$\vec{n} = \begin{bmatrix} n_t \\ n_x \\ n_y \end{bmatrix} \tag{3.1}$$

or in polar coordinates

$$\vec{n} = \begin{bmatrix} n_t \\ n_x \\ n_y \end{bmatrix} = \begin{bmatrix} -r \\ \cos\theta \\ \sin\theta \end{bmatrix} \tag{3.2}$$

A bicharacteristic ray is defined as a line of tangency between the characteristic surface and a characteristic plane. This tangential characteristic plane is defined as

$$\vec{n} \cdot \begin{bmatrix} \Delta t \\ \Delta x \\ \Delta y \end{bmatrix} = -r\,\Delta t + \Delta x \cos\theta + \Delta y \sin\theta = 0 \tag{3.3}$$

A bicharacteristic ray along a characteristic surface that is presented as a characteristic cone is shown in Figure 3.1.

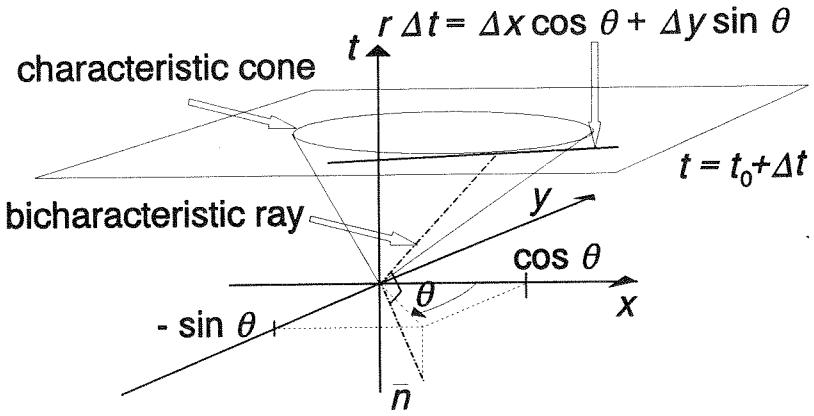

Figure 3.1

In a time interval t-t_0, a disturbance travels from (x_0, y_0) to (x, y), with

$$r(t-t_0) - \cos\theta(x-x_0) - \sin\theta(y-y_0) = 0 \tag{3.4}$$

Analogeously to the Huyghens' construction, a point at the curve (relative to the point of origin) can be approximated by the intersection of two tangential lines.

$$\begin{aligned}(r-\Delta r)\Delta t - (x - x_0)\cos(\theta-\Delta\theta) - (y - y_0)\sin(\theta-\Delta\theta) &= 0 \\ r\Delta t - (x - x_0)\cos\theta - (y - y_0)\sin\theta &= 0\end{aligned} \qquad \textbf{3.5}$$

(see Figure 3.1).
For $\Delta\theta \rightarrow 0$ this can be rewritten as

$$\Delta x = \Delta t\left[r\cos\theta - \frac{dr}{d\theta}\sin\theta\right] \;;\; \Delta y = \Delta t\left[r\sin\theta + \frac{dr}{d\theta}\cos\theta\right] \qquad \textbf{3.6}$$

Consequently, small disturbances travel along bicharacteristics that are described with

$$\begin{bmatrix}1\\ c_x\\ c_y\end{bmatrix} = \begin{bmatrix}1\\ \frac{\partial x}{\partial t}\\ \frac{\partial y}{\partial t}\end{bmatrix} = \begin{bmatrix}1\\ r\cos\theta - \frac{dr}{d\theta}\sin\theta\\ r\sin\theta + \frac{dr}{d\theta}\cos\theta\end{bmatrix} \qquad \textbf{3.7}$$

with r as well as the derivative of r to θ to be determined from the characteristic condition (Section 3.2.2). Equation 3.7 enables the construction of characteristic surfaces intersected after a reference time interval.

3.2.2. Characteristic condition for uniform material.

The system of equations is described by Eqs 2.1, 2.2, 2.3, 2.7 and 2.11 (see also Appendix A.1). The total derivative of a variable ξ is defined as

$$\frac{D\xi}{Dt} = \begin{bmatrix}n_t\\ n_x\\ n_y\end{bmatrix}^T \cdot \begin{bmatrix}\frac{\partial\xi}{\partial t}\\ \frac{\partial\xi}{\partial x}\\ \frac{\partial\xi}{\partial y}\end{bmatrix} = n_t \cdot \frac{\partial\xi}{\partial t} + n_x \cdot \frac{\partial\xi}{\partial x} + n_y \cdot \frac{\partial\xi}{\partial y} \qquad \textbf{3.8}$$

Multiplication of the system of partial-differential equations A.2 with $\vec{n}^T \vec{n}$ enables rewriting this system as

$$Q \cdot \begin{bmatrix} \mathrm{D}u/\mathrm{D}t \\ \mathrm{D}v/\mathrm{D}t \\ \mathrm{D}a/\mathrm{D}t \\ \mathrm{D}z_b/\mathrm{D}t \\ \mathrm{D}c/\mathrm{D}t \end{bmatrix} = \vec{n}^T \cdot \vec{n} \begin{bmatrix} 0 \\ g_x - \tau_{bx}/\rho a \\ g_y - \tau_{by}/\rho a \\ 0 \\ c_e - c \end{bmatrix} \qquad \textbf{3.9}$$

with the matrix Q

$$Q = \begin{vmatrix} R & 0 & -g_z n_x & -g_z n_x & 0 \\ 0 & R & -g_z n_y & -g_z n_y & 0 \\ a n_x & a n_y & R & 0 & 0 \\ T_1 n_x + T_3 n_y & T_3 n_x + T_2 n_y & 0 & n_t & aR \\ 0 & 0 & 0 & 0 & P \end{vmatrix} \qquad \textbf{3.10}$$

where

$$R = n_t + u n_x + v n_y \;\; ; \;\; P = T_A n_t + L_x n_x + L_y n_y \qquad \textbf{3.11}$$

As stated in Section 3.2.1, along the characteristic surfaces, the gradients in variables can have multiple solutions, or in other words, the deteminant of the matrix Q is zero. Stating $|Q| = 0$ yields the characteristic condition

$$|Q| = R\,P\left[g_z a n_t \left(n_x^2 + n_y^2\right) + n_t R^2 + g_z R\left(n_x^2 T_1 + n_y^2 T_2 + 2 n_x n_y T_3\right)\right] = 0 \qquad \textbf{3.12}$$

Because each characteristic corresponds to a variable in the system of equations, in total five roots can be found. The roots of the characteristic condition $Q = 0$ describe three families of surfaces. $R = 0$ and $P = 0$ lead to characteristic normal planes. The third family describes a characteristic normal cone that can be identified as a Monge cone.

The two normal planes are described by

$$r = u\cos\theta + v\sin\theta \;\; ; \;\; r = \frac{L_x}{T_A}\cos\theta + \frac{L_y}{T_A}\sin\theta \qquad \textbf{3.13}$$

which yields with Eq.3.3

$$\frac{\Delta x}{\Delta t}\cos\theta + \frac{\Delta y}{\Delta t}\sin\theta = u\cos\theta + v\sin\theta$$

$$\rightarrow \qquad \textbf{3.14}$$

$$\frac{\Delta x}{\Delta t} = c_x = u \;\wedge\; \frac{\Delta y}{\Delta t} = c_y = v$$

representing the streamlines and

$$\frac{\Delta x}{\Delta t}\cos\theta + \frac{\Delta y}{\Delta t}\sin\theta = \frac{L_x}{T_A}\cos\theta + \frac{L_y}{T_A}\sin\theta \rightarrow c_x = \frac{L_x}{T_A} \wedge c_y = \frac{L_y}{T_A} \qquad \textbf{3.15}$$

representing relaxation-effects of the sediment in suspension.

The characteristic normal cone is described by

$$r^3 - 2r^2[u\cos\theta + v\sin\theta] +$$

$$+ r\left[(g_z a + g_z T_1 + u^2)\cos^2\theta + (uv + g_z T_3)\sin 2\theta + (v^2 + g_z T_2 + g_z a)\sin^2\theta\right] + \qquad \textbf{3.16}$$

$$- \frac{g_z}{2}(u\cos\theta + v\sin\theta)\left(T_1 + T_2 + (T_1 - T_2)\cos 2\theta + 2T_3\sin 2\theta\right) = 0$$

For example, the intersection of the coupled characteristic surfaces at Δt = 1 s in supercritical flow conditions is

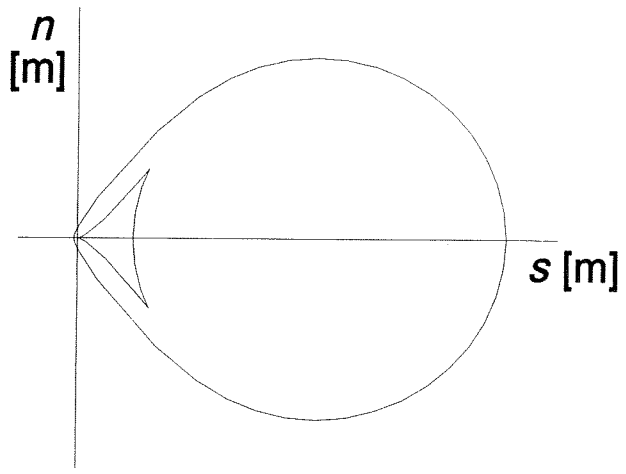

Figure 3.2

3.2.3. Characteristic condition for a single-layer model.

The system of partial-differential equations consists of Eqs 2.1, 2.2, 2.3, 2.19, 2.25 and 2.26 and is described in non-conservative form in Appendix A.2.

In the case of N size fractions, the number of variables and equations becomes 4 + 2*N. Three equations describe the conservation of fluid mass and momentum, N equations describe the relaxation effects per size-fraction in suspension, N mass balances per sediment size-fraction, and, additionally, the statement that the summation of N fractions equals unity. The latter condition enables elimination of one variable.

Consequently, the characteristic equation will be of the 3 + 2*N-th order. In analogy with Eq.3.15, the characteristics $P_i = 0$ describing the relaxation in suspended load can be easily recognized from this characteristic equation (Sloff, 1992). Similarly, the vorticity characteristic $R = 0$ (Eq.3.14) can be eliminated from the characteristic condition.

Because changes in composition can be related to changes in bed level (Section 2.3.3), no additional characteristic surfaces are introduced and a 2+N-th order equation remains, describing the coupled characteristic surfaces that are related to velocity, depth and level and composition of the bed. If $N = 2$, the roots can still be solved analytically, which is considered convenient for this analysis.

Analogeously to Section 3.2.2, the system of equations A.3 can be rewritten as

$$Q \cdot \begin{bmatrix} \mathrm{D}a/\mathrm{D}t \\ \mathrm{D}u/\mathrm{D}t \\ \mathrm{D}v/\mathrm{D}t \\ \mathrm{D}z_b/\mathrm{D}t \\ \mathrm{D}p_{s1}/\mathrm{D}t \\ \mathrm{D}p_{s2}/\mathrm{D}t \\ \mathrm{D}p_{m1}/\mathrm{D}t \end{bmatrix} = \vec{n}^T \cdot \vec{n} \begin{bmatrix} 0 \\ g_x - \tau_{bx}/\rho a \\ g_y - \tau_{by}/\rho a \\ 0 \\ p_{e1} - p_{s1} \\ p_{e2} - p_{s2} \\ 0 \end{bmatrix} \qquad 3.17$$

and the characteristic condition is

$$|Q| = \begin{bmatrix} R & an_x & an_y & 0 & 0 & 0 & 0 \\ -g_z n_x & R & 0 & -g_z n_x & 0 & 0 & 0 \\ -g_z n_y & 0 & R & -g_z n_y & 0 & 0 & 0 \\ 0 & 0 & 0 & 0 & P_1 & 0 & 0 \\ 0 & 0 & 0 & 0 & 0 & P_2 & 0 \\ 0 & K_{11}n_x+K_{21}n_y & K_{21}n_x+K_{31}n_y & \beta_1 n_t & aR & 0 & S_1 \\ 0 & K_{12}n_x+K_{22}n_y & K_{22}n_x+K_{32}n_y & (1-\beta_1)n_t & 0 & aR & S_2 \end{bmatrix} = 0 \qquad \textbf{3.18}$$

with

$$\begin{aligned} R &= n_t + un_x + vn_y \;\; ; \;\; P_i = T_{Ai}n_t + L_{xi}n_x + L_{yi}n_y \\ S_1 &= \delta_m n_t + (K_{41} + K_{51}(D_1-D_2))(un_x + vn_y) \\ S_2 &= -\delta_m n_t + (-K_{42} + K_{52}(D_1-D_2))(un_x + vn_y) \end{aligned} \qquad \textbf{3.19}$$

The characteristic equation can be rewritten as

$$\begin{gathered} R = 0 \;\vee\; P_1 = 0 \;\vee\; P_2 = 0 \\ \vee \\ n_t(R^2 + g_z a(n_x^2 + n_y^2))((\beta_1-1)S_1 + \beta_1 S_2) + \\ + g_z R[n_x^2(K_{11}S_2-K_{12}S_1) + 2n_x n_y(K_{21}S_2-K_{22}S_1) + n_y^2(K_{31}S_2-K_{32}S_1)] = 0 \end{gathered} \qquad \textbf{3.20}$$

The three roots of the characteristic equation that can be decoupled yield the following characteristic planes

$$\begin{aligned} R = 0 &\rightarrow c_x = u \;\wedge\; c_y = v \\ P_i = 0 &\rightarrow c_x = \frac{L_{xi}}{T_{Ai}} \;\wedge\; c_y = \frac{L_{yi}}{T_{Ai}} \end{aligned} \qquad \textbf{3.21}$$

representing the streamline and suspended-sediment retardation effects (in analogy with Eqs 3.14 and 3.15).

The coupled part of the characteristic equation, that represent the Monge cone, can be written as

$$Ar^4 + B(u\cos\theta + v\sin\theta)r^3 + (C\cos^2\theta + D\sin^2\theta + E\sin 2\theta)r^2 + \\ + (F\cos^3\theta + G\cos^2\theta\sin\theta + H\cos\theta\sin^2\theta + I\sin^3\theta)r + \\ + J\cos^4\theta + K\cos^3\theta\sin\theta + L\cos^2\theta\sin^2\theta + M\cos\theta\sin^3\theta + N\sin^4\theta \qquad 3.22$$

The coefficients are described in Appendix C.1.

For example, the intersection of the characteristic surfaces at Δt = 1 s in supercritical flow conditions is

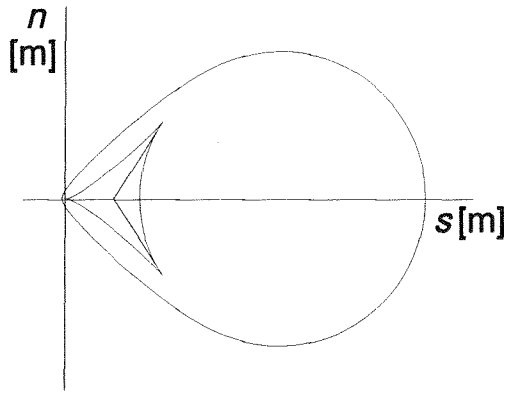

Figure 3.3

When Figures 3.2 and 3.3 are compared, the additional characteristic surface can be found that is introduced by distinction of size fractions.

3.2.4. Characteristic condition for a double-layer model.

The system of equations consists of Eqs 2.1, 2.2, 2.3, 2.19, 2.46 and 2.47 together with the statement by Eq.2.23 which can be applied for p_{pi} and p_{spi}. This system of partial-differential equations is described in non-conservative form in Appendix A.4.

From Eq.2.47 it can be concluded that changes in the subpavement are only related to changes in bed level and composition in the subpavement. Therefore, no additional characteristic direction will be introduced.

Again, the system of partial-differential equations can be written as

$$Q \cdot \begin{bmatrix} \mathrm{D}a/\mathrm{D}t \\ \mathrm{D}u/\mathrm{D}t \\ \mathrm{D}v/\mathrm{D}t \\ \mathrm{D}z_b/\mathrm{D}t \\ \mathrm{D}p_{s1}/\mathrm{D}t \\ \mathrm{D}p_{s2}/\mathrm{D}t \\ \mathrm{D}p_{p1}/\mathrm{D}t \\ \mathrm{D}p_{sp1}/\mathrm{D}t \end{bmatrix} = \vec{n}^T \cdot \vec{n} \begin{bmatrix} 0 \\ g_x - \tau_{bx}/\rho a \\ g_y - \tau_{by}/\rho a \\ 0 \\ p_{e1} - p_{s1} \\ p_{e2} - p_{s2} \\ 0 \\ 0 \end{bmatrix} \qquad \textbf{3.23}$$

with the matrix Q

$$\begin{bmatrix} R & an_x & an_y & 0 & 0 & 0 & 0 & 0 \\ -g_z n_x & R & 0 & -g_z n_x & 0 & 0 & 0 & 0 \\ -g_z n_y & 0 & R & -g_z n_y & 0 & 0 & 0 & 0 \\ 0 & 0 & 0 & 0 & P_1 & 0 & 0 & 0 \\ 0 & 0 & 0 & 0 & 0 & P_2 & 0 & 0 \\ 0 & g(1+\alpha_1)(K_{11}n_x + K_{21}n_y) & g(1+\alpha_1)(K_{21}n_x + K_{31}n_y) & \beta_{o1}n_t & aR & 0 & S_1 & T_1 \\ 0 & g(1+\alpha_2)(K_{12}n_x + K_{22}n_y) & g(1+\alpha_2)(K_{22}n_x + K_{32}n_y) & (1-\beta_{o1})n_t & 0 & aR & S_2 & T_2 \\ 0 & 0 & 0 & (\beta_{o1} - \kappa(1+\alpha_1)\beta_{p1})n_t & 0 & 0 & -\alpha_1\delta_p n_t & \delta_s n_t \end{bmatrix}$$

where **3.24**

$$R = n_t + un_x + vn_y \;\; ; \;\; P_i = T_{Ai}n_t + L_{xi}n_x + L_{yi}n_y$$

$$S_1 = \delta_p n_t + g(K_{41} + K_{51}(D_1 - D_2))(un_x + vn_y)$$

$$S_2 = -\delta_p n_t + g(-K_{42} + K_{52}(D_1 - D_2))(un_x + vn_y)$$

3.25

$$T_1 = \delta_s n_t + g\alpha_1\left(K_{41}\frac{p_{p1}}{p_{sp1}} + K_{51}\frac{D_{mp}}{D_{ms}}(D_1 - D_2)\right)(un_x + vn_y)$$

$$T_2 = -\delta_s n_t + g\alpha_2\left(-K_{42}\frac{1-p_{p1}}{1-p_{sp1}} + K_{52}\frac{D_{mp}}{D_{ms}}(D_1 - D_2)\right)(un_x + vn_y)$$

with

$$\alpha_2 = \alpha_1 \frac{1-p_{sp1}}{p_{sp1}} \frac{p_{p1}}{1-p_{p1}} \left(\frac{D_{mp}}{D_{ms}}\right)^{l_2-l_1} \qquad \textbf{3.26}$$

The definition of K_{ij} can be found in appendix B.

The characteristic determinant can be written as

$$R = 0 \vee P_1 = 0 \vee P_2 = 0 \vee n_t = 0$$

$$\vee$$

$$\begin{aligned}
&n_t\left(R^2 + g_z a(n_x^2+n_y^2)\right)\left[(1-\beta_{o1})(\delta_s S_1+\alpha_1\delta_p T_1) - \beta_{o1}(\delta_s S_2+\alpha_1\delta_p T_2)\right] + \\
&+ g_z g R n_x^2\left[(1+\alpha_2)K_{12}(\delta_s S_1+\alpha_1\delta_p T_1) - (1+\alpha_1)K_{11}(\delta_s S_2+\alpha_1\delta_p T_2)\right] + \\
&+ 2g_z g R n_x n_y\left[(1+\alpha_2)K_{22}(\delta_s S_1+\alpha_1\delta_p T_1) - (1+\alpha_1)K_{21}(\delta_s S_2+\alpha_1\delta_p T_2)\right] + \\
&+ g_z g R n_y^2\left[(1+\alpha_2)K_{32}(\delta_s S_1+\alpha_1\delta_p T_1) - (1+\alpha_1)K_{31}(\delta_s S_2+\alpha_1\delta_p T_2)\right] + \\
&\left(R^2 + g_z a(n_x^2+n_y^2)\right)(T_2 S_1 - T_1 S_2)(\kappa\beta_{p1}(1+\alpha_1) - \beta_{o1}) = 0
\end{aligned} \qquad \textbf{3.27}$$

The part of the characteristic equation that represents the coupled roots of Eq.3.37 can again be written as

$$\begin{aligned}
&Ar^4 + B(u\cos\theta + v\sin\theta)r^3 + (C\cos^2\theta + D\sin^2\theta + E\sin 2\theta)r^2 + \\
&+ (F\cos^3\theta + G\cos^2\theta\sin\theta + H\cos\theta\sin^2\theta + I\sin^3\theta)r + \\
&+ J\cos^4\theta + K\cos^3\theta\sin\theta + L\cos^2\theta\sin^2\theta + M\cos\theta\sin^3\theta + N\sin^4\theta
\end{aligned} \qquad \textbf{3.28}$$

with the coefficients of the equation described in Appendix C.2.

Chapter 4

Analysis of characteristic surfaces.

4.1. Introduction.

In this Chapter, the coupled characteristic roots of Eq.3.22 (single-layer model) and Eq.3.28 (double-layer model) are analysed by constructing the characteristic surfaces with the help of Huyghens' construction Eq.3.7.

In the analysis of the coupled characteristic surfaces, three families will be distinguished (Figure 3.2); a family of large characteristic surface that can be described as a "balloon"-shaped surface (Section 4.2), and two families of small bicharacteristic surfaces (Figure 3.3); a "fast" and "slow"-travelling "star"-shaped surface (Section 4.3).

Throughout the analysis, the analogy between one-dimensional and two-dimensional models is used; the characteristics in 1-DH models are equivalent with the bicharacteristic rays in or against the direction of the stream.

In Section 4.1, the characteristics of flow variables are approximated with the help of the quasi-steady approach (instantaneous adjustment of the flow variables compared to changes in the morphological variables). The validity of this quasi-steady approach for subcritical and supercritical flow is investigated for two-dimensional models.

The "star"-shaped characteristic surfaces are analysed in Section 4.2. Different approximations are investigated, and the validity of decoupling changes in bed level from changes in composition is tested.

In Section 4.3.6 and 4.4.3, the mathematical character of the single-layer and double-layer model are analysed. Approximative criteria for maximum thickness of the mixing layers have been derived to ensure the hyperbolicity of the models. Some remarks on the relevance of this maximum layer thickness are added in Section 4.3.7.

4.2. Family of large ("balloon"-shaped) characteristic surfaces.

4.2.1. Analysis of characteristic roots.

To predict the behaviour of the characteristics, the roots of the characteristic equation are analysed.

In Figure 4.1, all characteristics relative to velocity are presented for varying Froude numbers and sediment transport. The broken lines represent the characteristics in the case of a larger sediment-transport rate.

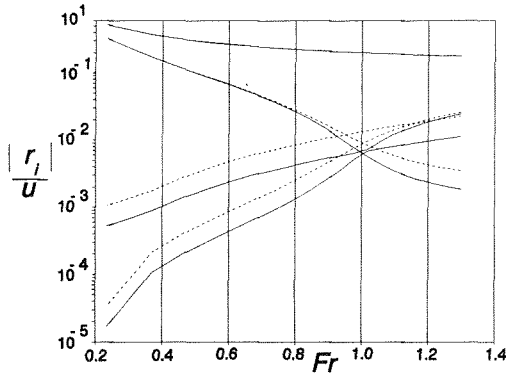

Figure 4.1

For situations with $s_b/ua << 1$, $Fr < 0.8$ and $Fr > 1.2$, the large characteristics are not significantly affected by the mobility of the bed (see also De Vries, 1993). This allows simplified solutions for the characteristics, which will be derived in the following.

4.2.2. Approximation of characteristics.

Perpendicular to the flow the effect of the transported volume of sediment on the family of large characteristic surfaces increases. In the case of $v = 0$ m/s, and with $n_x = 0$ and $n_y = 1$, the characteristic roots of Eq.3.20 are

$$n_t = 0 \quad \vee \quad P_1 = -\frac{L_{y1}}{T_{A1}} \quad \vee \quad P_2 = -\frac{L_{y2}}{T_{A2}}$$

$$\vee \qquad \textbf{4.1}$$

$$-\delta_m n_t^2 = 0 \quad \vee \quad n_t = \pm\sqrt{-g_z(a + K_{31} + K_{32})} = \pm\sqrt{-g_z\left(a + \frac{s_{b1}+s_{b2}}{u}\right)}$$

The latter roots can be interpretated as the maximum width of the "balloon"-shaped wave front perpendicular to the direction of flow. It appears that the characteristic surface can be partially approximated with a circle (Figure 4.2).

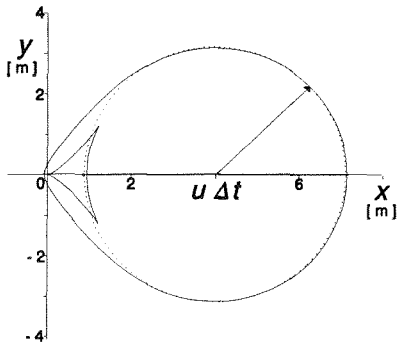

Figure 4.2

This implies that the largest bicharacteristic ray in flow direction can be approximated with

$$r = -n_t = u + \sqrt{-g_z(a + K_{31} + K_{32})} = u + \sqrt{-g_z a\left(1 + \frac{s_{b1} + s_{b2}}{ua}\right)} \qquad 4.2$$

For $s_b/q << 1$ (with $q = ua$), this expression approaches

$$r = u + \sqrt{-g_z a} \qquad 4.3$$

(De Vries, 1993). The relative errors of Eqs 4.2 and 4.3 are represented in Figure 4.3 by ϵ_1 and ϵ_0 respectively. ϵ_2 represents the situation with a sediment transport twice as much relative to ϵ_1.

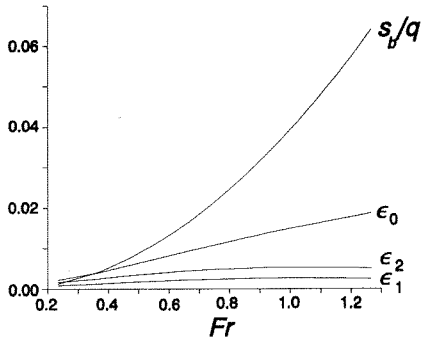

Figure 4.3

Similarly it can be found

$$r = -n_t = u - \sqrt{-g_z(a + K_{31} + K_{32})} = u - \sqrt{-g_z a\left(1 + \frac{s_{b1} + s_{b2}}{ua}\right)} \qquad 4.4$$

In Figure 4.4, all characteristics for the single-layer model are plotted. The approximations Eqs 4.2 and 4.4 are represented with the broken lines.

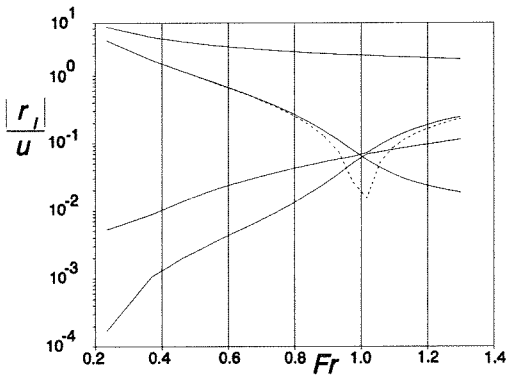

Figure 4.4

It is noted that this second approximation cannot be applied for Fr near unity. As a result, from this analysis it appears that a "quasi-steady" approach (no effect of the

mobility of the bed on the celerities of the water level) can be applied for one-dimensional models with $Fr < 0.8$ and $s_b/q << 1$. At larger rates of sediment transport, the approximations by Eqs 4.2 and 4.4 perform better than the "fixed-bed" characteristic Eq.4.3.

4.2.3. Decoupling of hydraulic and morphological processes.

At supercritical flows for $Fr > 1.2$ this approach seems justified also (Figure 4.4), but for two-dimensional models, this is not the case. If the characteristic surfaces for uniform sediment are calculated for two situations with different transport rates, the following Figures 4.5-a to 4.5-f can be constructed for varying values of Fr.

As can be concluded, decoupling of hydraulic and morphological processes in two-dimensional supercritical flows cannot be applied. The scale of Figures 4.5 is not constant. For $Fr < 0.6$, however, changes in hydraulic conditions (depth and velocity) can be assumed instantaneous relative to the "slow" changes in bed level and composition.

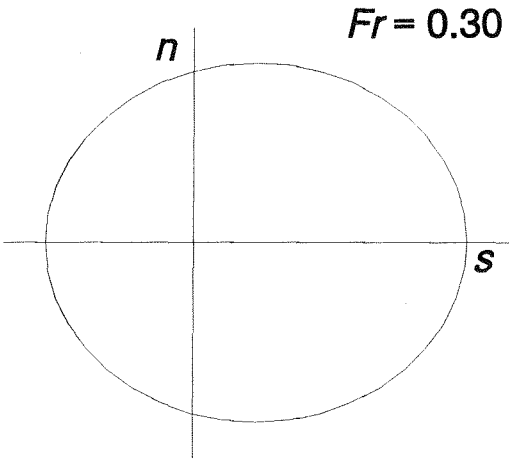

Figure 4.5-a

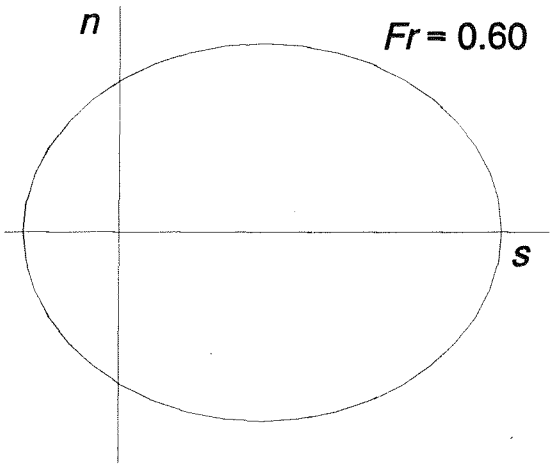

Figure 4.5-b

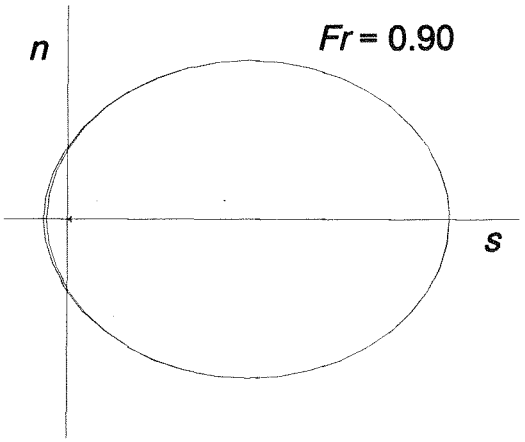

Figure 4.5-c

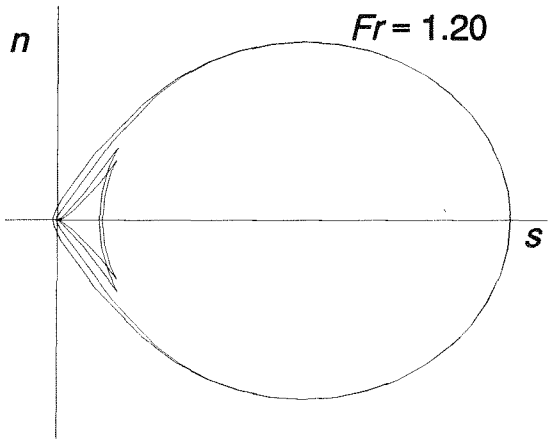

Figure 4.5-d

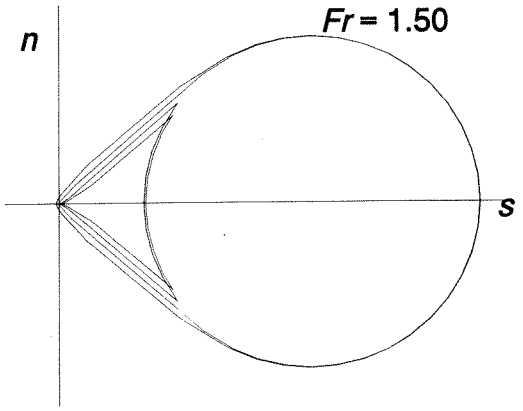

Figure 4.5-e

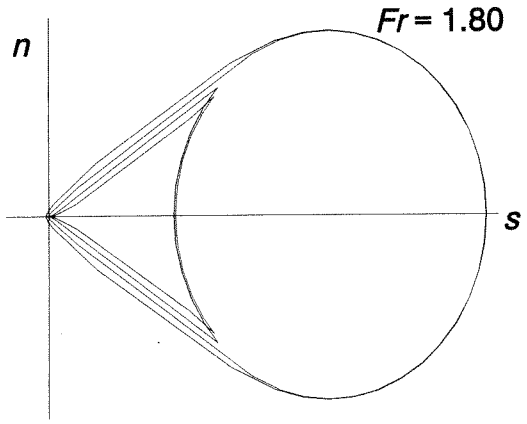

Figure 4.5-f

4.3. Family of small ("star"-shaped) characteristic surfaces for the single-layer model.

4.3.1. Physical conditions.

The families of small bicharacteristic surfaces are strongly related to the composition of the layers and of the vertical fluxes between the layers. Different conditions can be distinguished.

	$\beta_{pi} = p_{oi}$	$\beta_{pi} = p_{mi}$
$p_{m1} < p_{o1}$	erosion of an armoured riverbed	deposition of coarse material at a fine river bed
$p_{m1} \geq p_{o1}$	erosion of a coarse river bed covered with fine material	deposition of fine material at a coarse river bed

Table 4.1

As a result, sedimentation and erosion conditions yield different characteristic surfaces; in the following figures, the bicharacteristics are presented that are related to bed level and composition in the case of sedimentation of fine material at a coarser river bed (Figure 4.6-a), and in the case of erosion of an armoured river bed (Figure 4.6-b).

The star-shaped curves that are shown represent travelling fronts of small-scale disturbances. The wave fronts can be constructed from roots of the characteristic equation as described in section 3. For the two situations described, the wave fronts are of opposite shape.

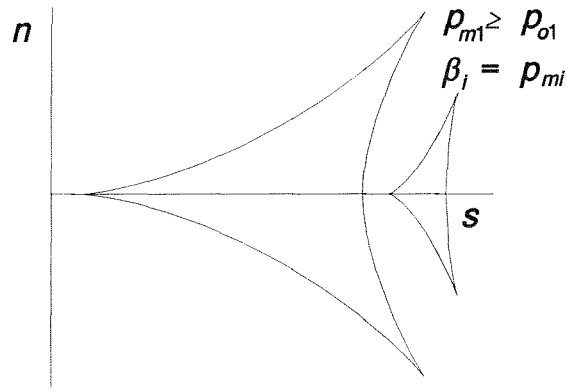

Figure 4.6-a

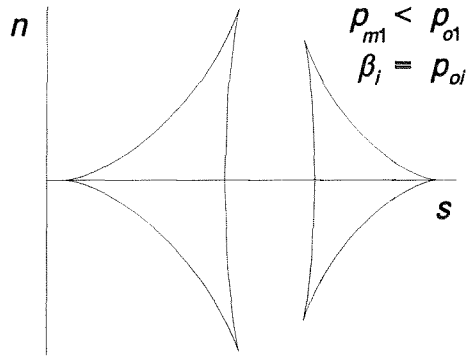

Figure 4.6-b

4.3.3. Analysis of characteristic roots.

If Eq. 3.22 is applied for the situation of one-dimensional flow, the equation of the charactistics is

$$Ar^4 + Bur^3 + Cr^2 + Dr + E = 0 \qquad 4.5$$

with

$$A = -\delta_m \;;\; B = 2\delta_m + X \;;\; C = -2u^2X - \delta_m\left[g_z(a+K_{11}+K_{12})+u^2\right]$$

$$D = g_z u\left(\delta_m(K_{11} + K_{12}) + aX + Y\right) + u^3X \;;\; E = -g_z u^2 Y$$

$$X = (1-\beta_1)(D_1-D_2)K_{51} + (D_2-D_1)\beta_1 K_{52} + (1-\beta_1)K_{41} + \beta_1 K_{42}$$

$$Y = (D_1 - D_2)(K_{12}K_{51} - K_{11}K_{52}) + K_{12}K_{41} + K_{11}K_{42}$$

Two ways of approaching roots of Eq.4.5 have been applied here. The first is the simplification of the coefficients of Eq.4.5, the second way is to simplify the system of equation that yield the characteristic equation by the decoupling of physical processes. The latter method directly yields insight whether processes can be decoupled.

Simplification of coefficients.

If $X = \delta_m$, Eq.4.5 can be written as

$$(u-r)\left[\delta_m\, r\left(g_z(a + K_{11} + K_{12}) + (r-u)^2\right) + g_z u Y\right] = 0 \qquad 4.6$$

which yields for one of the roots $r = u$. The condition $X = \delta_m$ is satisfied at the lines drawn in the following figures for different size-distributions.

In the figures 4.7-a and 4.7-b, sedimentation and armouring conditions are represented respectively.

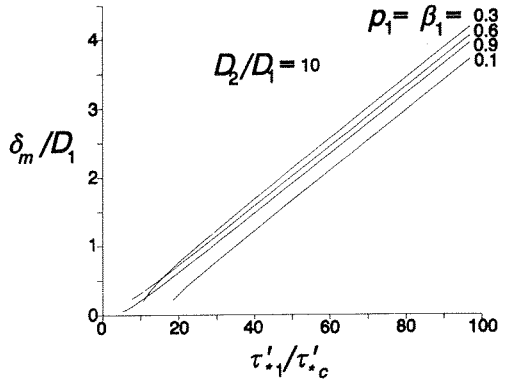

Figure 4.7-a

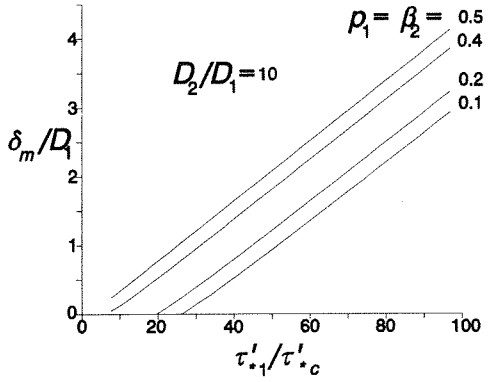

Figure 4.7-b

The mixing layer should be very thin to satisfy this condition, and usually the characteristics related to morphological parameters are smaller than u.

If $Y = (K_{11} + K_{12})\, X$, Eq.4.5 can be written as

$$\left(\delta_m r - u\, X\right)\left(r\, g_z\, a + (r-u) g_z (K_{11} + K_{12}) + r(r-u)^2\right) = 0 \qquad \textbf{4.7}$$

which yields

$$r = \frac{uX}{\delta_m} \qquad \textbf{4.8}$$

The assumption $Y = (K_{11} + K_{12})\, X$ is satisfied if

$$\beta_1 = \frac{K_{11}}{K_{11} + K_{12}} \quad \vee \quad (D_1 - D_2)(K_{51} + K_{52}) + K_{41} - K_{42} = 0 \qquad \textbf{4.9}$$

In Figure 4.8-a, the left-hand root of Eq.4.9 is shown. At high shear-stresses β_1 approaches p_1. At $\tau_{*1}/\tau_{*c} > 50$, this condition is satisfied in sedimentation processes only.

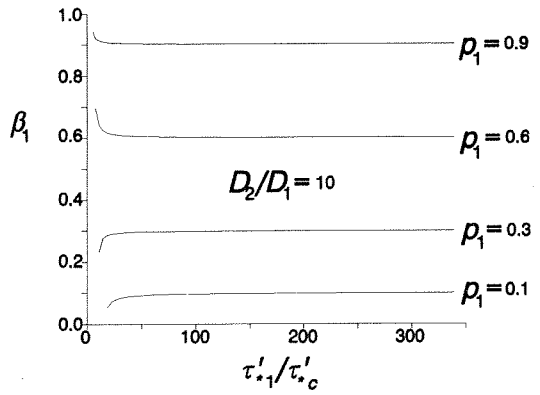

Figure 4.8-a

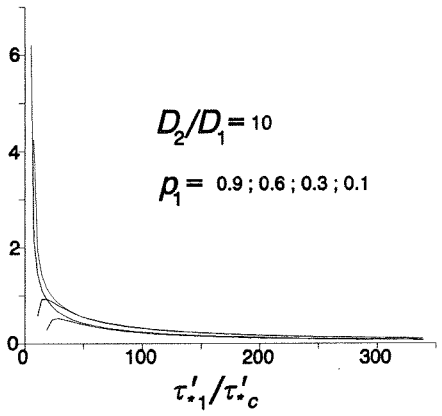

Figure 4.8-b

The expression at the left-hand side of the second root in Eq.4.9 is presented in Figure 4.8-b. This can be rewritten as

$$\frac{s_1(1-p_1)}{s_2 p_1} = \frac{m_1}{m_2} u^{n_1-n_2} D_m^{l_2-l_1} = \frac{D_m - (D_2-D_1)l_2(1-p_1)}{D_m + (D_2-D_1)l_1 p_1} \qquad 4.10$$

which is satisfied for $\tau_{*m}/\tau_{*c} \rightarrow \infty$. Consequently, $r \rightarrow uX/\delta_m$ in sedimentation processes at high shear-stresses.

Ribberink (1980) uses a quasi-steady approch and neglects effects of gradients in the median grain diameter. The additional characteristic is approximated with

$$r = u \frac{K_{41}(1-\beta_1) + K_{42}\beta_1}{\delta_m} \qquad 4.11$$

which is equivalent to Eq.4.8 apart from the effect of gradients in median grain diameter.

Decoupling of changes in bed level and composition.

If the quasi-steady approach is applied, ($Fr < 0.6$ and $Fr > 1.2$ for one-dimensional models), the characteristics that remain coupled refer to the composition and level of the bed. If changes in bed level and composition can be decoupled, two options exists: either the level or the composition adjusts intantaneously.

If the adjustment of the bed level is assumed intantane, the remaining characteristic root is

$$r = \frac{Y}{\delta_m(K_{11} + K_{12})} \qquad 4.12$$

Substitution into Eq.4.5 in combination with Eqs 4.2 and 4.4 yields for the fourth root

$$r = \frac{u^2(K_{11} + K_{12})}{a(1 - Fr^2 + (K_{31} + K_{32})/a)} \qquad 4.13$$

If on the other hand the adjustment of the bed composition is assumed intantaneous, the remaining characteristic root corresponding to the bed level is

$$r = \frac{uY}{(1-Fr^2)aX} \qquad 4.14$$

again substitution of Eq.4.14 into Eq.4.5 in combination with Eqs 4.2 and 4.3 yields for the fourth root

$$r = \frac{u(1-Fr^2)X}{\delta_m(1 - Fr^2 + (K_{31} + K_{32})/a)} \qquad 4.15$$

In Figure 4.9, the error ϵ in approximation by Eqs 4.8, 4.11, 4.13 and 4.15 relative to the exact characteristic is presented at varying Fr. The conditions represent the erosion

of an armoured river bed.

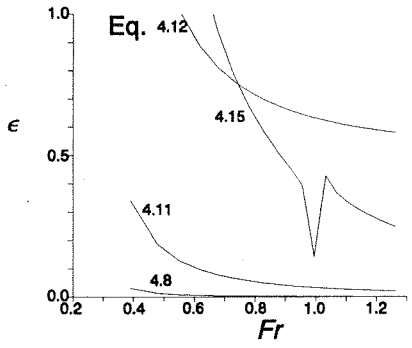

Figure 4.9

From Figure 4.9 can be concluded that $r = uX/\delta_m$ performes best compared to the other expressions. The difference in behaviour of Eqs 4.8 and 4.11 results from gradients in median grain size, which apparently is significant at low shear-stresses. Because the relative errors in Eqs 4.13 and 4.15 are significant, it can be concluded that composition of the bed cannot be decoupled from changes in bed level.

4.3.3. Approximation of characteristics.

In Figure 4.10, the characteristic roots in stream-direction at different shear-stresses are presented. As can be seen from the figure, two intersecting characteristics are composed by two different roots. The dotted line represents X/δ_m, which approaches one of the characteristics that correspond to the star-shaped characteristic surface.

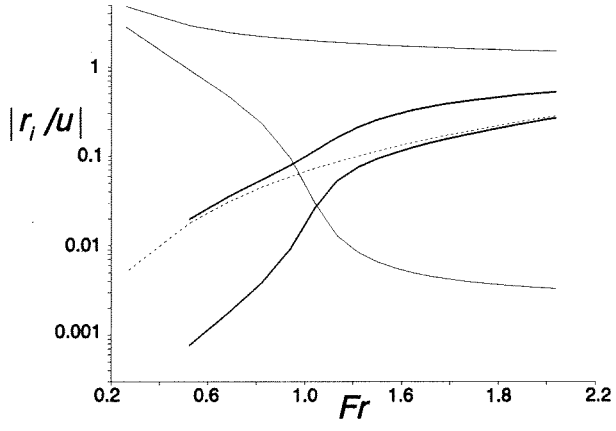

Figure 4.10

It appears from Section 4.3.8 that Eq.4.8 represents the tail of the largest, star-shaped characteristic surface, whereas the bicharacteristic ray in the direction of the stream, which is the equivalent of the characteristic in one-dimensional models, is represented by the front of the "star".

Consequently, the error made by using Eq.4.8 equals the length of the star which subsequently represents the two-dimensionality of a propagating disturbance. The error changes with flow conditions and sediment properties; in Figure 4.10 the error grows with Fr. In the case of sedimentation, the bicharacteristic ray is underestimated, whereas in the case of erosion of an armoured bed the bicharacteristic ray is overestimated.

The expression $r = uX/\delta_m$ approaches for $\tau_{*m}/\tau_{*c} \rightarrow \infty$

$$r = \frac{uX}{\delta_m} = \frac{s_{b1}}{p_{m1}\delta_m} \qquad \textbf{4.16}$$

The characteristic root is approximately linearly related with the reciproke of δ_m.

When subsituting the approximations Eqs 4.2, 4.4 and 4.8 into the characteristic equation Eq.4.5, the fourth bicharacteristic ray can be found

$$r = \frac{g_z\, uY}{X\left(u^2 + g_z(a + K_{31} + K_{32})\right)} \qquad \textbf{4.17}$$

For $\tau_{*m}/\tau_{*c} \rightarrow \infty$, Eq.4.17 approaches

$$r \approx n\, u \frac{s_{b1}}{p_{m1}a} \frac{1}{\left(\frac{u^2}{g_z a} + 1 + \frac{(s_{b1}+s_{b2})}{ua}\right)} \qquad \textbf{4.18}$$

which corresponds with the characteristic for uniform material (De Vries, 1993).

In Figure 4.11, the characteristics of the single-layer model are shown. The broken lines represent the approximations by Eqs 4.2, 4.4, 4.8 and 4.17. Near Fr is unity, the approximations fail.

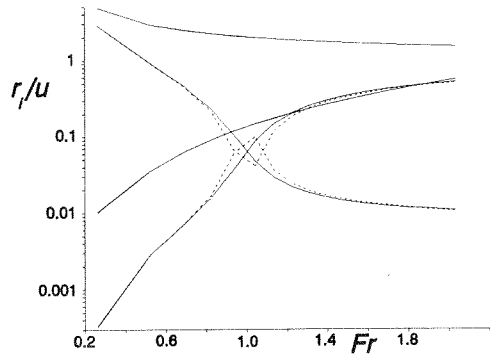

Figure 4.11

If the bicharacteristic rays that correspond to the star-shaped wave fronts are plotted linearly (Figure 4.12), the performance of the approximations by Eq.4.8 and Eq.4.17 become more clear. It can be seen that for $Fr < 0.8$, Eq.4.17 slightly overestimates the characteristic, whereas for $Fr > 1.2$, the error appears to be larger and the characteristic

is underestimated.

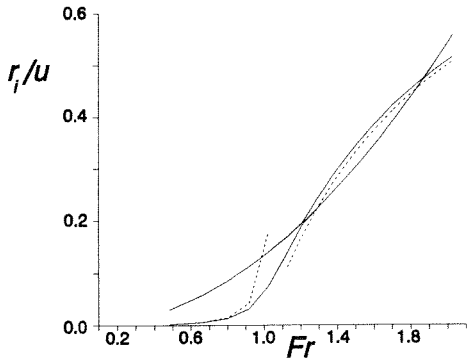

Figure 4.12

4.3.4. Sensitivity of characteristics to the mixing-layer thickness.

The sensitivity of both star-shaped bicharacteristics to changes in δ_m is presented in Figure 4.13. Here, the characteristic roots in stream-direction are shown of both star-shaped characteristic surfaces. No principal differences can be found under sedimentation and erosion of armoured beds.

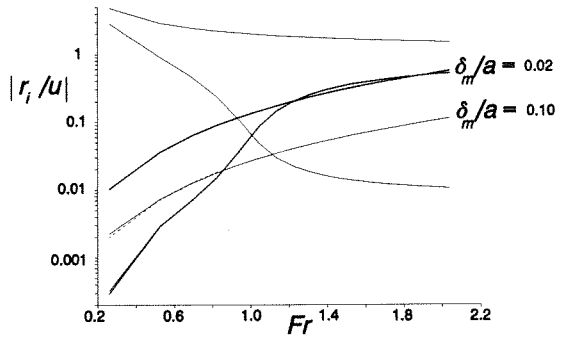

Figure 4.13

It can be concluded that for higher shear-stresses, only the additional characteristic that is introduced is sensitive to changes in δ_m (Ribberink, 1980). As a result, the selection of δ_m does not *directly* affect the dynamic behaviour of the bed level, which can be considered beneficial.

If δ_m is chosen sufficiently large, the characteristics intersect. After intersection in the case of sedimentation, the characteristics are combined into one wave front and only the intermediate point ($r = uX/\delta_m$) changes with varying δ_m. This will be illustrated in Section 3.4.4. Under the conditions of erosion of an armoured bed, the characteristics become imaginary at the point of intersection.

4.3.5. Effect of sediment mixture relative to uniform material.

To compare the behaviour of the single-layer model with the general mobile bed model, the relative differences in characteristics of both models are presented in Figure

4.14 for varying values of Fr.

The characteristics with subscript *un* refer to a uniform material, the subscript *nu* refers to a mixture with $D_2 = 2\ D_1$. The two situations described have an equal mean diameter and the rate of total sediment transport is similar at high shear stresses where hiding effects can be neglected.

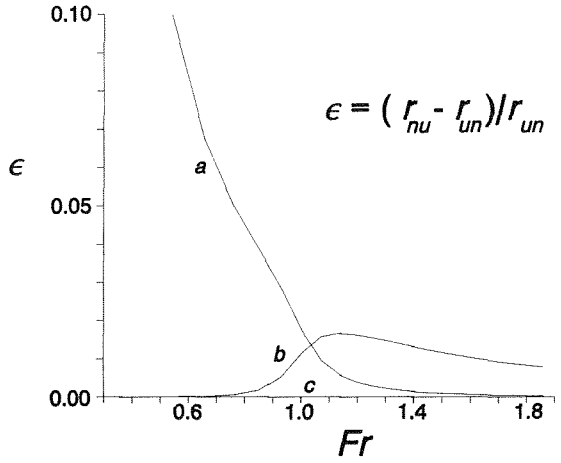

Figure 4.14

The changes in bed level are related to the characteristics indicated with *a* for subcritical flow and *b* for supercritical flow, and appear to be sensitive to the distinction of size-fractions. At low Fr, hiding effects have a significant influence on the morphology. At high Fr, the effect of fractions on the characteristics reduces, which can also be concluded from Eq.4.18. Consequently, distinguishing different fractions is most significant for flows when shear-stresses are low.

In Figure 4.15, the effect of changes in fraction is presented: characteristics with subscript 1 and 2 refer to a bed composition with $p_{m1} = 0.30$ and $p_{m1} = 0.20$ respectively. For subcritical flow, the characteristics that correspond to propagation of changes in water level are indicated with *b* an *c*, and *a* and *d* refer to changes in bed level and composition. It can be concluded that for the range $0.6 < Fr < 1.3$, the single-layer model is very sensitive to the composition of the bed.

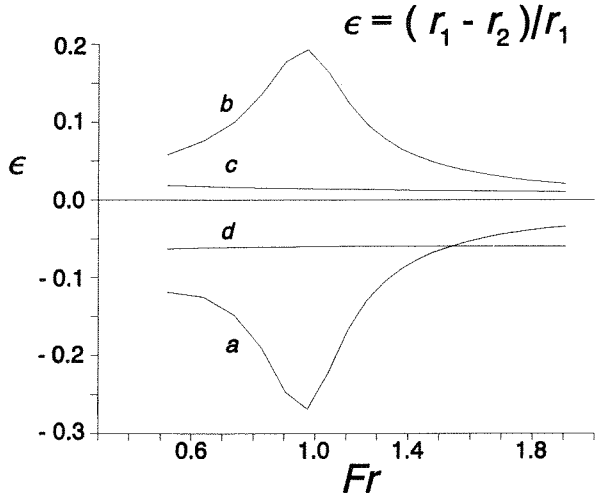

Figure 4.15

It should, however, taken into account that this analysis is based on the use of the Meyer-Peter and Müller sediment-transport formula, which application is restricted to relatively small shear stresses.

4.3.6. Mathematical character of the single-layer model.

As described by Ribberink (1987), the characteristics of a single-layer model can become complex. If the partial-differential equations yield complex characteristics, the system is elliptic. Then future conditions influences the present and the model is physically unrealistic. The application of the single-layer model is therefore limited.

One condition, but not sufficient, for the system to become elliptic in the case of erosion with the mixing layer coarser than the substrate

$$\frac{D_{m\text{-}mix}}{D_{m\text{-}sub}} > 1 \qquad \textbf{4.19}$$

where D_m is the median grain size. To increase the range of hyperbolic character of the model, a transition layer can be introduced to replace $D_{m\text{-}sub}$ with a smaller, intermediate diameter (Ribberink, 1987).

The characteristics become complex if the two star-shaped characteristic surfaces intersect. This point of intersection is affected by the flow conditions, sediment properties and the thickness of the mixing layer; by selecting a smaller value of δ_m, the intersection can be avoided or extended to higher shear-stresses.

Consequently, a maximum value of δ_m can be found to assure the hyperbolicity of the system. If the physical situation is included in the interval of proper δ_m, the single-layer model can be applied.

Although Eq.4.8 does not represent the front of the star-shaped bicharacteristic but the tail at the back, the critical value of δ_m is estimated for $Fr < 0.8$ with the help of Eqs 4.8 and 4.17

$$\frac{\delta_m}{a} \approx \frac{X^2}{Y}\left(\frac{u^2}{g_z a} + 1 + \frac{s_{b1}+s_{b2}}{ua}\right) \qquad \textbf{4.20}$$

For $\tau_{*m}/\tau_{*c} \rightarrow \infty$ Eq.4.20 approaches

$$\frac{\delta_m}{a} \approx \frac{1}{n\,u}\left(1 + \frac{s_{b1}}{p_{m1} ua} - Fr^2\right) \qquad \textbf{4.21}$$

For $Fr > 1.2$, the critical value of δ_m can be approximated with Eq.4.4

$$\frac{\delta_m}{a} \approx \frac{X}{a\left(1 - \frac{\sqrt{-g_z a}}{u}\sqrt{1 + \frac{K_{31}}{a} + \frac{K_{32}}{a}}\right)} \qquad \textbf{4.22}$$

which approaches for $\tau_{*m}/\tau_{*c} \rightarrow \infty$

$$\frac{\delta_m}{a} \approx \frac{s_{b1}}{p_{m1}\,a\,u}\,\frac{Fr}{Fr - \sqrt{1 + \frac{s_{b1}}{p_{m1} ua}}} \qquad \textbf{4.23}$$

In Figure 4.16, the critical value of δ_m and Eqs 4.20 and 4.22 (broken lines) are plotted.

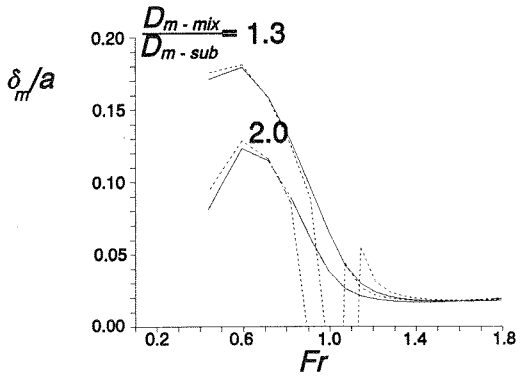

Figure 4.16

As can be concluded from the figure, the approximations slightly overestimate the exact critical value of δ_m because Eq.4.8 overestimates the bicharacteristic ray.

In the Figure 4.17, the critical values of δ_m are presented for a coarse material (D_1 = 4.0 mm, D_2 = 10.0 mm) with varying values of D_m in the mixing layer relative to the substrate.

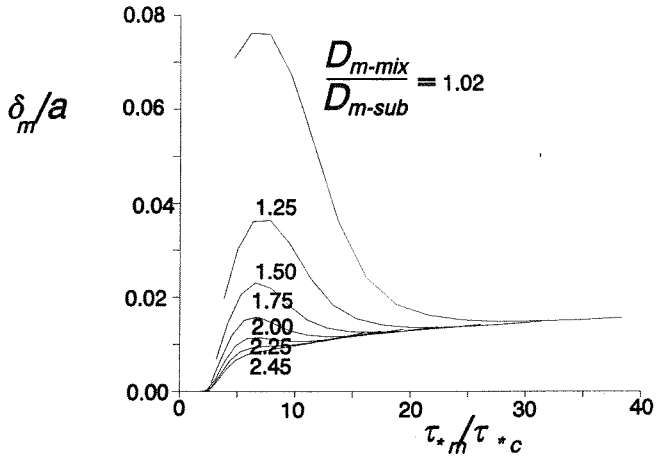

Figure 4.17

Because δ_m is often taken constant, problems can occur if flow conditions vary widely. At high shear-stresses, the hyperbolicity criterion becomes less sensitive to differences in composition of the mixing layer and substratum. Reducing the difference by distinction of a transition layer clearly improves the hyperbolicity of the mathematical model.

The propagation of disturbances in composition reduces with increasing D_m. As a result, the bicharacteristic rays will intersect more easily and the maximum values of δ_m will also be smaller.

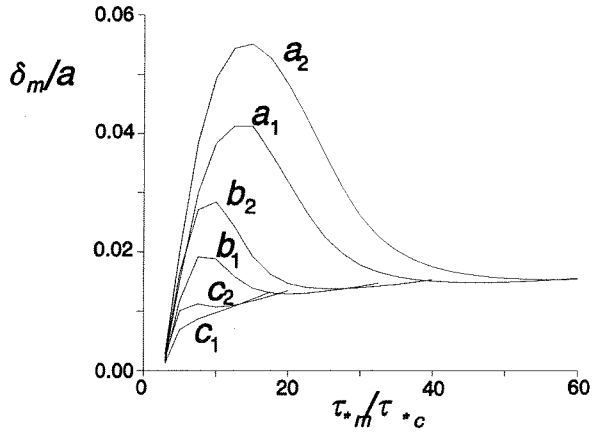

Figure 4.18

In Figure 4.18, the critical values of δ_m are presented against the mean shear-stress relative to the critical shear-stress. Herein, the sediment diameters are for *a*: D_1 = 1.0 mm, D_2 = 2.5 mm, for *b*: D_1 = 2.0 mm, D_2 = 5.0 mm, and for *c*: D_1 = 4.0 mm, D_2 = 10.0 mm. The fraction of fine sediment in the mixing layer are p_1 = 0.01 for set 1 and p_1 = 0.30 for set 2. The fraction of fine material in the substratum are for all sets p_1 = 0.99.

4.3.7. Relevance of maximum mixing-layer thickness.

The vertical mixing in the mixing layer should be instantaneous compared to morphological changes (Section 2.3.2). In general, the mixing process is assumed to be in an equilibrium state (e.g. developed bed forms). However, if this mixing is still in progress (developing armour layer), a time interval can be chosen to limit the extend of the vertical mixing and subsequently to satisfy the criterion of a maximum thickness of the mixing layer.

In other words, the applicability of the single-layer model can be extended when the time scale of the predictions are adjusted to the time interval that is needed to achieve the maximum thickness of the mixing layer.

In the application of numerical solution procedures, this implies that in the case of armouring, the maximum time interval ΔT is determined by the maximum value of the mixing layer thickness and the rate of mixing w

$$\Delta T \leq \frac{\delta_{m-\max}}{w} \qquad \textbf{4.24}$$

If the maximum thickness of the mixing layer is of the order of a few grains at the surface of the bed, the time scale to be used is nearly instantaneous, which results in small time steps. At larger values of the critical thickness, the mixing process has developed to a larger extend an the maximum time step can be larger as well.

The introduction of the rate of vertical mixing w, requires the definition of this rate. The vertical mixing is related to the frequency and magnitude of fluctuations in the bed, and subsequently to the shear stress and the size and composition of the top layers at the river bed.

In the following, this rate is assumed proportional to the average grain-velocity in the bed load layer. This grain velocity of fraction i is defined as

$$u_{gi} = \frac{s_{bi}}{p_{mi}\,\delta_b} \qquad \textbf{4.25}$$

After substitution of the maximum value of δ_m, Figure 4.19 can be constructed where u_{gi}/u is represented for different compositions of the river bed and for varying Fr.

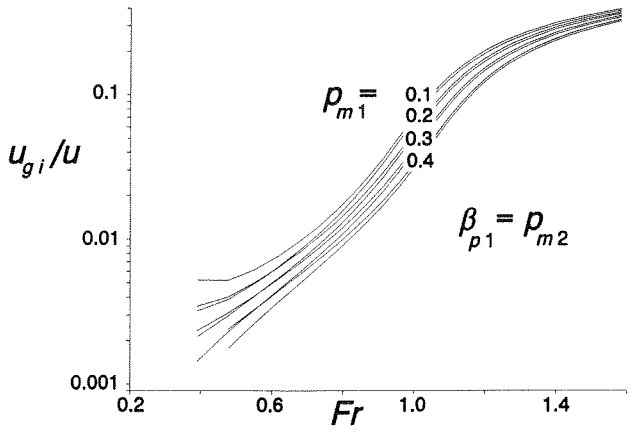

Figure 4.19

It should be noticed that at high shear-stresses, the fraction of bed load in the total load decreases relative to the amount of suspended load, which can result in an overestimation of the grain velocity at high shear-stresses.

With Eqs 4.24 and 4.25, an estimation for the maximum time interval can be found

$$\Delta T \leq \frac{\delta_m}{w} \approx \frac{p_{pi}\,\delta_m^2}{s_{bi}} \qquad \textbf{4.26}$$

With the help of this estimation Figure 4.20 can be constructed.

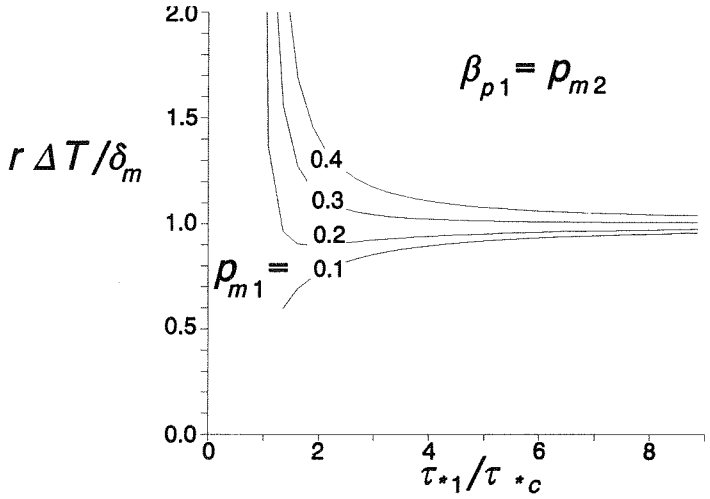

Figure 4.20

It appears that at high shear-stresses, this maximum time interval is not a realistic one for morphological modelling; the travelling distance of disturbances in bed level and composition equals the thickness of the mixing layer. However, in Section 2.3.4 it has been shown that at high shear-stresses, armour layers are not stable which makes this condition of maximum ΔT a hypothetical one.

Near the initiation of motion, where armour layers can be stable, the maximum time interval can be large. To indicate the magnitude of this time interval, ΔT is presented in dimensional form in Figure 4.21 for varying relative shear-stresses τ_{*m}/τ_{*c} .

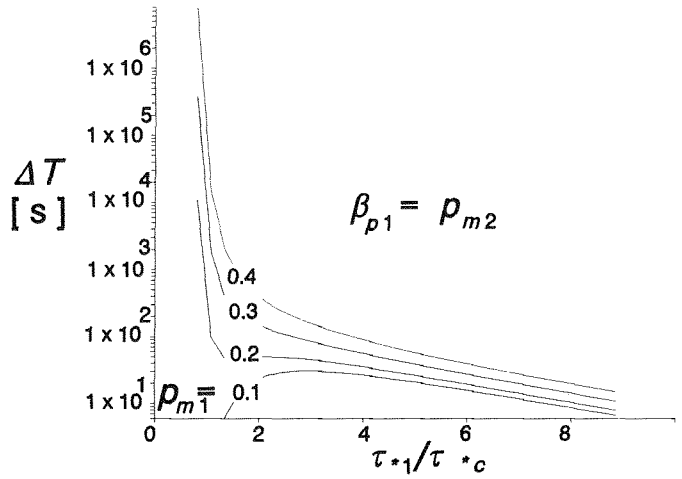

Figure 4.21

However, it should be questioned whether the vertical mixing can still be considered instantaneous relative to changes in bed level and composition at the time scales estimated.

In the single-layer model as analysed above, the thickness of the mixing layer is taken constant. However, because changes in mixing-layer thickness can be related to local variables in stead of gradients in these variables, (shear stress, average grain-velocity in the bed load, development of bed forms etc.), including changes in mixing-layer thickness only implies the introduction of source terms in the sediment mass balances. Consequently, the characteristics of the model are not affected.

4.3.8. Behaviour of characteristic surfaces.

Two-dimensional effects illustrate this behaviour in the following analysis, where depths are constant (1 m) and the ratio τ_{*1}/τ_{*c} ranges from 2 to 200. The black dots in the graphs represent $r = uX/\delta_m$.

Sedimentation ($D_{m\text{-}mix} = D_{m\text{-}sub}$).

In the first set of figures, the mean diameter of the mixing layer equals that of the substratum. The size and fraction of the finer material is 0.4 mm and 0.8 repectively, the size of the coarse fraction is 1 mm. The thickness of the mixing layer is taken 0.08 m.

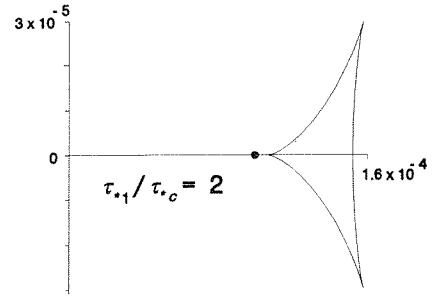

Figure 4.22-a

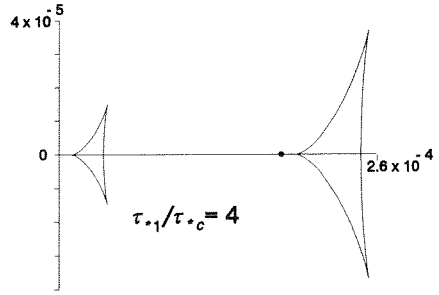

Figure 4.22-b

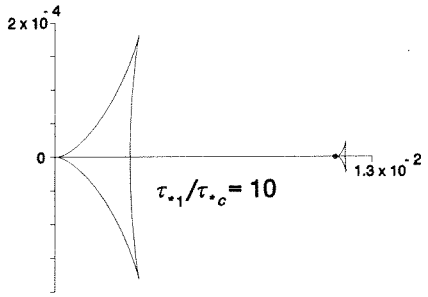

Figure 4.22-c

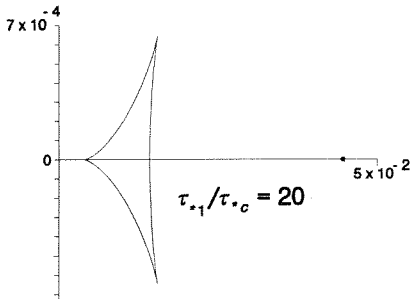

Figure 4.22-d

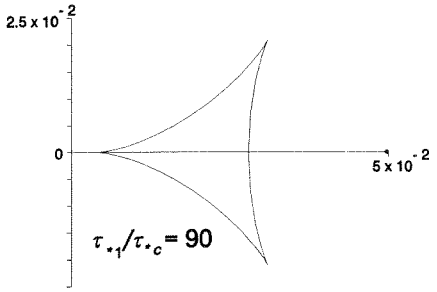

Figure 4.22-e

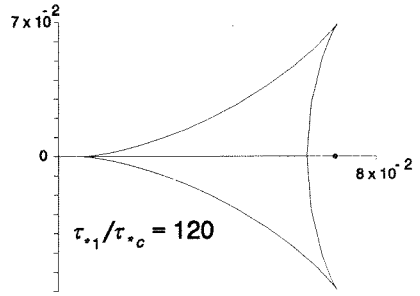

Figure 4.22-e

At $20 < \tau_{*1}/\tau_{*c} < 120$, the fastest wave front approaches $r = uX/\delta_m$. As a result, in this interval its dimensions become negligible relative to the other wave front. It appears that the fastest wave front declines for shear stresses left of the transition line (where the characteristic root equals uX/δ_m) and grows at higher shear stresses. At higher velocities the bicharacteristic rays in stream direction intersect and the two wave fronts

coincide. In that case, distinguishing size fractions becomes superfluous.

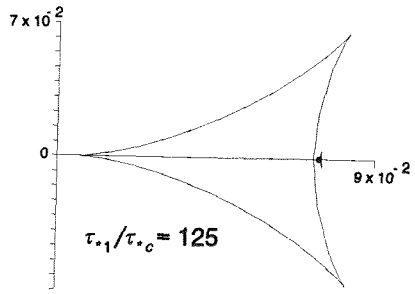

Figure 4.22-f

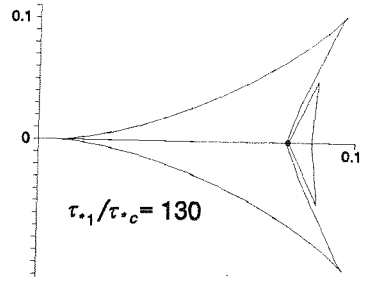

Figure 4.22-g

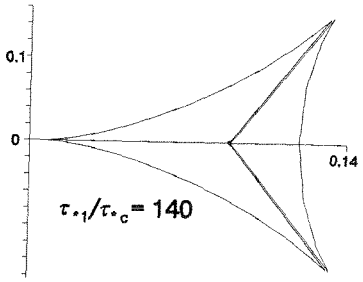

Figure 4.22-h

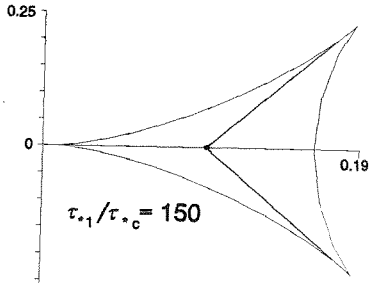

Figure 4.22-i

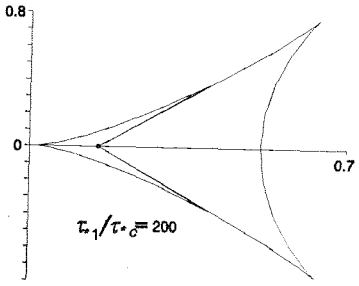

Figure 4.22-j

Erosion of an armoured bed ($D_{m\text{-}mix} = 1.55\ D_{m\text{-}sub}$).

In the second set, a coarse mixing layer at a fine substratum is considered. The size fraction of the fine material in the mixing layer and substratum are 0.25 mm and 0.75 respectively. The mixing-layer thickness is taken 0.01 m.

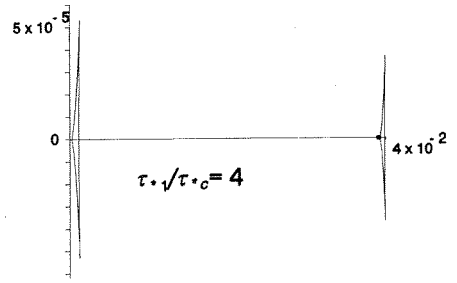

Figure 4.23-a

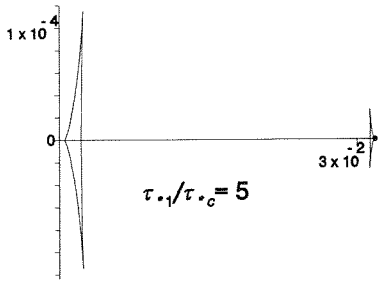

Figure 4.23-b

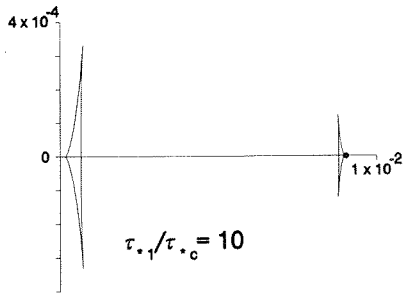

Figure 4.23-c

In the range $4 < \tau_{*1}/\tau_{*c} < 5$, the bicharacteristic ray approaches uX/δ_m, and the wave front changes its shape. Because the mixing layer is chosen sufficiently small, the bicharacteristic surfaces do not intersect in this example and, in contrast with the joining fronts in sedimentation conditions, the two wave fronts remain seperate.

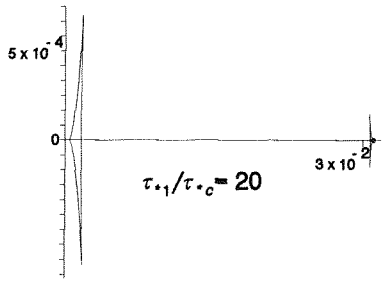

Figure 4.23-d

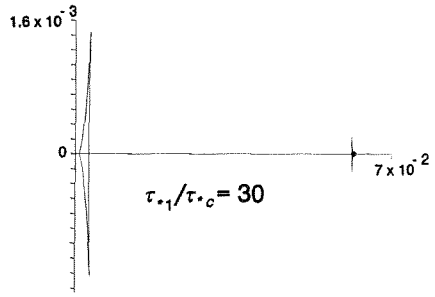

Figure 4.23-e

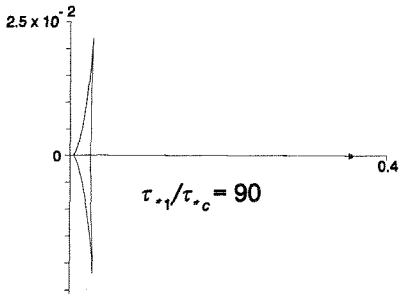

Figure 4.23-f

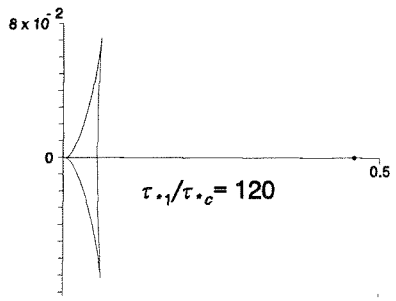

Figure 4.23-g

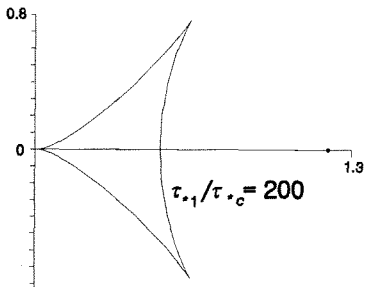

Figure 4.23-h

Due to the orientation of the characteristic surfaces, approximating the bicharacteristic ray in stream direction with Eq.4.8 yields an underestimation in sedimentation conditions and an overestimation in the case of an eroding, armoured bed.

4.4. Family of small ("star"-shaped) characteristic surfaces for the double-layer model.

4.4.1. Analysis of characteristic roots.

Similar to the single-layer model, and expression can be found that approximates the largest front of the wave-shaped bicharacteristics.

$$r = \frac{uX}{\delta_p \delta_s (1+\alpha_1)} \qquad \textbf{4.27}$$

with

$$X = g\,K_{41}\left[\delta_s(1 - \kappa\,\beta_{p1}(1+\alpha_1)) + \delta_p\alpha_1\frac{p_{p1}}{p_{sp1}}\left[(\kappa\beta_{p1}-\beta_{o1})(1+\alpha_1) + \alpha_1\right]\right] +$$

$$+ g\,K_{42}(1+\alpha_1)\left[\delta_s\kappa\beta_{p1} + \delta_p\alpha_2(\beta_{o1} - \kappa\beta_{p1})\frac{1-p_{p1}}{1-p_{sp1}}\right] +$$

$$+ g\,K_{51}\frac{(D_1-D_2)}{D_{ms}}\left[\,\delta_s D_{ms}(1 - \kappa\beta_{p1}(1+\alpha_1)) + \delta_p\alpha_1 D_{mp}\left[(\kappa\beta_{p1}-\beta_{o1})(1+\alpha_1)+\alpha_1\right]\,\right] +$$

$$+ g\,K_{52}\frac{(D_2-D_1)}{D_{ms}}(1+\alpha_1)\left[\,\delta_s D_{ms}\kappa\beta_{p1} + \delta_p\alpha_2 D_{mp}(\beta_{o1} - \kappa\beta_{p1})\,\right]$$

For $\tau_{*m}/\tau_{*c} \to \infty$, this approximation is

$$r = \frac{\left(\delta_s p_{p1} g^2 + \delta_p p_{sp1}(1-g)^2\right)}{g p_{p1}} \frac{s_{b1}}{p_{p1}\delta_p\delta_s(1+\alpha_1)} \qquad \textbf{4.28}$$

Again with Eqs 4.2, 4.4 and 4.27, the remaining characteristic root can be approximated

$$r = \frac{u\left(g_z(Z + aY) + u^2 Y\right)}{X\left[u^2 + g_z(a + g(1+\alpha_1)K_{31} + g(1+\alpha_2)K_{32})\right]} \qquad \textbf{4.29}$$

with Z and Y described in Appendix C.2.

For $\tau_{*m}/\tau_{*c} \to \infty$, Eq.4.29 approaches

$$r \approx \frac{n\,s_{b1}}{a\,p_{p1}} \frac{1}{1 - Fr^2 + \dfrac{s_{b1}}{p_{p1}ua}} \qquad \textbf{4.30}$$

which corresponds with the characteristics for uniform material.

4.4.2. Sensitivity of characteristics to layer thickness and sediment flux.

Similar to the single-layer model (Figure 4.13), the fronts of the star-shaped characteristics in stream-direction in case of sedimentation and erosion of armoured beds can be shown at varying shear stresses for different layer thicknesses. The effect of g on the bicharacteristic rays in the direction of flow is represented in the Figure 4.24.

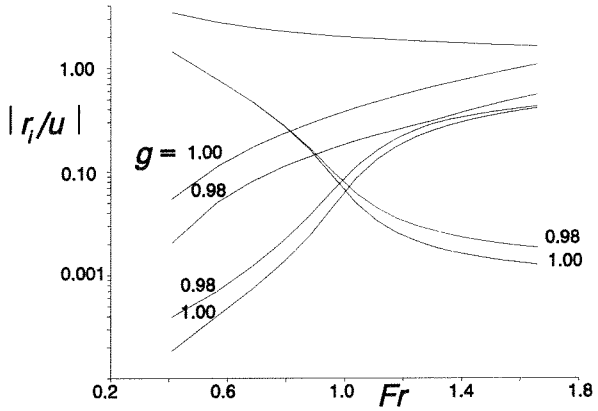

Figure 4.24

From Figure 4.24 it can be concluded that in contrast with the single-layer model where only one characteristic is clearly affected by the layer-parameters in the model, contributions by the subpavement layer *directly* affect the transport rate and subsequently the morphological behaviour (see also section 2.3.3.).

To illustrate this conclusion, the relative differences in characteristics for $g = 1.00$ (subscript 1) and $g = 0.90$ (subscript 2) are presented in Figure 4.25.

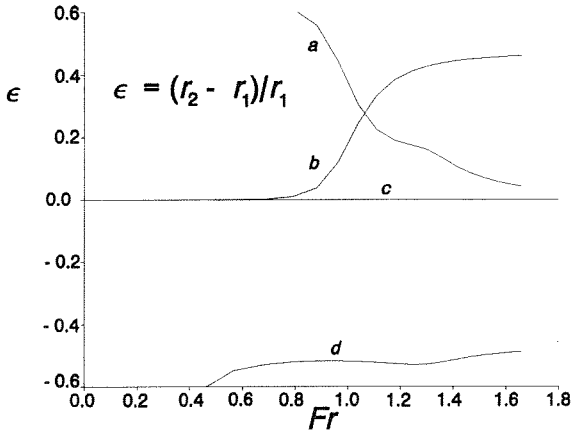

Figure 4.25

This figure clearly shows that the effect of the subpavement on morphology is present in subcritical flow (line *a*) and supercritical flow (line *b*). Also at low shear-stresses near at the initiation of motion, the effect of fine material contributed by the subpavement can be significant.

In supercritical flows, the magnitude of the negative characteristic that can be related to the propagation of changes in bed level, is increased with increasing exposure of the fine subpavement.

Consequently, the selection of the relative exposure coefficient g and the layer thickness significantly affect the behaviour of composition as well as level of the river bed in the model.

4.4.3. Mathematical character of the double-layer model.

In Figure 4.26, the maximum value of the pavement layer δ_p is presented. The sediment diameters are D_1 = 1 mm and D_2 = 2 mm, and p_{p1} = 0.30 for the pavement, p_{sp1} = 0.60 for the subpavement and β_{o1} = 0.90 for the substratum. The effect of exposure of the subpavement is investigated by taking different values of g.

The broken line in Figure 4.26 represents the maximum layer-thickness of the single-layer model with equivalent conditions.

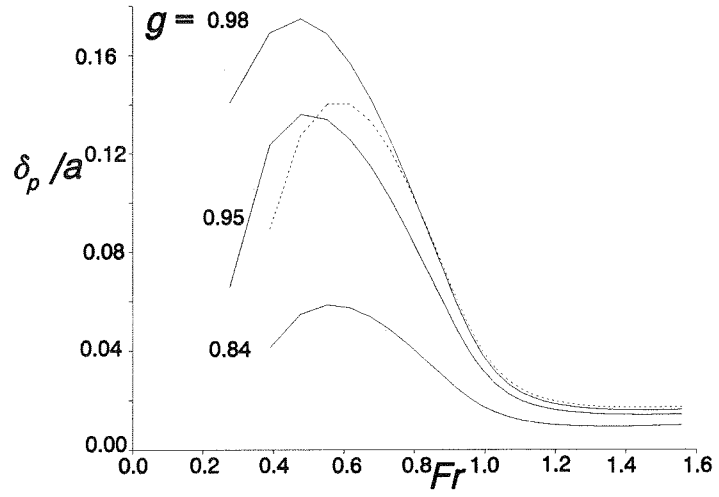

Figure 4.26

Consequently, for small contributions of the fine subpavement layer and at low values of Fr, the range of hyperbolicity of the mathemetical model improves by distinction of a transition or subpavement layer between coarse mixing layer and fine substratum. This can also be understood from Figure 4.17.

However, if the contribution of the fine transition layer to the horizontal sediment transport increases, the gain in maximum value of pavement-layer thickness diminishes. As a result, at large values of g and Fr, the double-layer model becomes elliptic more easily than the single-layer model.

With Eqs 4.27 and 4.28, the critical value of δ_p can be approximated for $Fr < 0.8$

$$\frac{\delta_p}{a} \approx \frac{1}{\delta_s(1+\alpha_1)} \frac{g_z X^2}{u\left(g_z(Z + aY) + u^2 Y\right)} \left(\frac{u^2}{g_z a} + 1 + \frac{g(1+\alpha_1)K_{31} + g(1+\alpha_2)K_{32}}{ua} \right) \qquad \textbf{4.31}$$

For $\tau_{*m}/\tau_{*c} \to \infty$, Eq.4.31 approaches

$$\frac{\delta_p}{a} \approx u \frac{\left(\epsilon g^2 p_{p1} + (1-g)^2 p_{sp1}\right)}{n \epsilon \left(g p_{p1} + (1-g) p_{sp1}\right)} \left(1 - Fr^2 + \frac{s_{b1}}{p_{p1} ua} \right) \qquad \textbf{4.32}$$

with $\epsilon = \delta_s/\delta_p$.

For $Fr > 1.2$, the critical value of δ_p can be approximated with Eq.4.4

$$\frac{\delta_p}{a} \approx \frac{1}{\delta_s(1+\alpha_1)} \frac{X}{a\left(1 - \frac{\sqrt{-g_z a}}{u}\sqrt{1 + g(1+\alpha_1)\frac{K_{31}}{a} + g(1+\alpha_2)\frac{K_{32}}{a}}\right)} \qquad \textbf{4.33}$$

For $\tau_{*m}/\tau_{*c} \to \infty$, Eq.3.33 approaches

$$\frac{\delta_p}{a} \approx \frac{s_{b1}}{p_{p1}\, u\, a} \frac{\epsilon\, g^2\, p_{p1} + (1-g)^2\, p_{sp1}}{\epsilon\, g\, (1+\alpha_1)\, p_{p1}} \frac{Fr}{Fr - \sqrt{1 + \frac{s_{b1}}{p_{p1} ua}}} \qquad \textbf{4.34}$$

with $\epsilon = \delta_s/\delta_p$.

Again, it should be noticed that Eqs 4.31 and 3.33 overpredict the critical value of δ_p. In Figure 4.27, the exact critical values of δ_p and the approximations Eqs 4.31 and 4.33 are plotted for different values of g.

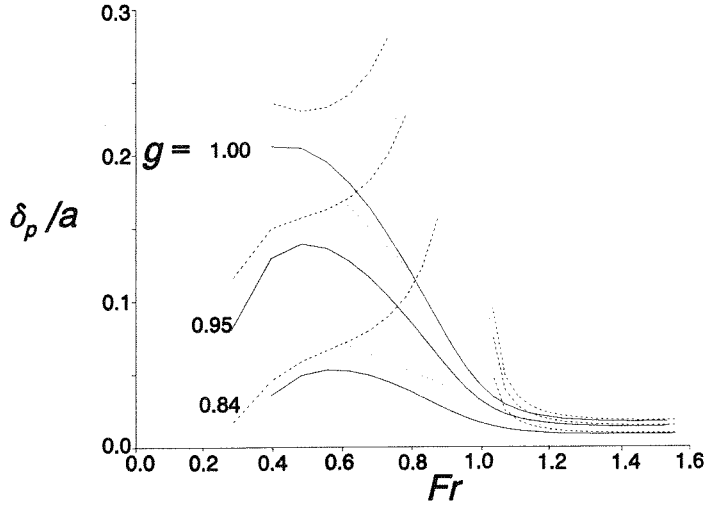

Figure 4.27

Chapter 5

Compatibility equations.

5.1. Introduction.

The characteristic equations of a system of partial-differential equations provide information on the dynamic behaviour of the mathematical model. The bicharacteristic surfaces present the propagation of information through the system, and the compatibility equations, or the gradients along the bicharacteristic rays provide insight in the magnitude of changes.

This can be of use when decoupling of hydraulic and morphological processes is applied; if gradients in different parameters along a bicharacteristic ray are of similar order of magnitude, parameters cannot be decoupled along this bicharacteristic. If parameters can be decoupled, the sign and magnitude of gradients can be analysed.

Secondly, the orientation of gradients in a two-dimensional system predicts differences in one- and two-dimensional models. In this section, the compatibility equations of a two-dimensional model are analysed, whereas the compatibility equations for a one-dimensional, double-layer model are described in Chapter 6.

From a numerical point of view, compatibility equations can be used for the construction of non-reflective boundaries (e.g. Hirsch, 1990).

The derivation procedure is described in the Section 5.2, and subsequently applied to the single-layer model (Section 5.3) and double-layer model (Section 5.7). The compatibility equations for the single-layer model are analysed in Section 5.4. Based on this analysis, the initial behaviour of disturbances in bed level and bed composition are analysed in Section 5.5 and 5.6.

5.2. Mathematical background.

If the system of partial-differential equations is hyperbolic, the three-dimensional basic equations can be combined to a form containing derivatives confined to a two-dimensional space (Hirsch, 1990); the three-dimensional space contructed by the t-, x- and y-axes is confined into a two-dimensional space constructed by τ, a curve parameter along a bicharacteristic ray and s, a parameter perpendicular to the bicharacteristic ray.

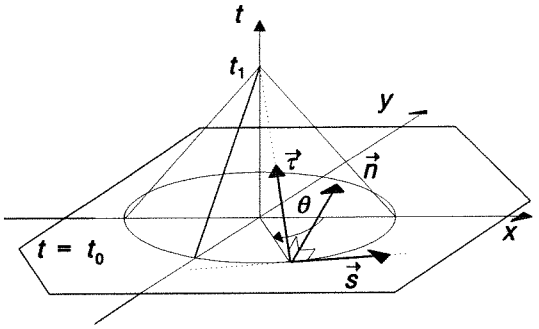

Figure 5.1

To obtain the compatibility equations, a procedure as described by Lin and Shen (1984) can be followed. The system of equations is combined linearly into one equation. Then the gradients in variables are stated to be along the bicharacteristics which yields the coefficients that should be used to summon the original equations.

Now, an equation has been found consisting of a linear combination of gradients in all variables along the characteristic surfaces. To seperate the unknown "time-components" in τ-direction from the known "space-components" components in s-direction (see Figure 5.1), a decomposition is applied.

5.3. Compatibility equations for the single-layer model.

The linear sum of the system of equations is

$$\begin{bmatrix} n_1 \\ un_1 - g_z n_2 \\ vn_1 - g_z n_3 \end{bmatrix}^T \nabla a + \begin{bmatrix} n_2 \\ an_1 + un_2 + K_{11} n_6 + K_{12} n_7 \\ vn_2 + K_{21} n_6 + K_{22} n_7 \end{bmatrix}^T \nabla u +$$

$$+ \begin{bmatrix} n_3 \\ un_3 + K_{21} n_6 + K_{22} n_7 \\ an_1 + vn_3 + K_{31} n_6 + K_{32} n_7 \end{bmatrix}^T \nabla v + \begin{bmatrix} \beta_1 n_6 + (1-\beta_1) n_7 \\ -g_z n_2 \\ -g_z n_3 \end{bmatrix}^T \nabla z_b +$$

$$+ \begin{bmatrix} T_{A1} n_4 + a n_6 \\ L_{x1} n_4 + uan_6 \\ L_{y1} n_4 + van_6 \end{bmatrix}^T \nabla p_{s1} + \begin{bmatrix} T_{A2} n_5 + a n_7 \\ L_{x2} n_5 + uan_7 \\ L_{y2} n_5 + van_7 \end{bmatrix}^T \nabla p_{s2} + \qquad \textbf{5.1}$$

$$+ \begin{bmatrix} \delta_m (n_6 - n_7) \\ u(K_{41} + K_{51}(D_1 - D_2)) n_6 + u(-K_{42} + K_{52}(D_1 - D_2)) n_7 \\ v(K_{41} + K_{51}(D_1 - D_2)) n_6 + v(-K_{42} + K_{52}(D_1 - D_2)) n_7 \end{bmatrix}^T \nabla p_{m1} =$$

$$= \left[g_x - \frac{\tau_{bx}}{\rho a} \right] n_2 + \left[g_y - \frac{\tau_{by}}{\rho a} \right] n_3 + \left[p_{e1} - p_{s1} \right] n_4 + \left[p_{e2} - p_{s2} \right] n_5$$

or

$$\vec{n}_a^T \nabla a + \vec{n}_u^T \nabla u + \vec{n}_v^T \nabla v + \vec{n}_z^T \nabla z_b + \vec{n}_{s1}^T \nabla p_{s1} + \vec{n}_{s2}^T \nabla p_{s2} + \vec{n}_m^T \nabla p_{m1} =$$

$$= \left[g_x - \frac{\tau_{bx}}{\rho a} \right] n_2 + \left[g_y - \frac{\tau_{by}}{\rho a} \right] n_3 + \left[p_{e1} - p_{s1} \right] n_4 + \left[p_{e2} - p_{s2} \right] n_5 \qquad \textbf{5.2}$$

Because the compatibility equation is valid along a characteristic surface, it can be stated for $\xi = a, u, v, z, s1, s2$ and m

$$\vec{n}_\xi{}^T \cdot \begin{pmatrix} n_{ti} \\ n_{xi} \\ n_{yi} \end{pmatrix} = 0 \qquad \textbf{5.3}$$

or

$$\begin{aligned}
&n_{ti}n_1 + n_{xi}(un_1 - g_z n_2) + n_{yi}(vn_1 - g_z n_3) = 0 \\
&n_{ti}n_2 + n_{xi}(an_1 + un_2 + K_{11}n_6 + K_{12}n_7) + n_{yi}(vn_2 + K_{21}n_6 + K_{22}n_7) = 0 \\
&n_{ti}n_3 + n_{xi}(un_3 + K_{21}n_6 + K_{22}n_7) + n_{yi}(an_1 + vn_3 + K_{31}n_6 + K_{32}n_7) = 0 \\
&n_{ti}(\beta_1 n_6 + (1-\beta_1)n_7) - n_{xi}g_z n_2 - n_{yi}g_z n_3 = 0 \\
&n_{ti}(an_6 + T_{A1}n_4) + n_{xi}(uan_6 + L_{x1}n_4) + n_{yi}(van_6 + L_{y1}n_4) = 0 \\
&n_{ti}(an_7 + T_{A2}n_5) + n_{xi}(uan_7 + L_{x2}n_5) + n_{yi}(van_7 + L_{y2}n_5) = 0 \\
&n_{ti}\delta_m(n_6 - n_7) + n_{xi}u\left[n_6\left(K_{41} + (D_1 - D_2)K_{51}\right) + n_7\left(-K_{42} + (D_1 - D_2)K_{52}\right)\right] + \\
&+ n_{yi}v\left[n_6\left(K_{41} + (D_1 - D_2)K_{51}\right) + n_7\left(-K_{42} + (D_1 - D_2)K_{52}\right)\right] = 0
\end{aligned} \qquad \textbf{5.4}$$

Equivalently, the multiplication coefficients can be determined with the matrix in Eq.3.18

$$Q \cdot \begin{bmatrix} n_1 \\ n_2 \\ n_3 \\ n_4 \\ n_5 \\ n_6 \\ n_7 \end{bmatrix} = \vec{0}$$

For all roots of the characteristic determinant ($i = 1,2,..,7$), a set values of n_1 to n_7 can found. These are described in the Appendix D.1.

The next step is to decompose the changes of f into gradients in τ- and s-directions, respectively along and perpendicular to a bicharacteristic ray (Figure 5.1). Therefore, all terms at the left-hand side of Eq.5.2 are written as

$$\vec{n}_\xi = T_\xi \vec{\tau} + S_\xi \vec{s} \rightarrow \vec{n}_\xi^T \nabla f = T_\xi \nabla f \cdot \vec{\tau} + S_\xi \nabla f \cdot \vec{s} \qquad 5.5$$

The components of the vectors $\vec{n}_\xi$ along a bicharacteristic ray are

$$T_\xi = \frac{\begin{pmatrix} 1 \\ c_{xi} \\ c_{yi} \end{pmatrix} \cdot \vec{n}_\xi}{\sqrt{1 + c_{xi}^2 + c_{yi}^2}} \qquad 5.6$$

The components of vectors perpendicular to a bicharacteristic ray are

$$P_\xi = \begin{pmatrix} 0 \\ -\sin\theta \\ \cos\theta \end{pmatrix} \cdot \vec{n}_\xi \qquad 5.7$$

Because gradients in f along s at the original time level $t = t_0$ can be prescribed, changes along the bicharacteristic rays can be calculated with

$$T_{ai}\frac{\partial a}{\partial \tau} + S_{ai}\frac{\partial a}{\partial s} + T_{ui}\frac{\partial u}{\partial \tau} + S_{ui}\frac{\partial u}{\partial s} + T_{vi}\frac{\partial v}{\partial \tau} + S_{vi}\frac{\partial v}{\partial s} + T_{zi}\frac{\partial z_b}{\partial \tau} + S_{zi}\frac{\partial z_b}{\partial s} +$$

$$+ T_{s1i}\frac{\partial p_{s1}}{\partial \tau} + S_{s1i}\frac{\partial p_{s1}}{\partial s} + T_{s2i}\frac{\partial p_{s2}}{\partial \tau} + S_{s2i}\frac{\partial p_{s2}}{\partial s} + T_{mi}\frac{\partial p_{m1}}{\partial \tau} + S_{mi}\frac{\partial p_{m1}}{\partial s} = \qquad 5.8$$

$$= \left(g_x - \frac{\tau_{bx}}{\rho a}\right) n_{2i} + \left(g_y - \frac{\tau_{by}}{\rho a}\right) n_{3i} + (p_{e1} - p_{s1}) n_{4i} + (p_{e2} - p_{s2}) n_{5i}$$

Consequently, the 2-DH compatibility relations for the single-layer model can be written as

$$T\left[\frac{\partial a}{\partial \tau}\ \frac{\partial u}{\partial \tau}\ \frac{\partial v}{\partial \tau}\ \frac{\partial z_b}{\partial \tau}\ \frac{\partial p_{s1}}{\partial \tau}\ \frac{\partial p_{s2}}{\partial \tau}\ \frac{\partial p_{m1}}{\partial \tau}\right]^T +$$

$$+ S\left[\frac{\partial a}{\partial s}\ \frac{\partial u}{\partial s}\ \frac{\partial v}{\partial s}\ \frac{\partial z_b}{\partial s}\ \frac{\partial p_{s1}}{\partial s}\ \frac{\partial p_{s2}}{\partial s}\ \frac{\partial p_{m1}}{\partial s}\right]^T = \qquad 5.9$$

$$= \left(g_x - \frac{\tau_{bx}}{\rho a}\right) K + \left(g_y - \frac{\tau_{by}}{\rho a}\right) L + (p_{e1} - p_{s1})\, M + (p_{e2} - p_{s2}) N$$

where T and S matrices, and K, L and M vectors described in Appendix D.1.

5.4. Analysis of compatibility coefficients.

With some numerical experiments, the magnitude of gradients in hydraulic and morphological parameters along the characteristic surfaces are analysed to provide insight in the two-dimensional behaviour at various conditions.
To enable mutual comparison, the parameters in the compatibility equation Eq.5.2 transformed into

$$a = a_0(1 + a') \;\; ; \;\; u = u_0(1 + u') \;\; ; \;\; z_b = a_0 z_b' \qquad \textbf{5.10}$$

$$p_{si} = p_{si\,0}(1 + p_{si}') \;\; ; \;\; p_{m1} = p_{m1\,0}(1 + p_{m1}')$$

The transformed compatibility equation is

$$\vec{n}_a^{\,T} a_0 \nabla a' + \vec{n}_u^{\,T} u_0 \nabla u' + \vec{n}_v^{\,T} v_0 \nabla v' + \vec{n}_z^{\,T} a_0 \nabla z_b' +$$

$$+ \vec{n}_{s1}^{\,T} p_{s1\,0} \nabla p_{s1}' + \vec{n}_{s2}^{\,T} p_{s2\,0} \nabla p_{s2}' + \vec{n}_m^{\,T} p_{m1\,0} \nabla p_{m1}' = \qquad \textbf{5.11}$$

$$= \left[g_x - \frac{\tau_{bx}}{\rho a} \right] n_2 + \left[g_y - \frac{\tau_{by}}{\rho a} \right] n_3 + \left[p_{e1} - p_{s1} \right] n_4 + \left[p_{e2} - p_{s2} \right] n_5$$

After decomposition of all terms in τ- and s-direction, for all bicharacteristic surfaces, the coefficients of gradients in τ-direction (T_ξ) are analysed at $0.25 \leq Fr \leq 1.50$, in every direction θ. In the following analysis, a = 1.00 m, δ_m = 0.016 m, D_1 = 0.0004 m, D_2 = 0.001 m and $p_{m1} = \beta_{o2}$ = 0.2. Consequently, a thin, coarse mixing layer at a fine substratum in erosion conditions.

The coefficients T_ξ are presented for varying values of θ and increasing values of Fr. $\theta = 0$, represents gradients in downstream direction s, $\theta = \pi/2$ is perpendicular to the flow (n- direction) and $\theta = \pi$ is directed upstream (see Figure 5.2).

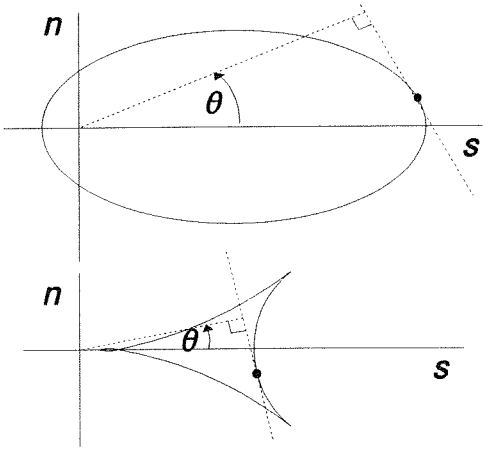

Figure 5.2

As can be understood, $0 \leq \theta/\pi \leq 1$ for the family of large characteristic surfaces ("balloon-shaped"), and $0 \leq \theta/\pi \leq 1/2$ for the families of small characteristic surfaces ("star-shaped").

The corresponding characteristic surfaces are

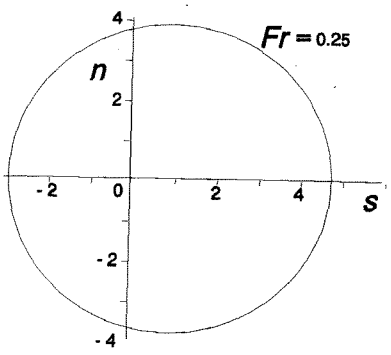

Figure 5.3-a

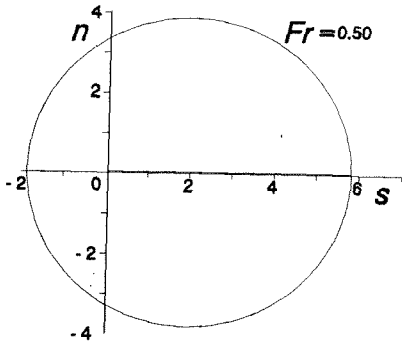

Figure 5.3-b

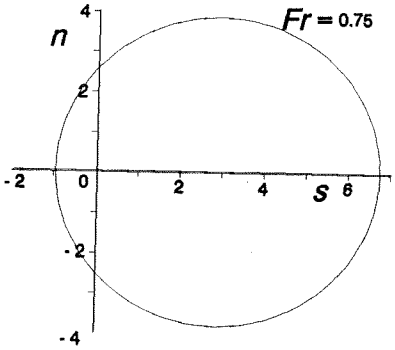

Figure 5.3-c

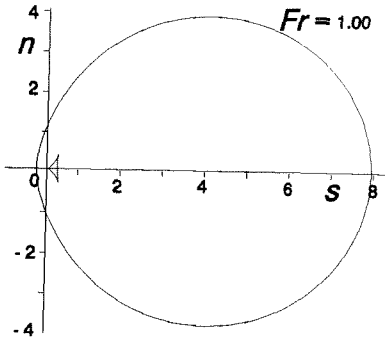

Figure 5.3-d

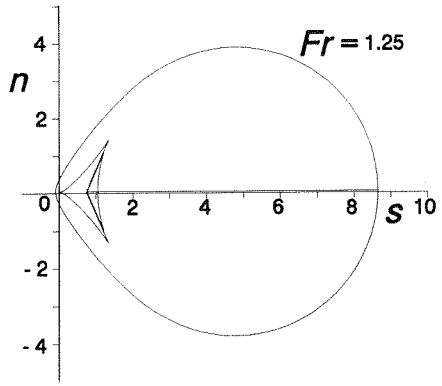

Figure 5.3-e

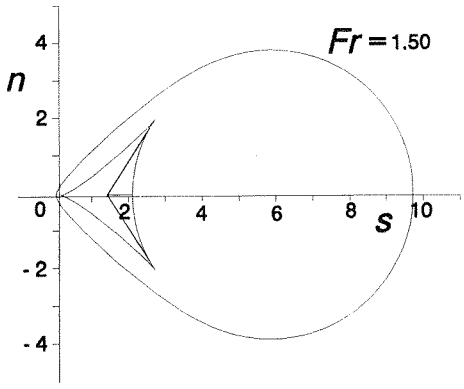

Figure 5.3-f

The coefficients of gradients in parameters along the family of large ("balloon-shaped") characteristic surfaces are

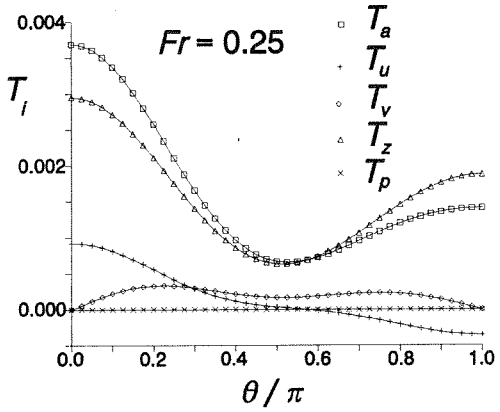

Figure 5.4-a

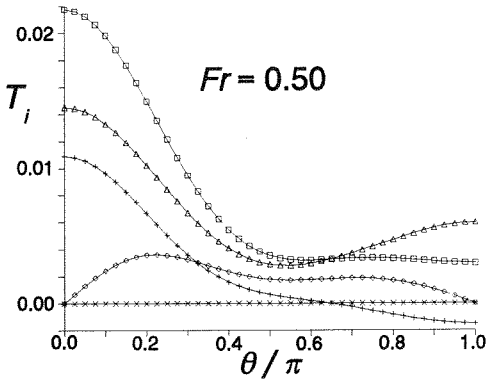

Figure 5.4-b

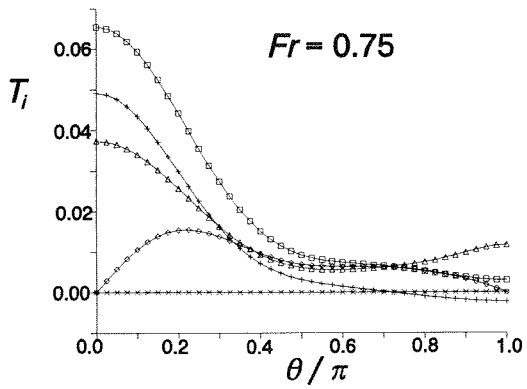

Figure 5.4-c

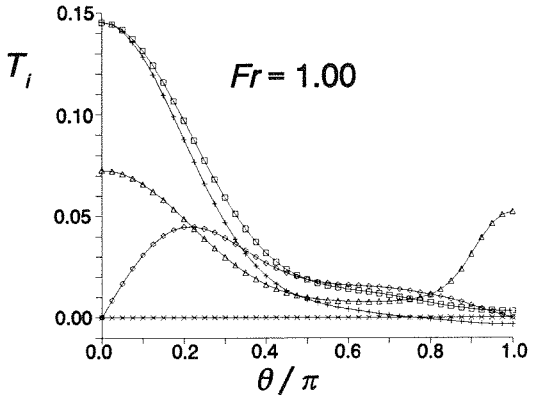

Figure 5.4-d

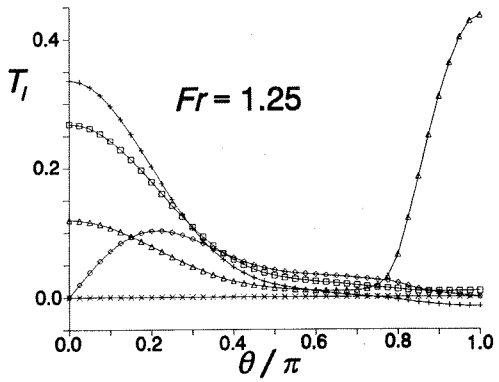

Figure 5.4-e

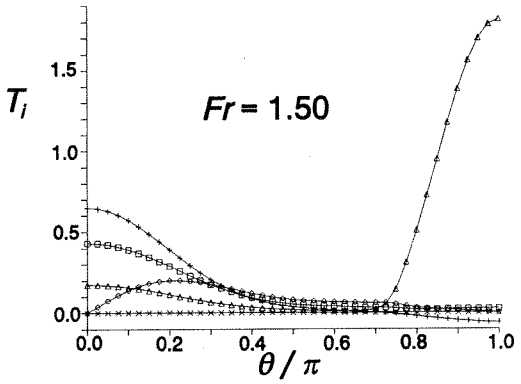

Figure 5.4-f

As can be understood, along this family of characteristic surfaces, the gradients in up- and downstream direction are more significant than gradients perpendicular to the flow. At low *Froude* numbers, the magnitudes of gradients in u and a in up- and downstream direction are are of similar order, whereas at increasing Fr, the downstream-orientated gradients. In supercritical flow, up-stream directed-gradients in u and a can be neglected relative to the gradients in bed level z_b.

Gradients in composition are relatively small along this bicharacteristic surface.

The coefficients of gradients along the family of small bicharacteristics (slow-travelling, "star-shaped" curve) are

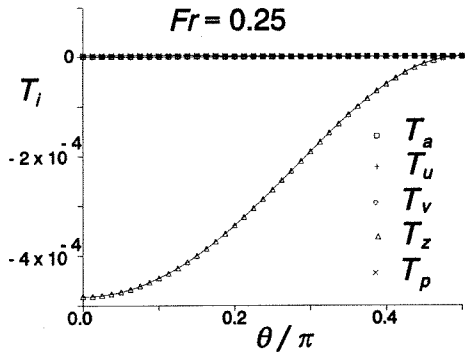

Figure 5.5-a

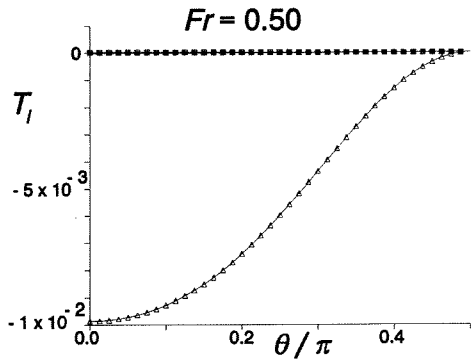

Figure 5.5-b

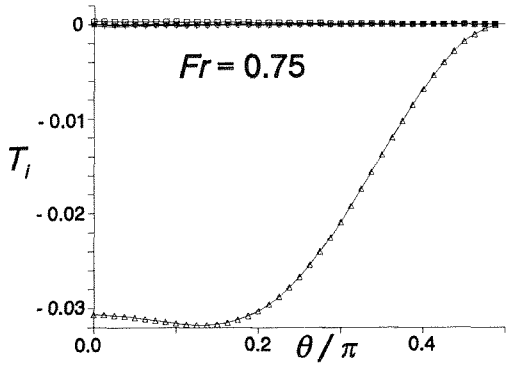

Figure 5.5-c

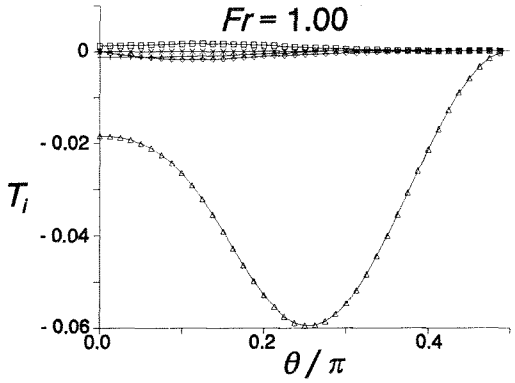

Figure 5.5-d

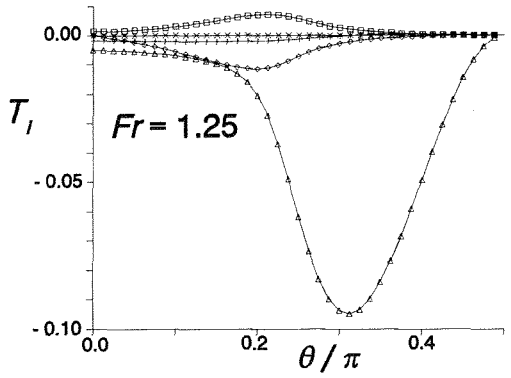

Figure 5.5-e

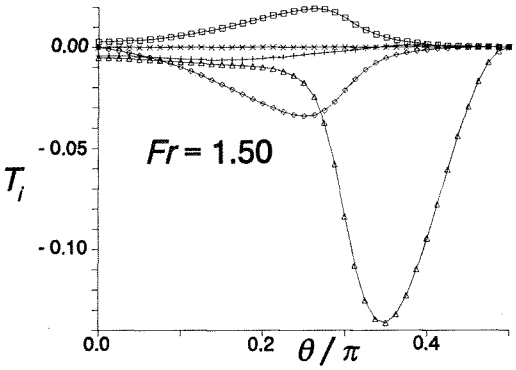

Figure 5.5-f

Along this characteristic surface at low *Froude* numbers, gradients in bed level and composition are significant.

At increasing *Fr*, gradients perpendicular to the flow increase relative to the gradients in up- and downstream direction. Consequently, under these conditions, the dynamic morphological behaviour in two-dimensional models will become different from that in from one-dimensional models, or, the effect of boundary conditions at the banks on the solution becomes more pronounced.

In stream direction, the magnitude of all gradients are of similar order, which indicates the coupled behaviour of flow and morphology.

At the tail of the star-shaped wave front ($\theta = \pi/2$), all coefficients are zero, which implies that gradients in parameters along this particular bicharacteristic ray cannot be determined with this compatibility equation. Parameters donot necessarily remain constant along this bicharacteristic ray.

The coefficients of gradients along the family of small bicharacteristics (fast-travelling, "star-shaped" curve) are

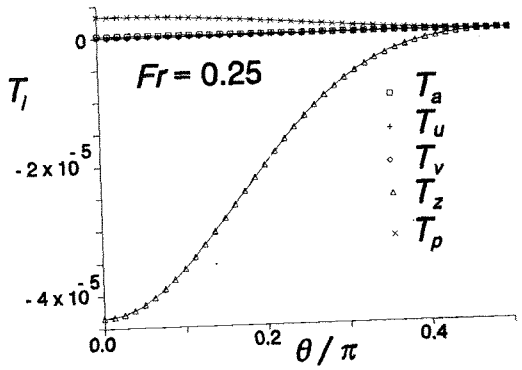

Figure 5.6-a

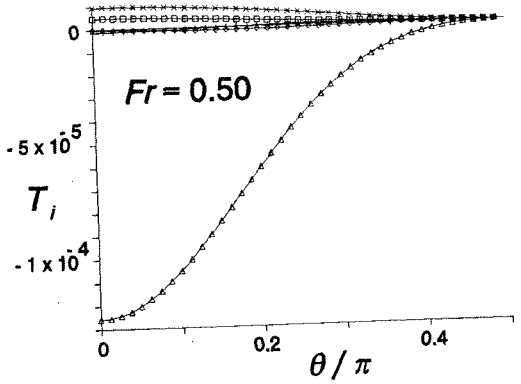

Figure 5.6-b

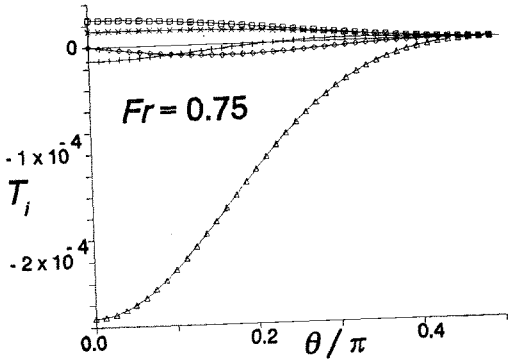

Figure 5.6-c

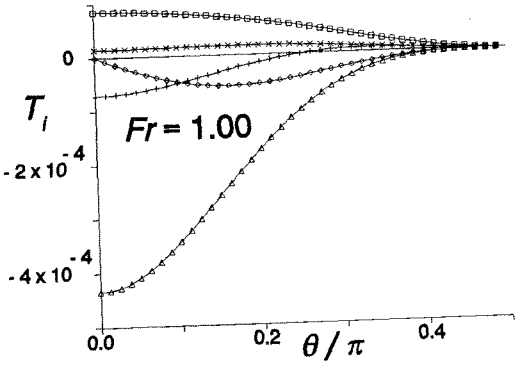

Figure 5.6-d

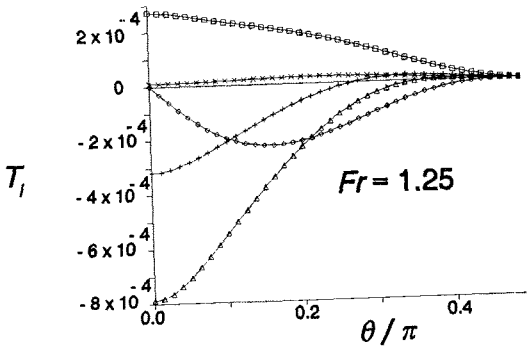

Figure 5.6-e

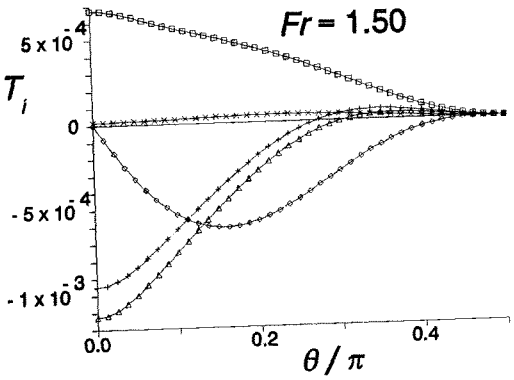

Figure 5.6-f

At increasing, subcritical *Froude* numbers, the gradients in bed level and composition are dominating along this characteristic surface. At supercritical flows, however, gradients in a, z_b and u are relevant again. Consequently, in general, changes in bed level and composition are coupled.

5.5. Initial behaviour of bed-level disturbances.

The numerical experiments as described above enable a rather simple analys f the gradients. In subcritical flows, downstream-directed gradients in bed level dominate along the slow-travelling, "star-shaped" wave front (Fig.3.7-a,b and c). In supercritical flows, gradients in bed level dominate at the upstream-directed part of the "balloon-shaped" wave front (Fig.3.6-d,e,f). Consequently, along those bicharacteristic rays, changes in bed level can be decoupled from gradients in other parameters. The corresponding compatibility equation can be written as

$$\frac{\partial z_b}{\partial \tau} = \left(g_x - \frac{\tau_{bx}}{\rho a}\right)\frac{n_2}{T_z} + (p_{e1} - p_{s1})\frac{n_4}{T_z} + (p_{e2} - p_{s2})\frac{n_5}{T_z} \qquad \textbf{5.12}$$

It can be concluded that two effects affect the initial growth or decline of bed-level disturbances along the corresponding bicharacteristic rays;

- slope effects and friction
- relaxation effects in the suspended material

5.5.1. Slope and friction effects.

For $\tau_{*m} >> \tau_{*c}$, the coefficient n_2 can be written as

$$\begin{aligned} n_2 &= P_1 P_2 R^2 (S_2 K_{11} - S_1 K_{12}) = \\ &= -P_1 P_2 (n_t + u)^2 \left(\delta_m n_t (n_1 s_{b1} + n_2 s_{b2}) + s_{b1} s_{b2}\left(\frac{n_1}{1-p_{m1}} + \frac{n_2}{p_{m1}}\right)\right) \end{aligned} \qquad \textbf{5.13}$$

In supercritical flows $n_t > 0$ and consequently $n_2 < 0$. In subcritical flows, Eq.4.17 can be substituted for $-n_t$, and n_2 also appears to be negative. The coefficient T_z can be written as

$$T_z = P_1 P_2 \frac{R}{\sqrt{1+n_t^2}} \left[(R^2 + g_z a)((1-\beta_1)S_1 - \beta_1 S_2) + g_z R n_t (S_2 K_{11} - S_1 K_{12})\right] \qquad \textbf{5.14}$$

which appears to be negative for subcritical and positive for supercritical flows. The ratio n_2/T_z is positive for subcritical and negative for supercritical flow.

If any inertia effects can be neglected, the flow is decelerating if $g_x < \tau_b/\rho a$, and the flow is accelerating if $g_x > \tau_b/\rho a$. Consequently, in subcritical flows, the height of bed forms (dunes) increase at accelerating flow and decrease at decelerating flow. In

supercritical flows, the opposite can be observed, bed forms (anti-dunes) develop in decelerating flow and diminish at accelerating flows.

If slope-effects are neglected, friction induces a development of bed-form heights in supercritical and a decline of bed-form heights at subcritical flow.

5.5.2. Relaxation effects.

These effects are due to the time- and length-scale of the adjustment of vertical concentration-profiles of suspended sediment, to local changes in conditions. As a result, these effects dominate if suspended load is large relative to bed load.

The coefficients n_4 and n_5 can be written as

$$n_4 = aR^2S_2P_2\left(g_z a + R^2\right) \quad ; \quad n_5 = - aR^2S_1P_1\left(g_z a + R^2\right) \qquad \textbf{5.15}$$

which appear to be negative at both sub- and supercritical flows. As a result, the ratios n_4/T_z and n_5/T_z are positive for subcritical and negative for supercritical flows.

If $p_{ei} > p_{si}$, the capacity is larger than the actual load and sediment is picked up from the bed, whereas if $p_{ei} < p_{si}$, the capacity is smaller than the actual load and sediment is deposited on the bed. Consequently, in subcritical flows, a sudden increase in sediment-transport capacity enlarges the height of bed forms, whereas a sudden decrease in sediment-transport capacity reduces the bed-form height.

In supercritical flows, again the opposite can be observed; a sudden decrease in sediment-transport capacity enlarges the height of bed forms, whereas a sudden increase of sediment-transport capacity reduces the bed-form height. This effect has been found by Sloff (1993) also, when carrying out numerical experiments on supercritical flows.

5.6. Initial behaviour of bed composition.

For low *Froude* numbers, ($Fr < 0.6$), the gradients in bed level and composition along the fast-travelling, "star-shaped" wave front are an order of magnitude larger than the gradients in flow variables (Figure 5.6-a,b).

The corresponding compatibility equation can be written as

$$T_z \frac{\partial z_b}{\partial \tau} + T_m \frac{\partial p_{m1}}{\partial \tau} = \left[p_{e1} - p_{s1}\right] n_4 + \left[p_{e2} - p_{s2}\right] n_5 \qquad \textbf{5.16}$$

or

$$\frac{\partial p_{m1}}{\partial \tau} = \frac{T_z}{T_m}\left(- \frac{\partial z_b}{\partial \tau} + \left[p_{e1} - p_{s1}\right] \frac{n_4}{T_z} + \left[p_{e2} - p_{s2}\right] \frac{n_5}{T_z}\right) \qquad \textbf{5.17}$$

The coefficient T_m can be written as

$$T_m = - R P_1 P_2 (R^2+g_z a) u \left[K_{41} - K_{42} + (K_{51}+K_{52})(D_1-D_2)\right] \delta_m \sqrt{1+r^2} \quad \textbf{5.18}$$

which is positive for the restriction $Fr < 0.6$. As a result, the ratio T_z/T_m is negative and Eq.5.17 can be written as

$$\frac{\partial p_{m1}}{\partial \tau} = \left|\frac{T_z}{T_m}\right| \left(\frac{\partial z_b}{\partial \tau} - \left[p_{e1}-p_{s1}\right] \frac{n_4}{T_z} - \left[p_{e2}-p_{s2}\right] \frac{n_5}{T_z} \right) \quad \textbf{5.19}$$

At accelerating flows, the fraction of fine material in the mixing layer increases (destruction of armour layer) due to a positive gradient in z_b. At decelerating flows, the mixing layer coarsens (armouring) due to negative gradients in z_b.

Because n_4/T_z and n_5/T_z are positive for subcritical flows, the relaxation of suspended sediment dampens the responses described.

5.7. Compatibility equations for the double-layer model.

The compatibility equations is for different families of characteristic surfaces

$$\vec{n}_a^T \nabla a + \vec{n}_u^T \nabla u + \vec{n}_v^T \nabla v + \vec{n}_z^T \nabla z_b + \vec{n}_{s1}^T \nabla p_{s1} + \vec{n}_{s2}^T \nabla p_{s2} +$$

$$+ \vec{n}_p^T \nabla p_{p1} + \vec{n}_{sp1} \nabla p_{sp1} = \quad \textbf{5.20}$$

$$= \left[g_x - \frac{\tau_{bx}}{\rho a}\right] n_2 + \left[g_y - \frac{\tau_{by}}{\rho a}\right] n_3 + \left[p_{e1}-p_{s1}\right] n_4 + \left[p_{e2}-p_{s2}\right] n_5$$

with

$$\vec{n}_a = \begin{bmatrix} n_1 \\ un_1 - g_z n_2 \\ vn_1 - g_z n_3 \end{bmatrix}^T \quad ; \quad \vec{n}_u = \begin{bmatrix} n_2 \\ an_1 + un_2 + g(1+\alpha_1)K_{11}n_6 + g(1+\alpha_2)K_{12}n_7 \\ vn_2 + g(1+\alpha_1)K_{21}n_6 + g(1+\alpha_2)K_{22}n_7 \end{bmatrix}^T$$

$$\vec{n}_v = \begin{bmatrix} n_3 \\ un_3 + g(1+\alpha_1)K_{21}n_6 + g(1+\alpha_2)K_{22}n_7 \\ an_1 + vn_3 + g(1+\alpha_1)K_{31}n_6 + g(1+\alpha_2)K_{32}n_7 \end{bmatrix}^T$$

$$\vec{n}_z = \begin{bmatrix} \beta_{p1}n_6 + (1-\beta_{p1})n_7 + (\beta_{o1} - \kappa\beta_{p1}(1+\alpha_1))n_8 \\ -g_z n_2 \\ -g_z n_3 \end{bmatrix}^T \quad ; \quad \vec{n}_{s1} = \begin{bmatrix} T_{A1}n_4 + an_6 \\ L_{x1}n_4 + uan_6 \\ L_{y1}n_4 + van_6 \end{bmatrix}^T$$

$$\vec{n}_{s2} \begin{bmatrix} T_{A2}n_5 + an_7 \\ L_{x2}n_5 + uan_7 \\ L_{y2}n_5 + van_7 \end{bmatrix}^T \quad ; \quad \vec{n}_{p1} = \begin{bmatrix} \delta_p(n_6 - n_7 - \alpha_1 n_8) \\ gu(K_{41} + K_{51}(D_1 - D_2))n_6 + gu(-K_{42} + K_{52}(D_1 - D_2))n_7 \\ gv(K_{41} + K_{51}(D_1 - D_2))n_6 + gv(-K_{42} + K_{52}(D_1 - D_2))n_7 \end{bmatrix}^T$$

$$\vec{n}_{sp1} = \begin{bmatrix} \delta_s(n_6 - n_7 + n_8) \\ g\alpha_1 u\left(K_{41}\frac{p_{p1}}{p_{sp1}} + K_{51}\frac{D_{mp}}{D_{ms}}(D_1 - D_2)\right)n_6 + g\alpha_2 u\left(-K_{42}\frac{1-p_{p1}}{1-p_{sp1}} + K_{52}\frac{D_{mp}}{D_{ms}}(D_1 - D_2)\right)n_7 \\ g\alpha_1 v\left(K_{41}\frac{p_{p1}}{p_{sp1}} + K_{51}\frac{D_{mp}}{D_{ms}}(D_1 - D_2)\right)n_6 + g\alpha_2 v\left(-K_{42}\frac{1-p_{p1}}{1-p_{sp1}} + K_{52}\frac{D_{mp}}{D_{ms}}(D_1 - D_2)\right)n_7 \end{bmatrix}$$

5.21

For all roots of the characteristic determinant (i = 1,2,..,7), a set values of n_1 to n_8 can be found. These are described in Appendix D.2.

Chapter 6

One-dimensional models.

6.1. Introduction.

In this chapter, the characteristic equations for the one-dimensional model are derived. In the first part, boundary conditions are described and the width-integrated system of partial-differential equations is described. Although banks are considered to be fixed, lateral sediment exchange of suspended load as well as bed load is included. Also lateral flow in or out the river is included. Directions of shear stresses and transversal exchange of flow and sediment are as represented in Figure 6.1.

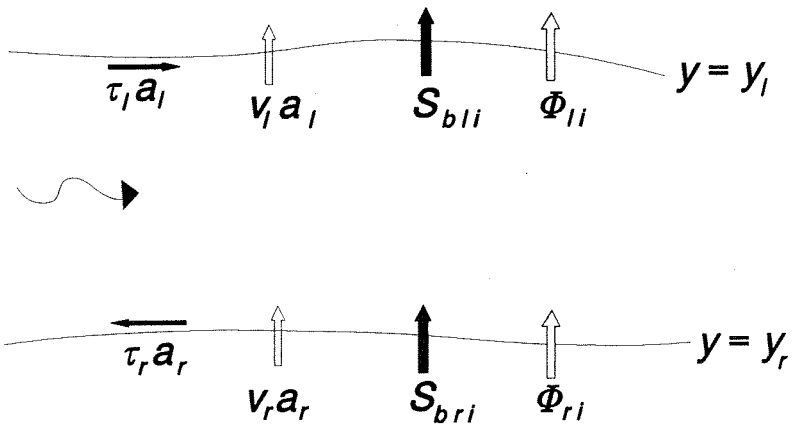

Figure 6.1

If the mass and momentum balances of flow and the sediment mass balances are integrated over the width, effects of two-dimensional phenomena are eliminated from the solution of the mathematical model that is obtained. In non-uniform mountain rivers, however, these phenomena can well be present. In the Sections 4.2 and 5.3, the significance of transversal changes in supercritical flows has already been described.

In the second part of this chapter (Sections 6.5 and 6.6), a brief analysis is given on the effects of parameters that are distributed non-uniformly over the width. Correction coefficients are derived and substituted in the system of equations. The effect of non-uniform width-distributions on the model is demonstrated with a simple model for uniform sediment.

6.2. Boundary conditions.

At the banks, the following boundaries conditions for the mass can be formulated, at the left bank $y = y_l$

$$\rho a\frac{\partial y_l}{\partial t} + \rho ua\frac{\partial y_l}{\partial x} - \rho(v-v_l)a = 0 \qquad \textbf{6.1}$$

and at the right bank $y = y_r$

$$-\rho a\frac{\partial y_r}{\partial t} - \rho ua\frac{\partial y_r}{\partial x} + \rho(v-v_r)a = 0 \qquad \textbf{6.2}$$

where v_l and v_r are exchange of mass at the banks .

The shear stresses at the left and right bank can be described as

$$\begin{bmatrix}\tau_{lx}\\ \tau_{ly}\end{bmatrix} = \tau_l\begin{bmatrix}\cos\theta_l\\ \sin\theta_l\end{bmatrix} \;;\; \begin{bmatrix}\tau_{rx}\\ \tau_{ry}\end{bmatrix} = \tau_r\begin{bmatrix}\cos\theta_r\\ \sin\theta_r\end{bmatrix} \qquad \textbf{6.3}$$

with

$$\cos\theta_l = \frac{1}{\sqrt{\left(\frac{\partial y_l}{\partial x}\right)^2 + 1}} \;;\; \sin\theta_l = \frac{1}{\sqrt{\left(\frac{\partial y_l}{\partial x}\right)^2 + 1}}\frac{\partial y_l}{\partial x} \qquad \textbf{6.4}$$

The boundary condition for x-directed momentum at the left bank is

$$\rho ua\frac{\partial y_l}{\partial t} + \rho u^2 a\frac{\partial y_l}{\partial x} - \rho uva_{y=y_l} +$$

$$-\frac{\rho g_z}{2}a^2\frac{\partial y_l}{\partial x} - \tau_l a\cos\theta_l + \rho uv_l a - p_l a\frac{\partial y_l}{\partial x} = 0 \qquad \textbf{6.5}$$

and at the right bank

$$-\rho ua\frac{\partial y_r}{\partial t} - \rho u^2 a\frac{\partial y_r}{\partial x} + \rho uva_{y=y_r} +$$

$$+\frac{\rho g_z}{2}a^2\frac{\partial y_r}{\partial x} + \tau_r a\cos\theta_r - \rho uv_r a + p_r a\frac{\partial y_r}{\partial x} = 0 \qquad \textbf{6.6}$$

The boundary condition for y-directed momentum at the right bank is

$$\rho va\frac{\partial y_l}{\partial t} + \rho uva\frac{\partial y_l}{\partial x} - \rho v^2 a_{y=y_l} +$$

$$+\frac{\rho g_z}{2}a^2 - \tau_l a\sin\theta_l + \rho v_l^2 a + p_l a = 0 \qquad \textbf{6.7}$$

and at the bank at the right-hand side

$$-\rho va\frac{\partial y_r}{\partial t} - \rho uva\frac{\partial y_r}{\partial x} + \rho v^2 a_{y=y_r} +$$

$$-\frac{\rho g_z}{2}a^2 + \tau_r a\sin\theta_r - \rho v_r^2 a - p_r a = 0 \qquad \textbf{6.8}$$

where p_l and p_r the pressure acting on the left and right bank respectively.

Regarding the mass balance of suspended load, it can be stated at the banks

$$\int_{z_b+\delta_b}^{z_s} p_{si}\mathrm{d}z\frac{\partial y_l}{\partial t} + \int_{z_b+\delta_b}^{z_s} up_{si}\mathrm{d}z\frac{\partial y_l}{\partial x} - \int_{z_b+\delta_b}^{z_s} vp_{si}\mathrm{d}z|_{y=y_l} + \Phi_{li} = 0$$

$$-\int_{z_b+\delta_b}^{z_s} p_{si}\mathrm{d}z\frac{\partial y_r}{\partial t} - \int_{z_b+\delta_b}^{z_s} up_{si}\mathrm{d}z\frac{\partial y_r}{\partial x} + \int_{z_b+\delta_b}^{z_s} vp_{si}\mathrm{d}z|_{y=y_r} - \Phi_{ri} = 0 \qquad \textbf{6.9}$$

where Φ_{li} and Φ_{ri} exchange of suspended sediment at the left and right bank respectively.

And, finally, the mass balance of bed load at the banks is

$$c_{bi}\delta_b\frac{\partial y_l}{\partial t} + g(1+\alpha_i)s_{bxi}\frac{\partial y_l}{\partial x} - g(1+\alpha_i)s_{byi}|_{y=y_l} + S_{bli} = 0$$

$$-c_{bi}\delta_b\frac{\partial y_r}{\partial t} - g(1+\alpha_i)s_{bxi}\frac{\partial y_r}{\partial x} + g(1+\alpha_i)s_{byi}|_{y=y_r} - S_{bri} = 0 \qquad \textbf{6.10}$$

with S_{bli} and S_{bri} the bed-load exchange at the left and right bank.

6.3. Width-integrated system of equations.

In the following, the transversal velocity component v is taken zero, gravity-component effects in y-direction are neglected and width-variations are taken small. The resulting system of partial-differential equations for the double layer model is written in non-conservative form. The mass balance is

$$a\frac{\partial B}{\partial t} + B\frac{\partial a}{\partial t} + ua\frac{\partial B}{\partial x} + uB\frac{\partial a}{\partial x} + aB\frac{\partial u}{\partial x} + va\Big|_{y_r}^{y_l} = 0 \qquad \textbf{6.11}$$

and the momentum balance is

$$Ba\frac{\partial u}{\partial t} + uaB\frac{\partial u}{\partial x} - g_x aB - g_z Ba\frac{\partial (a+z_b)}{\partial x} +$$
$$+ \frac{\overline{\tau_{bx}}}{\rho}B + uva\Big|_{y_r}^{y_l} - u\left(va\Big|_{y_r}^{y_l}\right) - \tau a\Big|_{y_r}^{y_l} = 0 \qquad \textbf{6.12}$$

The approximate solution of the depth- and width-integrated balance of suspended sediment can be written as

$$T_{Ai}\frac{\partial c_i}{\partial t} + L_{xi}\frac{\partial c_i}{\partial x} + (c_i - c_{ei}) = 0 \qquad \textbf{6.13}$$

where the relaxation coefficients should be determined with the boundary conditions at the bed and at the banks.

The mass balance for the bedload can be written as

$$g(1+\alpha_i)f_{iu}\frac{\partial u}{\partial x} + g\alpha_i f_{ip}\frac{\partial p_{pi}}{\partial x} + g\alpha_i f_{iD}\sum_{j=1}^{N} D_j\frac{\partial p_{pj}}{\partial x} +$$
$$+ g\alpha_i f_{ip}\frac{p_{pi}}{p_{spi}}\frac{\partial p_{spi}}{\partial x} + g\alpha_i f_{iD}\frac{D_{mp}}{D_{ms}}\sum_{j=1}^{N} D_j\frac{\partial p_{spj}}{\partial x} +$$
$$+ a\frac{\partial p_{si}}{\partial t} + ua\frac{\partial p_{si}}{\partial x} + \frac{\Phi_{li} - \Phi_{ri}}{B} + \delta_p\frac{\partial p_{pi}}{\partial t} + \delta_s\frac{\partial p_{spi}}{\partial t} + \qquad \textbf{6.14}$$
$$+ \beta_{oi}\frac{\partial z_b}{\partial t} + \frac{S_{bli} - S_{bri}}{B} + g(1+\alpha_i)\frac{s_{bxi}}{B}\frac{\partial B}{\partial x} = 0$$

and additionally

$$-\alpha_i\frac{\partial p_{pi}\delta_p}{\partial t} + \frac{\partial p_{si}\delta_s}{\partial t} + (\beta_{oi} - (1+\alpha_i)\ \kappa\ \beta_{pi})\frac{\partial z_b}{\partial t} = 0 \qquad \textbf{6.15}$$

Including changes in width implies the introduction of sediment-mass balances for the banks and formulae describing lateral exchange of bed load and supended load, analogeously to the mass balances of pavement and subpavement layers at the river bed. However, although transversal exchange of sediment is included, banks are considered to be fixed in the following.

6.4. Characteristic equations.

6.4.1. Characteristic condition.

The total derivative of a parameter is defined as

$$\frac{\mathrm{D}..}{\mathrm{D}t} = n_t \frac{\partial..}{\partial t} + \frac{\partial..}{\partial x} \qquad \textbf{6.16}$$

in analogy with Eq.3.8.
Analogeously to the system of two-dimensional equations, the total system can be written after multiplication with the characteristic normal vector $\vec{n}^T \vec{n}$.

$$Q \cdot \begin{bmatrix} \mathrm{D}a/\mathrm{D}t \\ \mathrm{D}u/\mathrm{D}t \\ \mathrm{D}z_b/\mathrm{D}t \\ \mathrm{D}p_{s1}/\mathrm{D}t \\ \mathrm{D}p_{s2}/\mathrm{D}t \\ \mathrm{D}p_{p1}/\mathrm{D}t \\ \mathrm{D}p_{sp1}/\mathrm{D}t \end{bmatrix} = \vec{n}^T \cdot \vec{n} \begin{bmatrix} -va\Big|_{y_r}^{y_l} - ua\dfrac{\mathrm{d}B}{\mathrm{d}x} \\ g_x aB - \overline{\tau_{bx}}B/\rho + u\left(va\Big|_{y_r}^{y_l}\right) - uva\Big|_{y_r}^{y_l} + \dfrac{\tau a}{\rho}\Big|_{y_r}^{y_l} \\ p_{e1} - p_{s1} \\ p_{e2} - p_{s2} \\ -(S_{bl1} - S_{br1})/B - (\Phi_{l1} - \Phi_{r1})/B + p_{s1}\left(va\Big|_{y_r}^{y_l}\right)/B \\ -(S_{bl2} - S_{br2})/B - (\Phi_{l2} - \Phi_{r2})/B + p_{s2}\left(va\Big|_{y_r}^{y_l}\right)/B \\ 0 \end{bmatrix} \qquad \textbf{6.17}$$

with

$$Q = \begin{bmatrix} R & a & 0 & 0 & 0 & 0 & 0 \\ -g_z & R & -g_z & 0 & 0 & 0 & 0 \\ 0 & 0 & 0 & P_1 & 0 & 0 & 0 \\ 0 & 0 & 0 & 0 & P_2 & 0 & 0 \\ 0 & g(1+\alpha_1)f_{1u} & \beta_{o1}n_t & aR & 0 & S_1 & T_1 \\ 0 & g(1+\alpha_2)f_{2u} & (1-\beta_{o1})n_t & 0 & aR & S_2 & T_2 \\ 0 & 0 & (\beta_{o1}-\kappa(1+\alpha_1)\beta_{p1})n_t & 0 & 0 & -\alpha_1\delta_p n_t & \delta_s n_t \end{bmatrix} \qquad \textbf{6.18}$$

where

$$R = n_t + u \quad ; \quad P_i = T_{Ai} n_t + L_{xi}$$

$$S_1 = \delta_p n_t + g(f_{1p} + f_{1D}(D_1 - D_2)) \quad ; \quad S_2 = -\delta_p n_t + g(-f_{2p} + f_{2D}(D_1 - D_2))$$

$$T_1 = \delta_s n_t + g\alpha_1 \left(f_{1p} \frac{p_{p1}}{p_{sp1}} + f_{1D} \frac{D_{mp}}{D_{ms}} (D_1 - D_2) \right) \qquad \textbf{6.19}$$

$$T_2 = -\delta_s n_t + g\alpha_2 \left(-f_{2p} \frac{1 - p_{p1}}{1 - p_{sp1}} + f_{2D} \frac{D_{mp}}{D_{ms}} (D_1 - D_2) \right)$$

The resulting characteristic equation equals Eq.4.5 which has been analysed in Section 4.3.3.

6.4.2. Compatibility equations.

The one-dimensional compatibility relations for the double-layer model can be written as (Section 5.7)

$$\begin{bmatrix} n_1 \\ un_1 - g_z n_2 \end{bmatrix}^T \nabla a + \begin{bmatrix} n_2 \\ an_1 + un_2 + g(1+\alpha_1) uf_{1u} n_5 + g(1+\alpha_2) uf_{2u} n_6 \end{bmatrix}^T \nabla u +$$

$$+ \begin{bmatrix} \beta_{p1} n_5 + (1-\beta_{p1}) n_6 + (\beta_{o1} - \kappa\beta_{p1}(1+\alpha_1)) n_7 \\ -g_z n_2 \end{bmatrix}^T \nabla z_b +$$

$$+ \begin{bmatrix} T_1 n_3 + an_5 \\ L_1 n_3 + uan_5 \end{bmatrix}^T \nabla p_{s1} + \begin{bmatrix} T_2 n_4 + an_6 \\ L_2 n_4 + uan_6 \end{bmatrix}^T \nabla p_{s2} +$$

$$+ \begin{bmatrix} \delta_p (n_5 - n_6 - \alpha_1 n_7) \\ (f_{1p} + f_{1D}(D_1 - D_2)) n_5 + (-f_{2p} + f_{2D}(D_1 - D_2)) n_6 \end{bmatrix}^T \nabla p_{p1} + \qquad \textbf{6.20}$$

$$+ \begin{bmatrix} \delta_{sp} (n_5 - n_6 + n_7) \\ g\alpha_1 \left(f_{1p} \frac{p_{p1}}{p_{sp1}} + f_{1D} \frac{D_{mp}}{D_{ms}} (D_1 - D_2) \right) n_5 + g\alpha_2 \left(-f_{2p} + f_{1D} \frac{D_{mp}}{D_{ms}} (D_1 - D_2) \right) n_6 \end{bmatrix} =$$

$$= -n_1 \left(\frac{va}{B} \Big|_{y_r}^{y_l} + \frac{ua}{B} \frac{\mathrm{d}B}{\mathrm{d}x} \right) + n_2 \left(\left[g_x - \frac{\tau_{bx}}{\rho a} + \frac{\tau}{\rho B} \Big|_{y_r}^{y_l} \right] + \frac{u \left(va \Big|_{y_r}^{y_l} \right) - uva \Big|_{y_r}^{y_l}}{B} \right) +$$

$$+ [p_{e1} - p_{s1}] n_3 + [p_{e2} - p_{s2}] n_4 +$$

$$+ \frac{(S_{bl1} - S_{br1} + \Phi_{l1} - \Phi_{r1})}{B} n_5 + \frac{(S_{bl2} - S_{br2} + \Phi_{l2} - \Phi_{r2})}{B} n_6$$

or

$$T_a \frac{Da}{Dt} + T_u \frac{Du}{Dt} + T_z \frac{Dz_b}{Dt} + T_{s1} \frac{Dp_{s1}}{Dt} + T_{a2} \frac{Dp_{s2}}{Dt} + T_{p1} \frac{Dp_{p1}}{Dt} + T_{sp1} \frac{Dp_{sp1}}{Dt} =$$

$$= - n_1 \left(\frac{ua}{B} \frac{dB}{dx} + \frac{va}{B} \Big|_{y_r}^{y_l} \right) + n_2 \left[g_x - \frac{\tau_{bx}}{\rho a} + \frac{\tau}{\rho B} \Big|_{y_r}^{y_l} + \frac{u \left(va \Big|_{y_r}^{y_l} \right) - uva \Big|_{y_r}^{y_l}}{aB} \right] + n_3 \left[p_{e1} - p_{s1} \right] +$$

$$+ n_4 \left[p_{e2} - p_{s2} \right] - \frac{\left(S_{bl1} - S_{br1} + \Phi_{l1} - \Phi_{r1} \right)}{B} n_5 - \frac{\left(S_{bl2} - S_{br2} + \Phi_{l2} - \Phi_{r2} \right)}{B} n_6 \qquad \textbf{6.21}$$

with

$$T_a = g_z \, n_t \, P_1 \, P_2 \, R^2 \, g \, u \left[(\delta_s S_2 + \delta_p \alpha_1 T_2)(1+\alpha_1) f_{1u} - (\delta_s S_1 + \delta_p \alpha_1 T_1)(1+\alpha_2) f_{2u} \right]$$

$$T_u = n_t \, P_1 \, P_2 \, g \, u \left[(\delta_s S_2 + \delta_p \alpha_1 T_2)(1+\alpha_1) f_{1u} - (\delta_s S_1 + \delta_p \alpha_1 T_1)(1+\alpha_2) f_{2u} \right]$$

$$T_z = g_z \, P_1 \, P_2 \, R^3 \, g \, u \left[(\delta_s S_2 + \delta_p \alpha_1 T_2)(1+\alpha_1) f_{1u} - (\delta_s S_1 + \delta_p \alpha_1 T_1)(1+\alpha_2) f_{2u} \right]$$

$$T_{s1} = n_t \, P_2 \, a \, R^2 \left(R^2 + g_z a \right) \left(\delta_s S_2 + \delta_p \alpha_1 T_2 \right) \left(u T_{A1} - L_1 \right) \qquad \textbf{6.22}$$

$$T_{s2} = n_t \, P_1 \, a \, R^2 \left(R^2 + g_z a \right) \left(\delta_s S_1 + \delta_p \alpha_1 T_1 \right) \left(L_2 - u T_{A2} \right)$$

$$T_{p1} = -P_1 P_2 R^2 \left(R^2 + g_z a \right) \delta_p \left[n_t \left(\delta_s S_2 + \delta_p \alpha_1 T_2 \right) + n_t \left(\delta_s S_1 + \delta_p \alpha_1 T_1 \right) + \alpha_1 \left(S_2 T_1 - S_1 T_2 \right) \right]$$

$$T_{sp1} = -P_1 P_2 R^2 \left(R^2 + g_z a \right) \delta_s \left[n_t \left(\delta_s S_2 + \delta_p \alpha_1 T_2 \right) + n_t \left(\delta_s S_1 + \delta_p \alpha_1 T_1 \right) + S_1 T_2 - S_2 T_1 \right]$$

6.4.3. Fixed-bed application.

In the case of a fixed bed, the compatibility relation can be reduced to

$$g_z \frac{Da}{Dt} + (n_t + u) \frac{Du}{Dt} =$$

$$= g_z (n_t + u) \frac{dz_b}{dx} - g_z \frac{ua}{B} \frac{dB}{dx} + (n_t + u) \left[g_x - \frac{\tau_{bx}}{\rho a} + \frac{\tau}{\rho B} \Big|_{y_r}^{y_l} + \frac{\left(u \left(va \Big|_{y_r}^{y_l} \right) - uva \Big|_{y_r}^{y_l} \right)}{aB} \right] \qquad \textbf{6.23}$$

with

$$n_t = - \frac{dx}{dt} \qquad \textbf{6.24}$$

The characteristic equation is

$$(n_t+u)^2 + g_z a = 0 \rightarrow n_t = -u \pm \sqrt{-g_z a} \qquad 6.25$$

Consequently, the compatibility relation is

$$\frac{Da}{Dt} \pm \frac{\sqrt{-g_z a}}{g_z}\frac{Du}{Dt} =$$

$$= \pm\sqrt{-g_z a}\frac{dz_b}{dx} - \frac{ua}{B}\frac{dB}{dx} \pm \frac{\sqrt{-g_z a}}{g_z}\left[g_x - \frac{\tau_{bx}}{\rho a} + \frac{\tau}{\rho B}\Big|_{y_r}^{y_l} + \frac{\left(u\left(va\Big|_{y_r}^{y_l}\right) - uva\Big|_{y_r}^{y_l}\right)}{aB}\right] \qquad 6.26$$

6.5. Non-uniform distribution of variables.

6.5.1. Introduction.

After integration of a variable over the depth or width, usually the average value of the variable is used in the equations. To account for additional terms that result from non-uniform distributions over the integration interval, correction terms are defined.

The application of a one-dimensional model with distribution-correction coefficients is justified if the correction coefficients are constant and can be decoupled from the conditions of flow. At larger deviations from the cross-sectionally averaged value (for instance in case of intermediate- and large-scale roughness) and for *Froude* numbers near unity ($0.6 \leq Fr \leq 1.2$), these coefficients are not only relatively large but also highly related to the conditions of flow.

Under these conditions, a flow is dominated by two- or even three-dimensional local phenomena and a one-dimensional mathematical model cannot be applied.

In the following analysis, the distribution coefficients are considered to be constant. Correction coefficients for the hydraulic as well as for the morphological variables are introduced.

The width B and the cross-sectionally averaged depth a are defined as

$$\bar{a} = \frac{\int_{y_r}^{y_l}\int_{z_b}^{z_s} dz\,dy}{\int_{y_r}^{y_l} dy} \quad ; \quad B = \int_{y_r}^{y_l} dy \qquad 6.27$$

6.5.2. Hydraulic distribution-coefficients.

To acount for non-uniform distributions of velocity over the depth and width and the depth over the width, the following coefficients are introduced

$$\alpha_u \, \bar{u} = \frac{\int_{y_r}^{y_l} \int_{z_b}^{z_s} u \, dz \, dy}{\int_{y_r}^{y_l} \int_{z_b}^{z_s} dz \, dy} = \frac{Q}{B\bar{a}} \quad ; \quad \beta_u \, \overline{u^2} = \frac{\int_{y_r}^{y_l} \int_{z_b}^{z_s} u^2 \, dz \, dy}{\int_{y_r}^{y_l} \int_{z_b}^{z_s} dz \, dy} \qquad \textbf{6.28}$$

Usually α_u and β_u are set unity. The non-uniform distribution of depth can be included by definition of

$$\beta_a \frac{\overline{a^2}}{2} = \frac{\int_{y_r}^{y_l} \int_{z_b}^{z_s} \int_{z}^{z_s} dz \, dz \, dy}{\int_{y_r}^{y_l} dy} \qquad \textbf{6.29}$$

6.5.3. Morphogical distribution-coefficients.

Apart from non-uniform distributions of velocity and depth, non-uniform distributions of bed load, suspended load and the river-bed composition can be taken into account.

Regarding a non-uniform distribution of p_{si} over the width, the following coefficients are introduced

$$\overline{p_{si}} = \frac{\int_{z_b}^{z_s} p_{si} \, dz}{\int_{z_b}^{z_s} dz} \quad ; \quad \alpha_{si} \, \overline{p_{si}} = \frac{\int_{y_r z_b}^{y_l z_s} p_{si} \, dz \, dy}{\int_{y_r z_b}^{y_l z_s} dz \, dy} \quad ; \quad \beta_{si} \, \overline{p_{si}} \, \bar{u} = \frac{\int_{y_r z_b}^{y_l z_s} p_{si} u \, dz \, dy}{\int_{y_r z_b}^{y_l z_s} dz \, dy} \qquad \textbf{6.30}$$

It is noted that α_{si} refers to an equilibrium distribution of p_{si} over the cross-section, whereas the relaxation coefficients refer to the adaption of the actual suspended load to the equilibrium total load.

To account for a non-uniform distribution of the bed load over the width, it is stated

$$\alpha_{bi}\overline{g(1+\xi_i)s_{bxi}} = \frac{\int_{y_r}^{y_l} g(1+\alpha_i)s_{bxi}\,dy}{\int_{y_r}^{y_l} dy} \qquad 6.31$$

If a power-law approximation is used, α_{bi} can be written as

$$\alpha_{bi} = \frac{\overline{g(1+\xi_i)p_{pi}m_i\frac{u^{n_i}}{D_m^{l_i}}}}{\overline{g}(1+\overline{\xi_i})\overline{p_{pi}}\;\overline{m_i}\frac{\overline{u}^{n_i}}{\overline{D_m}^{l_i}}} \qquad 6.32$$

This can be simplified by decoupling the width-distribution effects of the ratio of contributions from pavement and subpavement, velocity and sediment properties. It should be noticed that the exposure and contribution of the subpavement layer are related to the sediment properties.

The variation in sediment properties can be described with

$$\alpha_{pi} = \frac{\int_{y_r}^{y_l} \frac{p_{pi}}{D_m^{l_i}}\,dy}{\frac{\overline{p_{pi}}}{\overline{D_m}^{l_i}}\int_{y_r}^{y_l} dy} \approx \left(1+\frac{\Delta p_{pi}}{\overline{p_{pi}}}\right)\overline{D_m}^{l_i}\left(\sum_{i=1}^{N}\left(1+\frac{\Delta p_{pi}}{\overline{p_{pi}}}\right)\left(1+\frac{\Delta D_i}{\overline{D_i}}\right)p_{pi}D_i\right)^{-l_i} \qquad 6.33$$

The effect of a non-uniform velocity distribution over the width on the sediment transport is

$$\alpha_{ni} = \frac{\int_{y_r}^{y_l} u^{n_i}dy}{\overline{u}^{n_i}\int_{y_r}^{y_l} dy} \approx \left(1+\frac{\Delta u}{\overline{u}}\right)^{n_i} \qquad 6.34$$

6.5.4. Magnitude of distribution coefficients.

When introducing $\Delta\xi$ as the deviation from the cross-sectional averaged value ξ, the distribution coefficients for velocity can be written as

$$\alpha = \frac{\int_{y_r}^{y_l}\int_{z_b}^{z_s} u\,dz\,dy}{u_m a_m B} \approx 1 + \frac{\Delta u}{u_m}\frac{\Delta a}{a_m} \qquad 6.35$$

$$\beta = \frac{\int_{y_r}^{y_l}\int_{z_b}^{z_s} u^2\,dz\,dy}{u_m^2 a_m B} \approx 1 + \frac{\Delta u}{u_m}\frac{\Delta a}{a_m}\left(2 + \frac{\Delta u}{u_m}\right) + \left(\frac{\Delta u}{u_m}\right)^2$$

Hence, if the deviations are small, the following relation can be used

$$\alpha \approx \frac{\beta + 1}{2} \qquad 6.36$$

If, at large shear-stresses, the power n in the transport formula approaches 3, α_n can be considered similar to the *energy* or *Coriolis* coefficient.

With the help of Eq.6.36, the following table can be constructed, based on a reference by Chow (1959).

type	β_u			α_u			α_n		
	min	av	max	min	av	max	min	av	max
A	1.03	1.05	1.07	1.02	1.03	1.04	1.10	1.15	1.20
B	1.05	1.10	1.17	1.03	1.05	1.09	1.15	1.30	1.50
C	1.17	1.25	1.33	1.09	1.13	1.17	1.50	1.75	2.00

Table 6.1

Where type *A* stands for regular channels, flumes and spillways, type *B* refers to natural streams and torrents and type *C* represents river valleys that are overflooded.

6.6. Behaviour of 1-DH models with non-uniformly distributed variables.

6.6.1. System of equations.

If apart from non-uniform distributions, all gradients in y-direction are neglected, the mass balance can be rewritten as

$$a\frac{\partial B}{\partial t} + B\frac{\partial a}{\partial t} + \alpha_u ua\frac{\partial B}{\partial x} + \alpha_u uB\frac{\partial a}{\partial x} + \alpha_u aB\frac{\partial u}{\partial x} + va\Big|_{y_r}^{y_l} = 0 \qquad 6.37$$

and the momentum balance is

$$\left(\left(\alpha_u - \frac{\beta_u}{\alpha_u}\right)ua\frac{\partial B}{\partial t} + \left(\alpha_u - \frac{\beta_u}{\alpha_u}\right)Bu\frac{\partial a}{\partial t} + \alpha_u Ba\frac{\partial u}{\partial t} + \beta_u uaB\frac{\partial u}{\partial x} + \right.$$

$$\left. - g_x aB - g_z Ba\frac{\partial(a+z_b)}{\partial x} + \frac{\overline{\tau_{bx}}}{\rho}B + uva\Big|_{y_r}^{y_l} - \frac{\beta_u}{\alpha_u}u\left(va\Big|_{y_r}^{y_l}\right) - \tau a\Big|_{y_r}^{y_l} = 0 \right. \qquad 6.38$$

The mass balance of suspended sediment can be rewritten as

$$p_{si}a\left(\alpha_{si} - \frac{\beta_{si}}{\alpha_u}\right)\frac{\partial B}{\partial t} + p_{si}B\left(\alpha_{si} - \frac{\beta_{si}}{\alpha_u}\right)\frac{\partial a}{\partial t} + \alpha_{si}aB\frac{\partial p_{s_i}}{\partial t} + \beta_{si}auB\frac{\partial p_{si}}{\partial x} =$$

$$= \int_{y_r}^{y_l}\Phi_{si}dy + \Phi_{ri} - \Phi_{li} + \frac{\beta_{si}}{\alpha_u}p_{si}\left(va\Big|_{y_r}^{y_l}\right)$$

The approximate, first-order solution of the cross-sectional integrated balance of suspended sediment is

$$T_{Ai}\frac{\partial p_{si}}{\partial t} + L_{xi}\frac{\partial p_{si}}{\partial x} + (p_{si} - p_{ei}) = 0 \qquad 6.40$$

The mass balance for the bedload can be written as

$$g(1+\alpha_i)\alpha_{ni}\alpha_{pi}f_{iu}\frac{\partial u}{\partial x} + g\alpha_i\alpha_{ni}\alpha_{pi}f_{ip}\frac{\partial p_{pi}}{\partial x} + g\alpha_i\alpha_{ni}\alpha_{pi}f_{iD}\sum_{j=1}^{N}D_j\frac{\partial p_{pj}}{\partial x} +$$

$$+ g\alpha_i\alpha_{ni}\alpha_{pi}f_{ip}\frac{p_{pi}}{p_{spi}}\frac{\partial p_{spi}}{\partial x} + g\alpha_i\alpha_{ni}\alpha_{pi}f_{iD}\frac{D_{mp}}{D_{ms}}\sum_{j=1}^{N}D_j\frac{\partial p_{spj}}{\partial x} + \frac{\int_{y_r}^{y_l}\Phi_{si}dy}{B} + \qquad 6.41$$

$$+ \delta_p\frac{\partial p_{pi}}{\partial t} + \delta_s\frac{\partial p_{spi}}{\partial t} + \beta_{oi}\frac{\partial z_b}{\partial t} + \frac{S_{bli} - S_{bri}}{B} + g(1+\alpha_i)\alpha_{ni}\alpha_{pi}\frac{s_{bxi}}{B}\frac{\partial B}{\partial x} = 0$$

The system of partial-differential equations can be written as

$$Q \cdot \begin{bmatrix} \mathrm{D}a/\mathrm{D}t \\ \mathrm{D}u/\mathrm{D}t \\ \mathrm{D}z_b/\mathrm{D}t \\ \mathrm{D}p_{s1}/\mathrm{D}t \\ \mathrm{D}p_{s2}/\mathrm{D}t \\ \mathrm{D}p_{p1}/\mathrm{D}t \\ \mathrm{D}p_{sp1}/\mathrm{D}t \end{bmatrix} = \vec{n}^T \cdot \vec{n} \begin{bmatrix} -va\Big|_{y_r}^{y_l} - \alpha_u ua\dfrac{\mathrm{d}B}{\mathrm{d}x} \\ g_x aB - \overline{\tau_{bx}}B/\rho + u\left(va\Big|_{y_r}^{y_l}\right) - \dfrac{\beta_u}{\alpha_u}uva\Big|_{y_r}^{y_l} + \dfrac{\tau a}{\rho}\Big|_{y_r}^{y_l} \\ p_{e1} - p_{s1} \\ p_{e2} - p_{s2} \\ -(S_{bl1} - S_{br1})/B - (\Phi_{l1} - \Phi_{r1})/B + \dfrac{\beta_{s1}}{\alpha_u}p_{s1}\left(va\Big|_{y_r}^{y_l}\right)/B - g(1+\alpha_1)\alpha_{n1}\alpha_{p1}\dfrac{s_{bx1}}{B}\dfrac{\mathrm{d}B}{\mathrm{d}x} \\ -(S_{bl2} - S_{br2})/B - (\Phi_{l2} - \Phi_{r2})/B + \dfrac{\beta_{s2}}{\alpha_u}p_{s2}\left(va\Big|_{y_r}^{y_l}\right)/B - g(1+\alpha_2)\alpha_{n2}\alpha_{p2}\dfrac{s_{bx2}}{B}\dfrac{\mathrm{d}B}{\mathrm{d}x} \\ 0 \end{bmatrix} \qquad \textbf{6.42}$$

with Q

$$\begin{bmatrix} n_t+\alpha_u u & \alpha_u a & 0 & 0 & 0 & 0 & 0 \\ (\alpha_u-\beta_u/\alpha_u)un_t-g_z a & \alpha_u n_t a+\beta_u au & -g_z a & 0 & 0 & 0 & 0 \\ 0 & 0 & 0 & P_1 & 0 & 0 & 0 \\ 0 & 0 & 0 & 0 & P_2 & 0 & 0 \\ (\alpha_{s1}-\beta_{s1}/\alpha_u)c_1 n_t & g(1+\alpha_1)F_{u1} & \beta_{o1}n_t & a(\alpha_{s1}n_t+\beta_{s1}u) & 0 & S_1 & T_1 \\ (\alpha_{s2}-\beta_{s2}/\alpha_u)c_2 n_t & g(1+\alpha_2)F_{u2} & (1-\beta_{o1})n_t & 0 & a(\alpha_{s2}n_t+\beta_{s2}u) & S_2 & T_2 \\ 0 & 0 & (\beta_{o1}-\kappa\beta_{p1}(1+\alpha_1))n_t & 0 & 0 & -\alpha_1\delta_p n_t & \delta_s n_t \end{bmatrix} \qquad \textbf{6.43}$$

and where

$$\begin{aligned} F_{ui} &= \alpha_{ni}\,\alpha_{pi}\,f_{ui} \quad ; \quad P_i = T_{Ai}n_t + L_{xi} \\ S_1 &= \delta_p n_t + g\alpha_1\alpha_{n1}\alpha_{p1}\left(f_{1p} + f_{1D}(D_1-D_2)\right) \\ S_2 &= -\delta_p n_t + g\alpha_2\alpha_{n2}\alpha_{p2}\left(-f_{2p} + f_{2D}(D_1-D_2)\right) \\ T_1 &= \delta_s n_t + g\alpha_1\alpha_{n1}\alpha_{p1}\left(f_{1p}\frac{p_{p1}}{p_{sp1}} + f_{1D}\frac{D_{mp}}{D_{ms}}(D_1-D_2)\right) \\ T_2 &= -\delta_s n_t + g\alpha_2\alpha_{n2}\alpha_{p2}\left(-f_{2p}\frac{1-p_{p1}}{1-p_{sp1}} + f_{2D}\frac{D_{mp}}{D_{ms}}(D_1-D_2)\right) \end{aligned} \qquad \textbf{6.44}$$

Analogeously as in Section 6.4, the characteristics and compatibility equations can be determined for this system of equations.

6.6.2. Characteristics of fixed-bed model.

The matrix Q is reduced to

$$Q = \begin{bmatrix} n_t+\alpha_u & \alpha_u a \\ n_t u(\alpha_u-\beta_u/\alpha_u)-g_z a & a(\alpha_u n_t + \alpha\beta_u u) \end{bmatrix} \qquad 6.45$$

The characteristics for flows with non-uniform distributions over the width are

$$-\frac{n_t}{u} = \frac{r}{u} = \frac{\beta_u}{\alpha_u} \pm \frac{\sqrt{1 - \beta_u Fr^2(1-\beta_u/\alpha_u^2)}}{Fr} \qquad 6.46$$

The well-known circular bicharacteristic surface of a fixed-bed model remains a circle. As $\alpha_u < \beta_u < \alpha_u^2$, it appears that the radius of this circle reduces, whereas the center of the circle is larger then unity. Consequently, the most significant effect can be found at the upstream-orientated characteristic that is reduced. The transition from subcritical to supercritical flow will take place at $Fr = 1/\sqrt{\beta_u}$.

6.6.3. Characteristics of mobile-bed model.

The matrix Q is

$$Q = \begin{bmatrix} n_t+\alpha_u u & \alpha_u a & 0 \\ n_t u(\alpha_u-\beta_u/\alpha_u)-g_z a & a(\alpha_u n_t+\beta_u u) & -g_z a \\ 0 & \alpha_n f_u & n_t \end{bmatrix} \qquad 6.47$$

and the characteristic equation for a mobile bed model with uniform material is

$$\alpha_u n_t^3 + 2\beta_u u n_t^2 + \alpha_u\left(g_z a+\beta_u u^2+g_z\frac{\alpha_n}{\alpha_u}f_u\right)n_t + g_z\alpha_u u\alpha_n f_u = 0 \qquad 6.48$$

When applying Eq.6.46 (quasi-steady approach), the third root is

$$-\frac{n_t}{u} = \frac{r}{u} = \frac{\alpha_n f_u/a}{1 - \beta_u Fr^2} \qquad 6.49$$

Using the average values for the different type of rivers (Table 6.1), the characteristics are

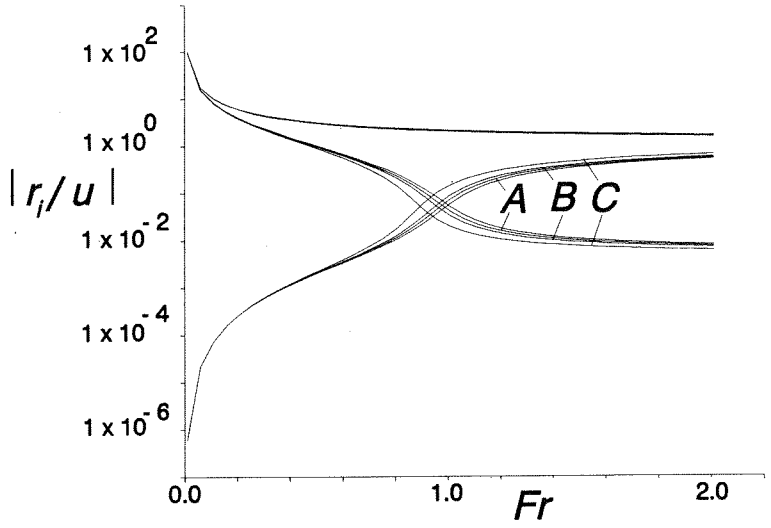

Figure 6.2

Because the effect of the velocity distribution on the transport capacity is usually accounted for by calibration coefficients, α_n is taken unity in Figure 6.2.

To compare with a uniform distribution (subscript 0), the relative difference in characteristics for $\alpha_n = 1$ (Figure 6.3) and $\alpha_n \neq 1$ (Figure 6.4) are represented.

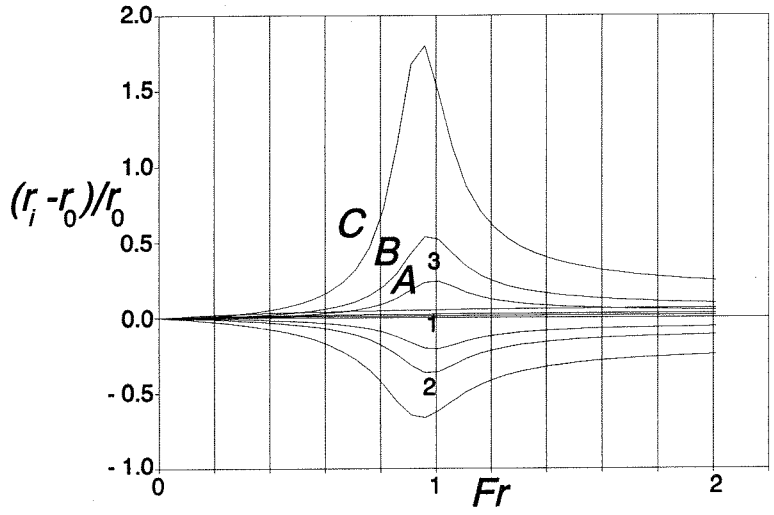

Figure 6.3

The largest characteristic (subscript 1) represents downstream travelling changes in water level appears to be insensitive to the distribution of parameters over the width. Whereas for $Fr > 0.2$, the distribution of parameters affects the dynamic behaviour of the model. For $0.6 \leq Fr \leq 1.2$, the transition interval between subcritical and

supercritival flow, the relative difference is large due to a shift in characteristics (see Figure 6.2).

The characteristic that can be related to the propagation of changes in bed level is marked by subscript 3 for subcritical flows and 2 for supercritical flows. This characteristic is very sensitive to changes in α_n (Figure 6.4)

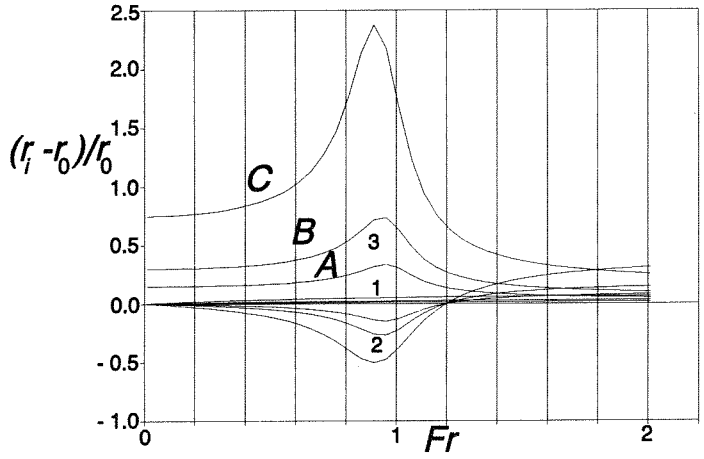

Figure 6.4

Because changes in the composition of the bed are coupled to changes in bed level, similar conclusions can be drawn for mobile bed models with graded sediment.

Chapter 7

Conclusions.

7.1. Introduction.

In this report, some aspects of the mathematical modelling of alluvial mountain rivers with graded sediment have been investigated. At present, the depth-averaged mathematical models that are generally used for alluvial low-land rivers are applied to simulate the hydraulics and morphology in alluvial mountain rivers.

However, the conditions in mountain rivers can be rather specific; large *Froude* numbers, small depths, extremely non-uniform geometries, large rates of transported material and graded sediments. Analysing such models with the theory of characteristics provides an indispensible insight on the dynamic behaviour of the model.

Based on this analysis, conclusions can be drawn on the effects of the dimensions of the model (2-DH or 1-DH), the number, type and thickness of sediment-exchange layers in the bed, the composition of the sediment, the time-scales of hydraulic and morphological changes and the initial behaviour of point disturbances.

According to Ribberink (1987), the number of fractions required to achieve a sufficiently accurate prediction of morphology should be four. The analysis in this report is based on a sediment mixture composed of two fractions which restricts the quantitative conclusions drawn in this report.

In Section 7.2, the effect of the flow regime on the behaviour of the model will be discussed. The effect of shear stress is mentioned in Section 7.3 and in Section 7.4, the single-layer and double-layer model are compared.

7.2. Effects of flow regime.

7.2.1. Initial behaviour of small morphological disturbances.

With the help of a simple analysis it has been shown that initial behaviour of small morphological disturbances in subcritical and supercritical flow are quite different (Section 5.4).

If inertia effects can be neglected in a hydrograph of a subcritical flow, disturbances in bed level grow whereas at the decelerating parts of the hydrograph, disturbances in bed level decrease.

With respect to the composition of the bed it can be concluded that the fraction of fine material in the bed increases at accelerating parts and the mixing layer coarsens at

decelerating parts. In general, this confirms that armour layers develop at the decelarating part of a flood.

The effect of relaxation in suspended load reinforces the response of the bed-level disturbances, whereas the response of the bed composition is surpressed.

During hydrographs in supercritical flows, small disturbances in bed level show an opposite behaviour.

Because the response on *non-uniform* flow in subcritical and supercritical flow regimes are different, sections of different flow regimes should not be eliminated by reach-averaging procedures if morphogical responses to a flood are predicted.

7.2.2. Coupled changes in morphology and hydraulics.

Because in *Froude* numbers in mountain rivers can vary significantly, hydraulic and morphological phenomena are coupled. This complicates the modelling of an alluvial mountain river relative to low-land rivers. The experience in using morphological models with *Fr* near unity and *Fr* larger than unity is scarce.

To a certain extend, the circle-shaped characteristic surfaces that are well-known from fixed-bed models can be recognised in the "balloon"-shaped characteristic surface of mobile bed models (Figure 4.2). The effect of the mobile bed can be understood from mutual comparison of both surfaces.

In line with conclusions drawn by De Vries (1959), it can be stated that for $Fr < 0.6$, separation of hydraulic and morphological changes can be applied at small rates of sediment transport. A transition interval at $0.6 < Fr < 1.2$ can be distinguished where characteristic roots change roles and changes in hydraulic and morphological variables are coupled.

Although in one-dimensional models with small rates of sediment transport the hydraulics and morphology for $Fr > 1.2$ can be decoupled, in two-dimensional models, transversal changes in hydraulics and morphology are coupled (Figures 4.5).

Changes in the morphological variables (bed level and bed composition) are coupled in general, irrespective of the regime of flow (Figure 4.9).

7.2.3. Transversal effects.

From analyzing the characteristic equations it can be concluded that not only the *propagation* of disturbances changes with varying *Fr*, also the *direction* of propagation is affected. With increasing *Fr*, the propagation of changes in bed level and composition in transversal direction increases.

Consequently, for higher values of *Fr*, the two-dimensional character of morphological changes becomes pronounced and the effect of boundary conditions on the solution increases.

7.2.4. Application of one-dimensional models.

As described in Section 7.2.3, the morphological behaviour of two-dimensional models in supercritical flow can be significantly affected by boundary conditions at the banks.

Consequently the performance of 1-DH models applied to supercritical flows in rivers with an extremely non-uniform geometry should be interpretated with care. Because the effect of the boundaries on the solution of the morphological model increases in supercritical flows, the reach-averaging of local geometrical parameters should be carried out carefully.

Due to a non-uniform distribution of roughness elements, parameters can vary over the cross-section of a river. The effect of non-uniform distributions over the depth and over the width increases with increasing *Fr*. As shown in Figures 6.2 and 6.3, the dynamic behaviour of fixed-bed and mobile-bed models is very sensitive to the distribution of parameters over the cross-section for $Fr \geq 0.6$. In subcritical flows, the rate of changes in morphology is increased, whereas in supercritical flows this rate is reduced by non-uniform transversal distributions.

However, in this range of *Fr*, the correcting distribution-coefficients can be expected to vary with *Fr*. Data on these coefficients at varying conditions of flow are rather scarce.

Consequently, when modelling flow at $Fr \geq 0.6$ in non-uniform rivers, transversal effects can be expected to be significant. The performance of one-dimensional models is very sensitive to the approach that is used to model the effects of non-uniform geometry.

7.3. Sediment transport.

At shear stresses close to the critical shear-stress, the correction by hiding effects has a large influence on the transport of fractions. At low shear-stresses, the coefficients in the power law that approximates the sediment transport, and the rate of sediment transport are very sensitive to changes in flow conditions and sediment properties. Due to the relative importance of turbulence and exposure at low shear-stresses, motions of particles are very hard to predict which implies that accurate prediction of for instance armouring phenomena is difficult.

In Appendix B, different shear-stress based transport formulae are compared (Meyer-Peter and Müller, 1948; Parker et al. (1982) modified by Diplas, 1987; Graf and Suzka, 1987). At low shear-stresses, the sensitivity of the sediment transport to shear stress and grain size can very significantly for different formulae. However, because general trends in the formulae correspond, the results of the analysis are considered of general relevance.

The composition of the sediment transport is fine relative to the river bed. At higher shear-stresses the influence of hiding reduces and the *relative* mobility of fine particles increases compared to that of coarser fractions. Then, the composition of the transported sediment becomes finer. At high shear-stresses, the composition of the sediment transport approaches that of the river bed.

7.4. Effects of sediment mixture.

7.4.1. Changes in composition.

The changes in composition of a river bed are related to

- the difference in composition of material picked-up (deposited) and material in the substratum (mixing layer) in case of erosion (sedimentation)
- changes in bed level relative to the mixing-layer thickness

The first factor is related to the type of transport formula used, the shear stresses relative to the critical shear-stress, the type of process (sedimentation or erosion) and the composition of the bed. This factor enables the derivation of a simple coarsening criterion to predict whether armouring can occur (Sections 2.3.4 and 2.4.6).

As a result of the relation with changes in bed level, the composition of the bed is coupled with hydraulic parameters, which significant for Fr near unity and super critical flows. This has been illustrated in Figure 4.15, where the characteristics appear to be very sensitive to changes in composition for $Fr > 0.6$.

7.4.2. Morphological behaviour.

The effect of distinguishing size-fractions on the morphology of an alluvial river is significant if shear stresses are low relative to the critical shear-stress (Figure 4.14). At this condition, the transport of a fraction is determined by the particle mobility which is controlled by size-specific hiding effects. Then, the effects of gradients in size fraction and even in median grain-diameter are significant.

At higher shear-stresses, the hiding effect diminishes and the morphological behaviour approaches that of a bed composed of uniform sediment with equivalent properties.

7.5. Mixing-layer thickness.

7.5.1. Relation to mixing mechanism.

The thickness of the mixing layer represents the extend of the bed that can be reworked to affect the sediment transport, within a relevant time interval. Predicton of the mixing-layer thickness for a wide range of flow conditions (and subsequent bed form regime) remains an interesting subject of research. However, it should be considered that the layer-thickness applied is not only related to physical conditions, but to the time-scale of bed level changes during the period of interest as well.

Because mixing layers and armour layer are different, the application of the single-layer model to simulate armouring phenomena could be erroneous.

7.5.2. Critical mixing layer-thickness.

In analyzing the single-layer model and the double-layer model, the thickness of the sediment layers in the river bed are taken constant. The mixing process that controls the composition of sediment transport is assumed instantaneous compared to morphological changes in bed level and composition.

In the case of erosion of an armoured bed, the model can loose its mathematical, hyperbolic character. Because armour layers can only be stable at relatively low shear-stresses, this problem of a non-realistic elliptical character is not relevant at high shear-stresses.

To insure the hyperbolicity of the system of partial-differential equations, the mixing-layer thickness should be smaller than a critical value which limits the vertical reworking of the top layers of the river bed. If this critical value is exceeded, the mathematical model is not valid.

This critical value of the mixing-layer thickness can be interpretated as the maximum ratio of the two characteristics that are related to morphological changes. Based on approximations of the longitudinal bicharacteristic rays, a criterion for subcritical and supercritical flow has been derived for the single- and double layer model which, however, fails for $0.8 < Fr < 1.2$.

It appears that the validity of the single-layer model can be improved by the introduction of a transition layer with intermediate composition (Figure 4.17), but at larger values of Fr and with increasing sediment contributions of the fine transition layer to the flow, this validity reduces (Figure 4.26).

7.5.3. Adjustment of time-scale.

If the mixing mechanism has not reached an equilibrium stage, the extend of vertical mixing can be limited by reduction of the time interval. Hence, the type of mixing mechanism and subsequently, the maximum value of the mixing layer can be related to a maximum time step for numerical calculations on the mathematical model.

It is noticed that this concerns changes in armoured river beds at very low shear-stresses with a relatively small time-scale. It should be questioned whether the small morphological changes in bed level and composition at these time-scales still can be decoupled from the mixing process.

7.6. Number of layers.

7.6.1. Single-layer model.

From the analysis of the longitudinal bicharacteristic rays it can be concluded that the effect of the additional characteristic surface in the single-layer model on the behaviour of the model is very small (Section 4.3.4). Consequently, the morphological behaviour of the model corresponds to that of a general mathematical model for uniform sediment with equivalent properties.

7.6.2. Double-layer model.

In contrast with the single-layer model, the morphological behaviour in the double-layer model is affected by distinction of layers and vertical fluxes (Section 4.4.2).

Ribberink (1987) and Di Silvio (1991) already concluded that double-layer models had a better performance in simulating their experiments. It is stated here that to enable the description of non-uniform armouring processes, contributions from the subpavement layer should be described that not only affect the composition, but also changes the rate of the transported sediment (Section 2.4.4). This has been illustrated in Figures 4.24 and 4.25.

The frequency of subpavement contributions is a rather important model parameter for the morphological behaviour, but at present, similar to the thickness of pavement and subpavement layer, predictions for this parameter at a wide range of flow conditions can not be made.

List of main symbols.

a	depth	[m]
B	width	[m]
c	actual concentration of suspended sediment	[-]
c_b	concentration of sediment in the bed-load layer	[-]
c_e	equilibrium concentration of suspended sediment	[-]
C	Chézy roughness parameter	[$m^{1/2}/s$]
D_i	particle diameter of sediment in the fraction i	[m]
D_{mp}	mean diameter of pavement, defined as $D_m = \sum p_{pi} D_i$ with i = 1 to N	[m]
u	velocity component in x-direction	[m/s]
v	velocity component in y-direction	[m/s]
f_{ij}	derivative of transport formula of fraction i to variable j	
Fr	Froude number, defined as $Fr = u/\sqrt{-g_z a}$	[-]
L_j	component in j-direction of adaption length of equilibrium concentration profile in z-direction	[m]
T_A	adaption period of equilibrium concentration profile in z-direction	[s]
g	gravitation constant	[m/s^2]
g_j	component of gravitation constant in j-direction	[m/s^2]
N	total number of fractions in the sediment mixture	[-]
n_j	component of characteristic normal in j-direction	
p	porosity of sediment	[-]
p_{si}	actual concentration of fraction i in suspension	[-]
p_{ei}	equilibrium concentration of fraction i in suspension	[-]
p_{Ti}	fraction i in the transported sediment	[-]
q	discharge per meter width in x-direction defined as $q = ua$	[m_2/s]
s	direction along characteristic surface perpendicular to bicharacteristic ray	
s_{bj}	component in j-direction of bed-load transport	[m^2/s]
s_{bji}	component in j-direction of fraction i in the bed-load	[m^2/s]
$w(z_b)$	vertical fluid velocity at level $z = z_b$	[m/s]
w_s	fall velocity of sediment particle	[m/s]
z_b	bed level	[m]
Z_b	spatial- and time-averaged bed-level	[m]
α_u	velocity distribution coefficient	[-]
α_{bi}	transversal-distribution coefficient of bed load	[-]
α_n	distribution coefficient of u^n	[-]
α_{pi}	transveral-distribution coefficient of fraction in pavement	[-]
α_{si}	transveral-distribution coefficient of suspended fraction	[-]
β_u	distribution coefficient of u^2	[-]
Δ	relative sediment density defined as $\Delta = \rho/\rho_s - 1$	[-]

θ	orientation of bicharacteristic ray	
τ	direction of bicharacteristic ray	
τ_{bj}	component of bed shear-stress in j-direction	[kg/ms^2]
τ_{*i}	particle shear-stress defined as $\tau_{*i} = u^2 / \Delta C^2 D_i$	[-]
τ_{*c}	critical particle shear-stress describing initiation of motion	[-]
ξ_i	particle shear-stress correction-coefficient for horizontal-hiding effects at fraction i	[-]
ρ	density of water	[kg/m^3]
ρ_s	density of sediment	[kg/m^3]

Single-layer model.

p_{mi}	fraction i in the mixing layer	[-]
β_i	fraction i at bed level $z = z_b - \delta_m$	[-]
δ_b	thickness of the transport-layer with bed load	[m]
δ_m	thickness of the mixing layer	[m]
ϵ_s	sediment mixing-coefficient	[m^2/s]
ϵ_{si}	sediment mixing-coefficient for fraction i	[m^2/s]
Φ_{si}	vertical sediment flux of fraction i between suspended load and bed load	[m/s]
Φ_{bi}	vertical sediment flux of fraction i between the mixing layer and the bed load	[m/s]
Φ_{oi}	vertical sediment flux of fraction i between the the substratum and the mixing layer	[m/s]

Double-layer model

g	probability of exposure of the pavement layer	[-]
p_{oi}	fraction i in the substratum	[-]
p_{pi}	fraction i in the pavement layer	[-]
p_{spi}	fraction i in the subpavement layer	[-]
α_i	ratio of vertical sediment fluxes of fraction i between layers and bedload transport, defined as $\alpha_i = \Phi_{bsi} / \Phi_{bpi}$	[-]
β_{pi}	fraction i at bed level $z = z_b - \delta_p$	[-]
β_{oi}	fraction i at bed level $z = z_b - \delta_p - \delta_{sp}$	[-]
δ_p	thickness of the pavement layer	[m]
δ_{sp}	thickness of the subpavement layer	[m]
Φ_{bpi}	vertical sediment flux of fraction i between the pavement layer and the bed load	[m/s]
Φ_{bsi}	vertical sediment flux of fraction i between the subpavement layer and the bed load	[m/s]
Φ_{pi}	vertical sediment flux of fraction i between the pavement and the subpavement	[m/s]
Φ_{oi}	vertical sediment flux of fraction i between the substratum and the subpavement	[m/s]

Literature.

Abbott, M.B. (1979); *Computational Hydraulics. Elements of the theory of free surface flows*, Pitman, London, 324 p.

Ashida K. and M. Michiue (1973); Studies on bed load transport rate in alluvial streams, Transactions of the ASCE, Vol.4.

Armanini, A and G. Di Silvio (1988); A one-dimensional model for the transport of a sediment mixture in non-equilibrium conditions, Journal of Hydraulic Research, Vol.26, No.3, p. 275-292.

Armanini, A and G. Di Silvio (1989); On the coexistence of bedload and suspended transport for a uniform grain size material, Sediment Transport Modeling, Proceedings of the International Symposium, S.S.Y.Wang (Ed), p581-587, New Orleans.

Borah, D.K.; C.V. Alonso and S.N. Prasad (1982); Routing graded sediments in streams; Formulations, ASCE, Journal of the Hydraulics Division, Vol.108, No.12, p. 1486-1503.

Chow, Ven Te (1958); *Open-Channel Hydraulics*, McGraw-Hill Inc., p.680.

Courant, R. and D. Hilbert (1962); *Methods of mathematical Physics. Vol.II: Partial differential equations*, Interscience Publishers, New York, 830 p..

Daubert, A. and O. Graffe (1967); Quelques apects des écoulements presque horizontaux a deux dimensions en plan et non permanents application aux estuaires. La Houille Blanche No.8, p. 847-860.

Diplas, P (1987); Bedload transport in gravel-bed streams, ASCE, Journal of Hydraulic Engineering, Vol.113, No.3, p. 277-292.

Egiazaroff, Par. I. (1965); Calculation of non-uniform sediment concentrations, ASCE, Journal of the Hydraulics Division, No.4.

Fletcher, C.A.J. (1988); *Computational Techniques for Fluid Dynamics. 1. Fundamentals and general techniques.*, Springer Berlin.

Fletcher, C.A.J. (1988); *Computational Techniques for Fluid Dynamics. 2. Specific techniques for different flow categories.*, Springer Berlin.

Galapatti, R. (1983); A depth-integrated model for suspended transport, Report No.83-7, Communications on Hydraulic and Geotechnical Engineering, Delft University of Technology, Faculty of Civil Engineering.

Graf, W.H. and L. Suzka (1987); Sediment transport in steep channels, Journal of Hydroscience and Hydraulic Engineering, Vol.5, No.1, pp.11-26.

Hirsch, C. (1988); *Numerical Computation of Internal and External Flows, Vol. 1: Fundamentals of Numerical Discretization.*, John Wiley and Sons.

Hirsch, C. (1990); *Numerical Computation of Internal and External Flows, Vol. 2: Computational methods for inviscid and viscous flows.*, John Wiley and Sons.

Jansen, P.Ph, L. van Bendegom, J. van den Berg, M. de Vries and A. Zanen (1978); *Principles of River Engineering, The non-tidal alluvial river*, Delftse Uitgevers Maatschappij, 509 p..

Karim, M.F.; F.M. Holly and J.F. Kennedy (1983); Bed armoring procedures in IALLUVIAL and application to the Missouri River, Iowa Institute of Hydraulic

Research Report No.269, Iowa.
Katopodes, N. and T. Strelkoff (1978); Computing two-dimensional dam-break flood wave, ASCE, Journal of the Hydraulics Division, Vol.104, No.9, p. 1269-1288.
Laguzzi M (1994); Modelling of sediment mixtures, Delft Hydraulics, Q1660.
Lai, C. (1986); Numerical modeling of unsteady open-channel flow, Advances in Hydrosciences, Vol.14, p. 161-333.
Lin, P.N. and H.W. Shen (1984); Two-D flow with sediment by the characteristic method, ASCE, Journal of Hydraulic Engineering Vol.110, No.5, p. 615-626.
Meyer-Peter, E and R. Müller (1948); Formulas for bed-load transport. Proceedings of the IAHR, Stockholm, Vol.2, paper 2, p.39-42.
Parker, G.; P.C. Klingeman and D.G. McLean (1982); Bedload and size distribution in paved gravel-bed streams, ASCE, Journal of Hydraulic Engineering, Vol.108, No.4, p. 544-571.
Peviani M. (1991): Modelling sediment transport in gravel bed rivers: three-dimensional effect of sorting, Grain Sorting Seminar, Ascona, Switzerland.
Rahuel, J.L, F.M.Holly, J.P.Chollet, P.J. Belleudy and G.Yang (1989); Modeling of riverbed evolution for bedload sediment mixtures, Journal of Hydraulic Engineering Vol.115, No.11, p. 1521-1542.
Ribberink, J.S. (1980); Morphological modelling for rivers with non-uniform sediment, Internal Report No.1-80, pp-144, Delft University of Technology, Department of Civil Engineering, Fluid Mechanics Group.
Ribberink, J.S. (1983); Experiments with non-uniform sediment in case of bed-load transport, Report No.83-2, Communications on Hydraulic and Geotechnical Engineering, Delft University of Technology, Faculty of Civil Engineering.
Ribberink, J.S. (1987); Mathematical modelling of one-dimensional morphological changes in rivers with non-uniform sediment, PhD-thesis, 200 p., Report No.87-2, Communications on Hydraulic and Geotechnical Engineering, Delft University of Technology, Faculty of Civil Engineering.
Silvio G. Di and S. Brunelli (1989); Experimental investigation on bedload and suspended transport in mountain rivers, Lecture Notes in Earth Sciences 37, Fluvial Hydraulics of Mountain Rivers, A. Armanini and G. Di Silvio (Eds.), Springer-Verlag, p. 443-457.
Silvio G. Di (1991); Sediment exchange between stream and bottom: a four layer model, VAW Mitteilungen 117, Proceedings of the International Grain Sorting Seminar, p.163-191, Ascona, Switzerland.
Silvio G. Di. and M. Peviani (1991); Transport of a mixture of sand and gravel in suspension and as bedload: experiments and mathematical modelling Symposium on " The Transport of Suspended Sediment and its Mathematical Modelling", Florence.
Sieben A (1993): Hydraulics and morphology of mountain rivers: a literature survey, Report No.93-4, Communications on Hydraulic and Geotechnical Engineering, Delft University of Technology, Faculty of Civil Engineering.
Sloff, C.J (1992); The method of characteristics applied to analyse 2DH hydraulic models, Report No.92-4, Communications on Hydraulic and Geotechnical

Engineering, Delft University of Technology, Faculty of Civil Engineering.
Sloff, C.J. (1993); Study on modelling the morphology of torrents on volcano slopes, Journal of the Hydraulic Research, Vol.31, No.3, p. 333-346.
Terzidis G. and T. Strelkoff (1970); Computation of open-channel surges and shocks, ASCE, Journal of the Hydraulics Division, Vol.96, No.12, p. 2581-2611.
Vriend, H.J. de (1987); 2DH mathematical modelling of morphological evolutions, Coastal Engineering, Vol.10, No.1.
Vriend, H.J. de (1987); Analysis of horizontally two-dimensional morphological evolutions in shallow water, Journal of Geophysical Research, Vol.92, No.C4, p. 3877-3893.
Vries, M. de (1965); Considerations about non-steady bedload transport in open channels, Proceedings IAHR Congress, Paper 3.8, Leningrad.
Vries, M. de (1993); River Engineering, Lecture Notes F10, Delft University of Technology, Faculty of Civil Engineering, Department of Hydraulic Engineering, 139 p..
Wolfram, S. (1991); *Mathematica: a system for doing mathematics by computer*, Second Edition, Addison-Wesley Publishing Company, Redwood City, California, p. 961.

Appendix A. System of equations.

A.1. 2-DH model with uniform material.

If ∇ is defined as

$$\nabla .. = \begin{bmatrix} \frac{\partial ..}{\partial t} \\ \frac{\partial ..}{\partial x} \\ \frac{\partial ..}{\partial y} \end{bmatrix} \qquad \text{A.1}$$

the system of equations for uniform material can be written as

$$\begin{bmatrix} 1 \\ u \\ v \end{bmatrix}^T \nabla a + \begin{bmatrix} 0 \\ a \\ 0 \end{bmatrix}^T \nabla u + \begin{bmatrix} 0 \\ 0 \\ a \end{bmatrix}^T \nabla v + \begin{bmatrix} 0 \\ 0 \\ 0 \end{bmatrix}^T \nabla z_b + \begin{bmatrix} 0 \\ 0 \\ 0 \end{bmatrix}^T \nabla c = 0$$

$$\begin{bmatrix} 0 \\ -g_z \\ 0 \end{bmatrix}^T \nabla a + \begin{bmatrix} 1 \\ u \\ v \end{bmatrix}^T \nabla u + \begin{bmatrix} 0 \\ 0 \\ 0 \end{bmatrix}^T \nabla v + \begin{bmatrix} 0 \\ -g_z \\ 0 \end{bmatrix}^T \nabla z_b + \begin{bmatrix} 0 \\ 0 \\ 0 \end{bmatrix}^T \nabla c = g_x - \frac{\tau_{bx}}{\rho a}$$

$$\begin{bmatrix} 0 \\ 0 \\ -g_z \end{bmatrix}^T \nabla a + \begin{bmatrix} 0 \\ 0 \\ 0 \end{bmatrix}^T \nabla u + \begin{bmatrix} 1 \\ u \\ v \end{bmatrix}^T \nabla v + \begin{bmatrix} 0 \\ 0 \\ -g_z \end{bmatrix}^T \nabla z_b + \begin{bmatrix} 0 \\ 0 \\ 0 \end{bmatrix}^T \nabla c = g_y - \frac{\tau_{by}}{\rho a} \qquad \text{A.2}$$

$$\begin{bmatrix} 0 \\ 0 \\ 0 \end{bmatrix}^T \nabla a + \begin{bmatrix} 0 \\ T_1 \\ T_3 \end{bmatrix}^T \nabla u + \begin{bmatrix} 0 \\ T_3 \\ T_2 \end{bmatrix}^T \nabla v + \begin{bmatrix} 1 \\ 0 \\ 0 \end{bmatrix}^T \nabla z_b + \begin{bmatrix} a \\ ua \\ va \end{bmatrix}^T \nabla c = 0$$

$$\begin{bmatrix} 0 \\ 0 \\ 0 \end{bmatrix}^T \nabla a + \begin{bmatrix} 0 \\ 0 \\ 0 \end{bmatrix}^T \nabla u + \begin{bmatrix} 0 \\ 0 \\ 0 \end{bmatrix}^T \nabla v + \begin{bmatrix} 0 \\ 0 \\ 0 \end{bmatrix}^T \nabla z_b + \begin{bmatrix} T_A \\ L_x \\ L_y \end{bmatrix}^T \nabla c = c_e - c$$

conform Lin and Shen (1984). The coefficients T_i are described in Eq.2.13

A.2. 2-DH single-layer model.

In the case of non-uniform sediment, additional mass conservation equations for the different size fractions are formulated.

$$\begin{bmatrix}0\\0\\0\end{bmatrix}\nabla a+\begin{bmatrix}0\\K_1\\K_2\end{bmatrix}\nabla u+\begin{bmatrix}0\\K_2\\K_3\end{bmatrix}\nabla v+\begin{bmatrix}1\\0\\0\end{bmatrix}\nabla z_b+\sum_{i=1}^{N}\begin{bmatrix}a\\ua\\va\end{bmatrix}\nabla p_{si}+\sum_{i=1}^{N}\begin{bmatrix}0\\uK_{5i}\\vK_{5i}\end{bmatrix}\nabla p_{mi}+\sum_{j=1}^{N}\begin{bmatrix}0\\uK_4D_j\\vK_4D_j\end{bmatrix}\nabla p_{mj}=0$$

$$\begin{bmatrix}0\\0\\0\end{bmatrix}\nabla a+\begin{bmatrix}0\\0\\0\end{bmatrix}\nabla u+\begin{bmatrix}0\\0\\0\end{bmatrix}\nabla v+\begin{bmatrix}0\\0\\0\end{bmatrix}\nabla z_b+\begin{bmatrix}T_{Ai}\\L_{xi}\\L_{yi}\end{bmatrix}\nabla p_{si}+\begin{bmatrix}0\\0\\0\end{bmatrix}\nabla p_{mi}=p_{ei}-p_{si} \qquad \text{A.3}$$

$$\begin{bmatrix}0\\0\\0\end{bmatrix}\nabla a+\begin{bmatrix}0\\K_{1i}\\K_{2i}\end{bmatrix}\nabla u+\begin{bmatrix}0\\K_{2i}v\\K_{3i}v\end{bmatrix}\nabla v+\begin{bmatrix}\beta_{oi}\\0\\0\end{bmatrix}\nabla z_b+\begin{bmatrix}a\\ua\\va\end{bmatrix}\nabla p_{si}+\begin{bmatrix}\delta_m\\uK_{5i}\\vK_{5i}\end{bmatrix}\nabla p_{mi}+\sum_{j=1}^{N}\begin{bmatrix}0\\uK_{4i}D_j\\vK_{4i}D_j\end{bmatrix}\nabla p_{mj}=0$$

A.3. 2-DH double-layer model.

The mass balance over the bed-load layer Eq.2.41 yields for constant g

$$\begin{aligned}
&g(1+\alpha_i)\left(\frac{\partial s_{bxi}}{\partial x}+\frac{\partial s_{byi}}{\partial y}\right)+(1-g)\frac{s_{bxi}}{p_{pi}}\left(\frac{D_{mp}}{D_{ms}}\right)^{l_i}\left(\frac{\partial p_{spi}}{\partial x}-\frac{p_{spi}}{p_{pi}}\frac{\partial p_{pi}}{\partial x}\right)+\\
&+(1-g)\frac{s_{bxi}}{p_{pi}}\frac{l_i\,p_{spi}}{D_{ms}}\left(\frac{D_{mp}}{D_{ms}}\right)^{l_i-1}\left(\sum_{j=1}^{N}D_j\frac{\partial p_{pj}}{\partial x}-\frac{D_{mp}}{D_{ms}}\sum_{j=1}^{N}D_j\frac{\partial p_{spj}}{\partial x}\right)+\\
&+(1-g)\frac{s_{byi}}{p_{pi}}\left(\frac{D_{mp}}{D_{ms}}\right)^{l_i}\left(\frac{\partial p_{spi}}{\partial y}-\frac{p_{spi}}{p_{pi}}\frac{\partial p_{pi}}{\partial y}\right)+\\
&+(1-g)\frac{s_{byi}}{p_{pi}}\frac{l_i\,p_{spi}}{D_{ms}}\left(\frac{D_{mp}}{D_{ms}}\right)^{l_i-1}\left(\sum_{j=1}^{N}D_j\frac{\partial p_{pj}}{\partial y}-\frac{D_{mp}}{D_{ms}}\sum_{j=1}^{N}D_j\frac{\partial p_{spj}}{\partial y}\right)+\\
&+\Phi_{si}+\delta_p\frac{\partial p_{pi}}{\partial t}+\delta_s\frac{\partial p_{spi}}{\partial t}+\beta_{oi}\frac{\partial z_b}{\partial t}=0
\end{aligned} \qquad \text{A.4}$$

In case of sedimentation, the size-specific exchange ratio is

$$\frac{\Phi_{bsi}}{\Phi_{bpi}} = \frac{1-g}{g} = \alpha \qquad \text{A.5}$$

and the bed load balance is

$$\frac{\partial s_{bxi}}{\partial x} + \frac{\partial s_{byi}}{\partial y} + \Phi_{si} + \delta_p \frac{\partial p_{pi}}{\partial t} + \delta_s \frac{\partial p_{spi}}{\partial t} + \beta_{oi} \frac{\partial z_b}{\partial t} = 0 \qquad \text{A.6}$$

Additionally, the mass balances of pavement and subpavement can be combined into

$$-\alpha_i \delta_p \frac{\partial p_{pi}}{\partial t} + \delta_{sp} \frac{\partial p_{spi}}{\partial t} + \left(\beta_{oi} - \kappa\ (1+\alpha_i)\ \beta_{pi}\right) \frac{\partial z_b}{\partial t} = 0 \qquad \text{A.7}$$

The mass balance of size fraction i can be formulated as

$$\begin{bmatrix} 0 \\ 0 \\ 0 \end{bmatrix}^T \nabla a + \begin{bmatrix} 0 \\ g(1+\alpha_i)K_{1i} \\ g(1+\alpha_i)K_{2i} \end{bmatrix}^T \nabla u + \begin{bmatrix} 0 \\ g(1+\alpha_i)K_{2i} \\ g(1+\alpha_i)K_{3i} \end{bmatrix}^T \nabla v + \begin{bmatrix} \beta_{oi} \\ 0 \\ 0 \end{bmatrix}^T \nabla z_b + \begin{bmatrix} a \\ ua \\ va \end{bmatrix}^T \nabla p_{si} +$$

$$+ \begin{bmatrix} \delta_p \\ guK_{4i} \\ gvK_{4i} \end{bmatrix}^T \nabla p_{pi} + \sum_{j=1}^{N} \begin{bmatrix} 0 \\ guK_{5i}D_j \\ gvK_{5i}D_j \end{bmatrix}^T \nabla p_{pj} + \qquad \text{A.8}$$

$$+ \begin{bmatrix} \delta_s \\ g\alpha_i uK_{4i}\dfrac{p_{pi}}{p_{spi}} \\ g\alpha_i vK_{4i}\dfrac{p_{pi}}{p_{spi}} \end{bmatrix}^T \nabla p_{spi} + \sum_{j=1}^{N} \begin{bmatrix} 0 \\ g\alpha_i uK_{5i}\dfrac{D_{mp}}{D_{ms}}D_j \\ g\alpha_i vK_{5i}\dfrac{D_{mp}}{D_{ms}}D_j \end{bmatrix} \nabla p_{spj} = 0$$

and

$$\begin{bmatrix} -\alpha_i\delta_p \\ 0 \\ 0 \end{bmatrix}^T \nabla p_{pi} + \begin{bmatrix} \delta_s \\ 0 \\ 0 \end{bmatrix}^T \nabla p_{spi} + \begin{bmatrix} \beta_{oi} - \kappa\ (1+\alpha_i)\beta_{pi} \\ 0 \\ 0 \end{bmatrix}^T \nabla z_b = 0 \qquad \text{A.9}$$

The coefficients K_{ij} are described in appendix B.

Appendix B. Power-law approximation.

B.1. Approximation of the Meyer-Peter and Müller formula.

Using a power-law to approximate the sediment transport is an often applied approach to
achieve a convenient expression for the derivative of the sediment transport to the variables in the model (e.g. Jansen et. al., 1978). The transport of suspended sediment and the bed load are combined into a total load approach. The Meyer-Peter Müller (1948) transport-formula, corrected for non-uniform sediment is

$$X_i = \frac{s_i}{p_{mi}\sqrt{g\Delta D_i^3}} = k\left(\tau'_{*i} - \xi_i\tau'_{*c}\right)^{3/2} \quad ; \quad \tau'_{*i} = \tau'_{*m}\frac{D_m}{D_i} \quad ; \quad \xi_i = f\left(\frac{D_i}{D_m}\right) \qquad \textbf{B.1}$$

where ξ_i represents the coefficient that corrects the critical shear stress of a size fraction i for exposure effects. This formula is approximated by

$$X'_i = \gamma\tau'^{\alpha}_{*i}\left(\frac{D_i}{D_m}\right)^{\beta} \qquad \textbf{B.2}$$

Stating that

$$X_i = X'_i \quad ; \quad \frac{\partial X_i}{\partial\tau'_{*i}} = \frac{\partial X'_i}{\partial\tau'_{*i}} \quad ; \quad \frac{\partial X_i}{\partial D_i/D_m} = \frac{\partial X'_i}{\partial D_i/D_m} \qquad \textbf{B.3}$$

α, β and γ can be found, as applied by Ribberink (1987)

$$\alpha = \frac{3}{2}\frac{1}{1-\xi_i\dfrac{\tau'_{*c}}{\tau'_{*i}}} = \frac{3}{2}\frac{1}{1-\xi_i\dfrac{D_i}{D_m}\dfrac{\tau'_{*c}}{\tau'_{*m}}} \qquad \textbf{B.4}$$

$$\beta = -\frac{3}{2}\frac{\dfrac{\partial\xi_i}{\partial D_i/D_m}\left(\dfrac{D_i}{D_m}\right)^2\dfrac{\tau'_{*c}}{\tau'_{*m}}}{1-\xi_i\dfrac{D_i}{D_m}\dfrac{\tau'_{*c}}{\tau'_{*m}}} \qquad \textbf{B.5}$$

$$\gamma = k\,\tau_{*m}^{3/2-\alpha}\left(\frac{D_i}{D_m}\right)^{\alpha-\beta-3/2}\left(1-\xi_i\frac{\tau'_{*c}}{\tau'_{*m}}\frac{D_i}{D_m}\right)^{3/2} = \qquad \textbf{B.6}$$

$$= k\left(\frac{u^2}{C^2\Delta D_m}\right)^{3/2-\alpha}\left(\frac{D_i}{D_m}\right)^{\alpha-\beta-3/2}\left(1-\xi_i\frac{\tau'_{*c}}{\tau'_{*m}}\frac{D_i}{D_m}\right)^{3/2}$$

The transport formula can be rewritten as

$$\frac{s_i}{p_{mi}} = m_i\frac{u_{tot}^{n_i}}{D_m^{l_i}} \qquad \textbf{B.7}$$

with

$$n_i = 2\alpha \;;\; l_i = \beta \;;\; m_i = \frac{\sqrt{g}}{C^{2\alpha}\Delta^{\alpha-1/2}}\gamma D_i^{\beta+3/2-\alpha} \qquad \textbf{B.8}$$

The coefficients of the power-law formula are related to τ_{*m}, D_i and D_m. As shown in the figures, n and l become constant for higher values of τ_{*m} relative to τ_{*c}. Consequently, the power-law approximation is suited for large particle shear-stresses.

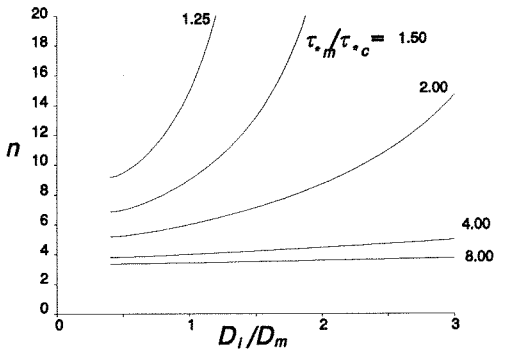

Fig.B.1

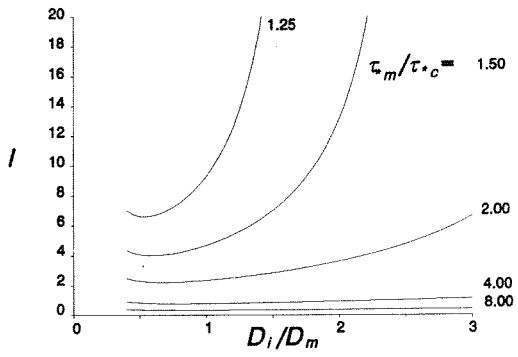

Fig.B.2

In Fig.B.3, the variation of s_{bi}/p_{mi} is shown with changes in shear stress and river bed composition.

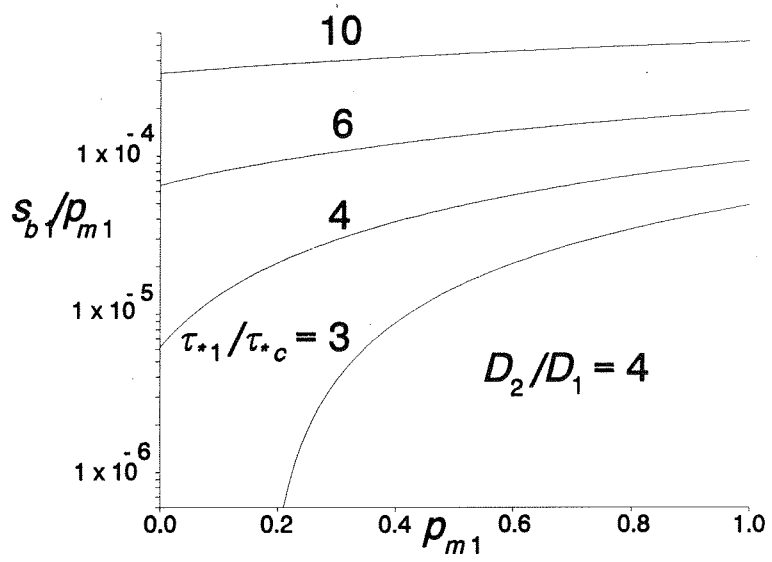

Fig.B.3

Due to the correction for hiding effects that is introduced by Egiazaroff's hiding coefficient, large-sized fractions are transported more easily at smaller values of τ_{*m}/τ_{*c}. At higher shear-stresses, the hiding effect diminishes, and the transported volume of smaller-sized material increases rapidly.

Consequently, the power-law approximation can be applied best for shear stresses that are large relative to the critical shear-stress. Gradients in the power-law coefficients m_i, n_i and l_i are taken constant in x-, y- and t-directions.
If $\tau_{*m}/\tau_{*c} \rightarrow \infty$, the sediment-transport formula approaches

$$s_i \approx k\, p_{mi} \sqrt{g\Delta D_i^3}\ \tau_{*m}^{3/2} \left(\frac{D_m}{D_i}\right)^{3/2} = p_{mi} \frac{k\sqrt{g}}{C^3\,\Delta}\ u^3 \qquad \textbf{B.9}$$

B.2. Horizontal-hiding.

For the correction coefficient ξ_i different empirical relations have been defined. Egiazaroff (1957, 1965) derived

$$\xi_i = \frac{\tau_{*c}(corrected)}{\tau_{*c}} = \left(\frac{\log 19}{\log\left(19\frac{D_i}{D_m}\right)}\right)^2 \qquad \textbf{B.10}$$

Ashida and Michiue (1973) applied Eq.10 to experiments and present for $D_i/D_m < 0.4$

$$\xi_i = 0.85\frac{D_m}{D_i} \qquad \textbf{B.11}$$

Differentation to D_i/D_m yields

$$\frac{\partial \xi_i}{\partial D_i/D_m} = -2\frac{D_m}{D_i}\frac{(\log 19)^2}{\left(\log\left(19\frac{D_i}{D_m}\right)\right)^3} \qquad \textbf{B.12}$$

and for $D_i/D_m < 0.4$

$$\frac{\partial \xi_i}{\partial D_i/D_m} = -\left(\frac{D_m}{D_i}\right)^{-2} \qquad \textbf{B.13}$$

B.3. Sediment-transport composition.

The composition of the transported sediment p_{Ti} at different shear-stresses and mixing-layer compositions is

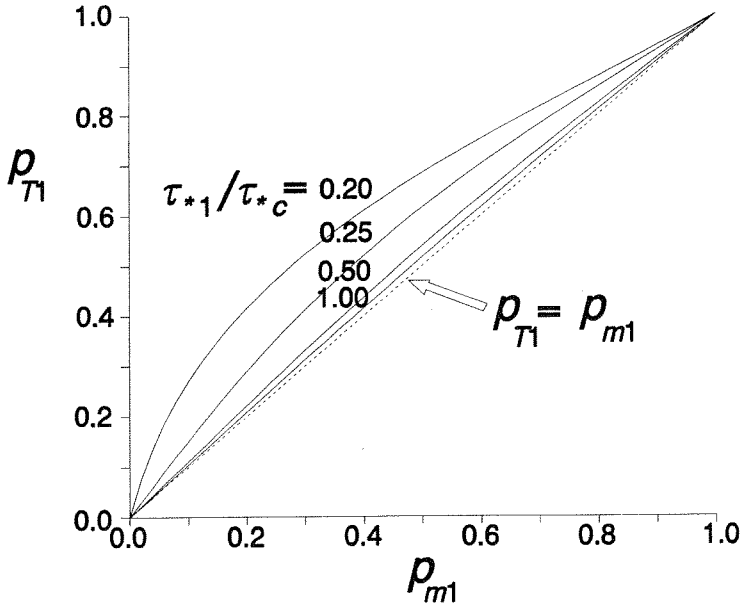

Fig.B.4

At extremely low particle shear-stress, only the finer fraction can be mobilised. Due to hiding effects, this fraction of finer material in the transported sediment reduces with increasing shear-stress.

However, at high shear-stresses, p_{Ti} approaches

$$p_{T1} = \frac{s_{b1}}{s_{b1} + s_{b2}} = \frac{p_{m1}}{p_{m1} + (1-p_{m1})} = p_{m1} \qquad \textbf{B.14}$$

Consequently, at low shear-stresses, the composition of the transported material is finer than the bed material, but at high shear-stresses, the transported material approaches the bed material.

B.4 Comparison with other sediment-transport formulae.

To check the main features of the approximated power law, a similar procedure has been carried out with a transport formula which has been developed by Parker et al. (1982), to predict bed-load transport in gravel-bed rivers, and a sediment transport formula suggested more recently by Graf and Suzka (1987) for coarse, uniform sediment at steep slopes.

Parker et al. (1982).

The formula proposed by Parker et al. (1982) has been modified by Diplas (1987) and reads for low shear-stresses ($\tau_{*m}/\tau_{*c} < 2.6$)

$$X_i = \tau_{*i}^{3/2} W_r \left[\frac{\tau_{*i}}{\tau_{r50}} \left(\frac{D_i}{D_{50}} \right)^c \right]^{a \left(\frac{D_i}{D_{50}} \right)^b} \qquad \textbf{B.15}$$

with

$$W_r = 0.0025 \;;\; a = 13.71 \;;\; b = 0.3214 \;;\; c = 0.943 \;;\; \tau_{r50} = 0.0873 \qquad \textbf{B.16}$$

The power-law coefficients are

$$\alpha_i = 1.5 + a \left(\frac{D_i}{D_{50}} \right)^b$$

$$\beta_i = a \left(\frac{D_i}{D_{50}} \right)^b \left(c + \ln \left(\frac{\tau_i}{\tau_{r50}} \left(\frac{D_i}{D_{50}} \right)^c \right)^b \right) \qquad \textbf{B.17}$$

For high shear-stresses ($\tau_{*m}/\tau_{*c} > 2.6$) the transport formula is

$$X_i = \tau_{*i}^{3/2} W_r \, a \, b^{c\left(1 - d\left[\frac{\tau_{*i}}{\tau_{r50}}\left(\frac{D_i}{D_{50}}\right)^g\right]^e \left(\frac{D_i}{D_{50}}\right)^f\right)} \qquad \textbf{B.18}$$

with

$$W_r = 0.0025 \;;\; a = 4 \;;\; b = 17 \;;\; c = 2.625 \;;\; d = 1.205$$
$$e = -1.843 \;;\; f = 0.3214 \;;\; g = 0.943 \;;\; \tau_{r50} = 0.0873 \qquad \textbf{B.19}$$

However, the calibration of Eq.B.18 at higher shear-stresses is rather poor.

The power-law coefficients are

$$\alpha_i = 1.5 - \ln b \; c \; d \; e \left[\frac{\tau_{*i}}{\tau_{r50}}\left(\frac{D_i}{D_{50}}\right)^g\right]^{e\left(\frac{D_i}{D_{50}}\right)^f} \left(\frac{D_i}{D_{50}}\right)^f$$
$$\beta_i = - \ln b \; c \; d \; e \left[\frac{\tau_{*i}}{\tau_{r50}}\left(\frac{D_i}{D_{50}}\right)^g\right]^{e\left(\frac{D_i}{D_{50}}\right)^f} \left(\frac{D_i}{D_{50}}\right)^f \left[g + \ln\left(\frac{\tau_{*i}}{\tau_{r50}}\left(\frac{D_i}{D_{50}}\right)^g\right)\right] \qquad \textbf{B.20}$$

Graf and Suzka (1987).

For bed load at steep slopes ($0.005 < |\partial z_b/\partial x| < 0.025$) with $Fr \geq 0.8$ and relatively coarse sediment (D_{50} = 12 mm and 24 mm). To account for non-uniform material, the Egiazaroff hiding-coefficient is introduced. It is suggested for
$\tau_{*m}/\tau_{*c} < 1.5$

$$X_i = 10.4 \cdot \tau_{*i}^{1.5} \cdot \left(\frac{D_i}{D_m}\right)^{1.5} \cdot \left(1 - \xi_i \frac{\tau_{*c}}{\tau_{*i}} \frac{D_m}{D_i}\right)^{2.5} \qquad \textbf{B.21}$$

and α_i and β_i are

$$\alpha_i = - \frac{2.5}{1 - \xi_i \frac{\tau_{*c}}{\tau_{*i}} \frac{D_m}{D_i}} - 1 \;;\; \beta_i = 2.5 \frac{1 - \xi_i' \frac{\tau_{*c}}{\tau_{*i}}}{1 - \xi_i \frac{\tau_{*c}}{\tau_{*i}} \frac{D_m}{D_i}} - 1 \qquad \textbf{B.22}$$

Although calibrated very poorly, for $\tau_{*m}/\tau_{*c} > 1.5$ is proposed

$$X_i = 10.4 \cdot \tau_{*i}^{2.5} \cdot \left(\frac{D_i}{D_m}\right)^{2.5} \qquad \textbf{B.23}$$

and $\alpha_i = 2.5$ and $\beta_i = 2.5$.
It should be noticed that Eqs B.21 and B.22 have been derived, calibrated and verified for the transport of uniform material.

In Figure B.5, the resulting transport of a fraction calculated by the Meyer-Peter and Müller formula (MPM), the Parker formula modified by Diplas (PD) and the formula suggested by Graf and Suzka (1987) (GS) are compared for varying shear stresses.

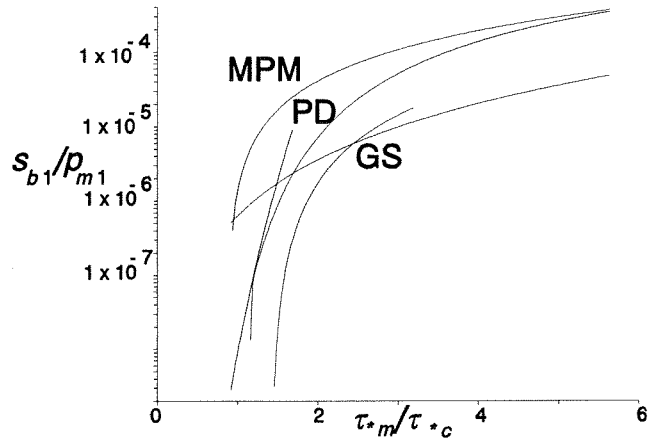

Fig.B.5

As can be expected, differences occur at low shear-stresses, where stochastic fluctuations in the bed load transport prevent accurate predictions. However, at high shear-stresses ($\tau_{*m}/\tau_{*c} > 2.5$), the calibration and verification of the original formulae is poor.

In Figure B.6 and B.7, n_i and l_i, the powers of velocity and median grain diameter in both formulae are compared.

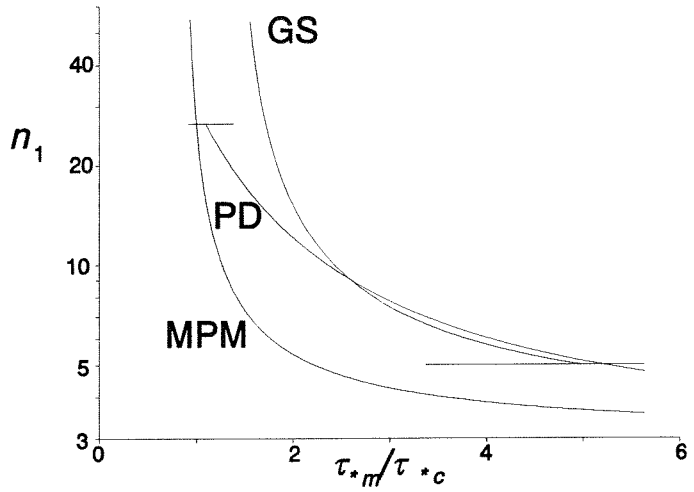

Fig.B.6

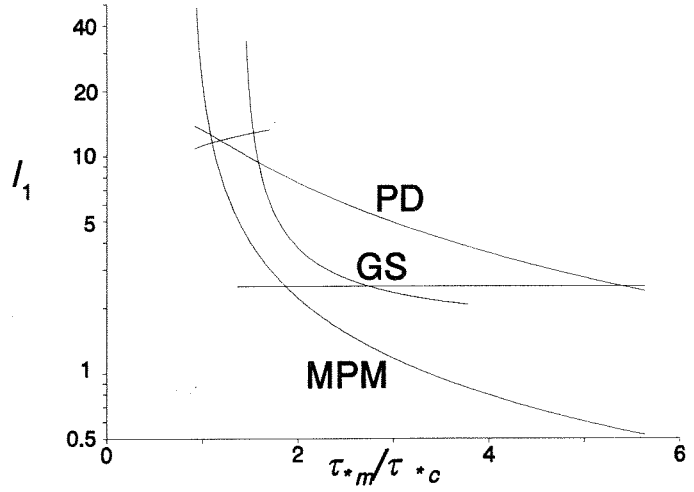

Fig.B.7

B.5. Gradients in sediment-transport.

The components of sediment transport are assumed as (De Vriend, 1987)

$$s_{bxi} = \frac{u}{u_{tot}} s_{bi} \quad ; \quad s_{byi} = \frac{v}{u_{tot}} s_{bi} \qquad \text{B.24}$$

Consequently, gradients in bed load are

$$\frac{\partial s_{bxi}}{\partial x} = \frac{s_{bi}}{u_{tot}}\left(1-\frac{u^2}{u_{tot}^2}\right)\frac{\partial u}{\partial x} - \frac{s_{bi}}{u_{tot}}\frac{uv}{u_{tot}^2}\frac{\partial v}{\partial x} + \frac{u}{u_{tot}}\frac{\partial s_{bi}}{\partial x}$$

$$\frac{\partial s_{byi}}{\partial y} = -\frac{s_{bi}}{u_{tot}}\frac{uv}{u_{tot}^2}\frac{\partial u}{\partial y} + \frac{s_{bi}}{u_{tot}}\left(1-\frac{v^2}{u_{tot}^2}\right)\frac{\partial v}{\partial y} + \frac{v}{u_{tot}}\frac{\partial s_{bi}}{\partial y} \qquad \textbf{B.25}$$

Herein is

$$\frac{\partial s_{bi}}{\partial x} = \frac{\partial s_{bi}}{\partial p_{mi}}\frac{\partial p_{mi}}{\partial x} + \frac{\partial s_{bi}}{\partial u_{tot}}\frac{\partial u_{tot}}{\partial x} + \frac{\partial s_{bi}}{\partial D_m}\frac{\partial D_m}{\partial x} =$$

$$= f_{ip}\frac{\partial p_{mi}}{\partial x} + f_{iu}\frac{\partial u_{tot}}{\partial x} + f_{iD}\frac{\partial D_m}{\partial x} \qquad \textbf{B.26}$$

with gradients in m_i, l_i and n_i neglected, and with

$$\frac{\partial D_m}{\partial x} = \frac{\partial \sum_{i=1}^{N} p_{mi}D_i}{\partial x} = \sum_{i=1}^{N}\left(p_{mi}\frac{\partial D_i}{\partial x} + D_i\frac{\partial p_{mi}}{\partial x}\right) = \sum_{i=1}^{N} D_i\frac{\partial p_{mi}}{\partial x} \qquad \textbf{B.27}$$

Substitution into Eq.16 yields

$$\frac{\partial s_{bxi}}{\partial x} = K_{1i}\frac{\partial u}{\partial x} + K_{2i}\frac{\partial v}{\partial x} + uK_{4i}\frac{\partial p_{mi}}{\partial x} + uK_{5i}\sum_{i=1}^{N} D_i\frac{\partial p_{mi}}{\partial x} \qquad \textbf{B.28}$$

$$\frac{\partial s_{byi}}{\partial y} = K_{2i}\frac{\partial u}{\partial y} + K_{3i}\frac{\partial v}{\partial y} + vK_{4i}\frac{\partial p_{mi}}{\partial y} + vK_{5i}\sum_{i=1}^{N} D_i\frac{\partial p_{mi}}{\partial y}$$

with

$$K_{1i} = \frac{s_{bi}}{u_{tot}}\left(1-\frac{u^2}{u_{tot}^2}\right) + f_{iu}\frac{u^2}{u_{tot}^2} \quad ; \quad K_{2i} = -\frac{s_{bi}}{u_{tot}}\frac{uv}{u_{tot}} + f_{iu}\frac{uv}{u_{tot}^2}$$

$$K_{3i} = \frac{s_{bi}}{u_{tot}}\left(1-\frac{v^2}{u_{tot}^2}\right) + f_{iu}\frac{v^2}{u_{tot}^2} \quad ; \quad K_{4i} = \frac{f_{ip}}{u_{tot}} \quad ; \quad K_{5i} = \frac{f_{iD}}{u_{tot}} \qquad \textbf{B.26}$$

Appendix C. Coefficients of coupled bicharacteristics.

C.1. Single-layer model.

The coupled part of the characteristic equation, that represent the Monge cone, can be written as

$$\begin{aligned} Q = {} & Ar^4 + B(u\cos\theta + v\sin\theta)r^3 + (C\cos^2\theta + D\sin^2\theta + E\sin 2\theta)r^2 + \\ & + (F\cos^3\theta + G\cos^2\theta\sin\theta + H\cos\theta\sin^2\theta + I\sin^3\theta)r + \\ & + J\cos^4\theta + K\cos^3\theta\sin\theta + L\cos^2\theta\sin^2\theta + M\cos\theta\sin^3\theta + N\sin^4\theta \end{aligned} \qquad \text{C.1}$$

with

$$\begin{aligned} A &= -d_m \\ B &= 2d_m + X \\ C &= -2u^2X - d_m\left[g_z(a+K_{11}+K_{12})+u^2\right] \\ D &= -2v^2X - d_m\left[g_z(a+K_{31}+K_{32})+v^2\right] \\ E &= -2uvX - d_m\left[g_z(K_{21}+K_{22})+uv\right] \end{aligned} \qquad \text{C.2}$$

and

$$\begin{aligned} F &= g_z u\left[\delta_m(K_{11}+K_{12}) + aX + Y\right] + u^3X \\ G &= 3u^2vX + 2g_z u\left[\delta_m(K_{21}+K_{22}) + Z\right] + g_z v\left[\delta_m(K_{11}+K_{12}) + aX + Y\right] \\ H &= g_z u\left[\delta_m(K_{31}+K_{32}) + aX + W\right] + 3uv^2X + 2g_z v\left[\delta_m(K_{21}+K_{22}) + Z\right] \\ I &= g_z v\left[\delta_m(K_{31}+K_{32}) + aX + W\right] + v^3X \;;\; J = -g_z u^2Y \;;\; K = -2g_z u(uZ + vY) \\ L &= -g_z(u^2W + 4uvZ + v^2Y) \;;\; M = -2g_z v(uW + vZ) \;;\; N = -g_z v^2W \end{aligned} \qquad \text{C.3}$$

with

$$
\begin{aligned}
X &= (1-\beta_1)(D_1-D_2)K_{51} + (D_2-D_1)\beta_1 K_{52} + (1-\beta_1)K_{41} + \beta_1 K_{42} \\
Y &= (D_1 - D_2)(K_{12}K_{51} - K_{11}K_{52}) + K_{12}K_{41} + K_{11}K_{42} \\
Z &= (D_1 - D_2)(K_{22}K_{51} - K_{21}K_{52}) + K_{22}K_{41} + K_{21}K_{42} \\
W &= (D_1 - D_2)(K_{32}K_{51} - K_{31}K_{52}) + K_{32}K_{41} + K_{31}K_{42}
\end{aligned}
\qquad \text{C.4}
$$

C.2. Double-layer model.

The part of the characteristic equation that represent the Monge cone can again be written as

$$
\begin{aligned}
Q = {} & Ar^4 + B(u\cos\theta + v\sin\theta)r^3 + (C\cos^2\theta + D\sin^2\theta + E\sin 2\theta)r^2 + \\
& + (F\cos^3\theta + G\cos^2\theta\sin\theta + H\cos\theta\sin^2\theta + I\sin^3\theta)r + \\
& + J\cos^4\theta + K\cos^3\theta\sin\theta + L\cos^2\theta\sin^2\theta + M\cos\theta\sin^3\theta + N\sin^4\theta
\end{aligned}
\qquad \text{C.5}
$$

with

$$
\begin{aligned}
A &= \delta_p\delta_s(1+\alpha_1) \;\; ; \;\; B = -2\delta_p\delta_s(1+\alpha_1) - X \\
C &= u^2(2X+Y) + \delta_p\delta_s(1+\alpha_1)\left[g_z(a + g(1+\alpha_1)K_{11} + g(1+\alpha_2)K_{12}) + u^2\right] \\
D &= v^2(2X+Y) + \delta_p\delta_s(1+\alpha_1)\left[g_z(a + g(1+\alpha_1)K_{31} + g(1+\alpha_2)K_{32}) + v^2\right] \\
E &= uv(2X+Y) + \delta_p\delta_s(1+\alpha_1)\left[g_z g((1+\alpha_1)K_{21} + (1+\alpha_2)K_{22}) + uv\right]
\end{aligned}
\qquad \text{C.6}
$$

and

$$F = -g_z u\left[\delta_p\delta_s g(1+\alpha_1)\left((1+\alpha_1)K_{11}+(1+\alpha_2)K_{12}\right) + aX + Z\right] - u^3(X+2Y)$$

$$G = -3u^2v(X+2Y) - 2g_z u\left[\delta_p\delta_s g(1+\alpha_1)\left((1+\alpha_1)K_{21}+(1+\alpha_2)K_{22}\right) + W\right] +$$
$$- g_z v\left[\delta_p\delta_s g(1+\alpha_1)\left((1+\alpha_1)K_{11}+(1+\alpha_2)K_{12}\right) + aX + Z\right]$$

$$H = -g_z u\left[\delta_p\delta_s g(1+\alpha_1)\left((1+\alpha_1)K_{31}+(1+\alpha_2)K_{32}\right) + aX + V\right] - 3uv^2(X+2Y) +$$
$$- 2g_z v\left[\delta_p\delta_s g(1+\alpha_1)\left((1+\alpha_1)K_{21}+(1+\alpha_2)K_{22}\right) + W\right] \qquad \textbf{C.7}$$

$$I = -g_z v\left[\delta_p\delta_s g(1+\alpha_1)\left((1+\alpha_1)K_{31}+(1+\alpha_2)K_{32}\right) + aX + V\right] - v^3(X+2Y)$$

$$J = u^2\left(g_z(Z + aY) + u^2Y\right)$$

$$K = 2g_z u(uW + vZ) + 2uv\left(2u^2 + g_z a\right)Y$$

$$L = g_z\left(u^2V + 4uvZ + v^2Z\right) + \left(g_z a(u^2 + v^2) + 6u^2v^2\right)Y$$

$$M = 2g_z v(vW + uV) + 2vu\left(2v^2 + g_z a\right)Y \quad ; \quad N = v^2\left(g_z(V + aY) + v^2Y\right)$$

with

$$X = g\,K_{41}\left[\delta_s(1 - \kappa\,\beta_{p1}(1+\alpha_1)) + \delta_p\alpha_1\frac{p_{p1}}{p_{sp1}}\left[(\kappa\beta_{p1}-\beta_{o1})(1+\alpha_1) + \alpha_1\right]\right] +$$

$$+ g\,K_{42}(1+\alpha_1)\left[\delta_s\kappa\beta_{p1} + \delta_p\alpha_2(\beta_{o1} - \kappa\beta_{p1})\frac{1-p_{p1}}{1-p_{sp1}}\right] +$$

$$+ g\,K_{51}\frac{(D_1-D_2)}{D_{ms}}\left[\,\delta_s D_{ms}(1 - \kappa\beta_{p1}(1+\alpha_1)) + \delta_p\alpha_1 D_{mp}\left[(\kappa\beta_{p1}-\beta_{o1})(1+\alpha_1)+\alpha_1\right]\,\right]$$

$$+ g\,K_{52}\frac{(D_2-D_1)}{D_{ms}}(1+\alpha_1)\left[\,\delta_s D_{ms}\kappa\beta_{p1} + \delta_p\alpha_2 D_{mp}(\beta_{o1} - \kappa\beta_{p1})\,\right]$$

$$Y = g^2\,K_{41}K_{52}\frac{(D_2-D_1)}{D_{ms}}\,(\kappa\beta_{p1}(1+\alpha_1) - \beta_{o1})\,\frac{(D_{ms}\alpha_1 p_{p1} - D_{mp}\alpha_2 p_{sp1})}{p_{sp1}} +$$

$$+ g^2\,K_{42}K_{51}\frac{(D_1-D_2)}{D_{ms}}\,(\kappa\beta_{p1}(1+\alpha_1) - \beta_{o1})\frac{(\alpha_1 D_{mp}(1-p_{sp1}) - \alpha_2 D_{ms}(1-p_{p1}))}{1-p_{sp1}} +$$

$$+ g^2\,K_{41}K_{42}(\kappa\beta_{p1}(1+\alpha_1) - \beta_{o1})\frac{(\alpha_1 p_{p1}(1-p_{sp1}) - \alpha_2 p_{sp1}(1-p_{p1}))}{p_{sp1}(1-p_{sp1})} +$$

$$+ g^2\,K_{51}K_{52}(D_2-D_1)^2\frac{D_{mp}}{D_{ms}}(\kappa\beta_{p1}(1+\alpha_1) - \beta_{o1})(\alpha_2-\alpha_1)$$

C.8

and

$$Z = g^2(1+\alpha_2)K_{51}K_{12}\frac{D_1-D_2}{D_{ms}}\left(D_{ms}\delta_s+D_{mp}\delta_p\alpha_1^2\right) +$$

$$+ g^2(1+\alpha_1)K_{11}K_{52}\frac{D_2-D_1}{D_{ms}}\left(D_{ms}\delta_s+D_{mp}\delta_p\alpha_1\alpha_2\right) +$$

$$+ g^2(1+\alpha_2)K_{12}K_{41}\frac{\left(\delta_s p_{sp1} + \delta_p\alpha_1^2 p_{p1}\right)}{p_{sp1}} +$$

$$+ g^2(1+\alpha_1)K_{11}K_{42}\frac{\left(\delta_s(1-p_{sp1}) + \delta_p\alpha_1\alpha_2(1-p_{p1})\right)}{1-p_{sp1}} \qquad \textbf{C.9}$$

$$W = g^2(1+\alpha_2)K_{51}K_{22}\frac{D_1-D_2}{D_{ms}}\left(D_{ms}\delta_s+D_{mp}\delta_p\alpha_1^2\right) +$$

$$+ g^2(1+\alpha_1)K_{21}K_{52}\frac{D_2-D_1}{D_{ms}}\left(D_{ms}\delta_s+D_{mp}\delta_p\alpha_1\alpha_2\right) +$$

$$+ g^2(1+\alpha_2)K_{22}K_{41}\frac{\left(\delta_s p_{sp1} + \delta_p\alpha_1^2 p_{p1}\right)}{p_{sp1}} +$$

$$+ g^2(1+\alpha_1)K_{21}K_{42}\frac{\left(\delta_s(1-p_{sp1}) + \delta_p\alpha_1\alpha_2(1-p_{p1})\right)}{1-p_{sp1}} \qquad \textbf{C.10}$$

$$V = g^2(1+\alpha_2)K_{51}K_{32}\frac{D_1-D_2}{D_{ms}}\left(D_{ms}\delta_s+D_{mp}\delta_p\alpha_1^2\right) +$$

$$+ g^2(1+\alpha_1)K_{31}K_{52}\frac{D_2-D_1}{D_{ms}}\left(D_{ms}\delta_s+D_{mp}\delta_p\alpha_1\alpha_2\right) +$$

$$+ g^2(1+\alpha_2)K_{32}K_{41}\frac{\left(\delta_s p_{sp1} + \delta_p\alpha_1^2 p_{p1}\right)}{p_{sp1}} +$$

$$+ g^2(1+\alpha_1)K_{31}K_{42}\frac{\left(\delta_s(1-p_{sp1}) + \delta_p\alpha_1\alpha_2(1-p_{p1})\right)}{1-p_{sp1}} \qquad \textbf{C.11}$$

Appendix D. Coefficients of 2DH-compatibility equations.

D.1. Single-layer model.

The coefficients used to summon the mass and momentum balances can be chosen

$$n_{1i} = g_z R P_1 P_2 \left[-S_1 \left(K_{12} n_{xi}^2 + 2K_{22} n_{xi} n_{yi} + K_{32} n_{yi}^2 \right) + S_2 \left(K_{11} n_{xi}^2 + 2K_{21} n_{xi} n_{yi} + K_{31} n_{yi}^2 \right) \right.$$

$$n_{2i} = S_1 P_1 P_2 \left[g_z a n_{yi} \left(K_{22} (n_{xi}^2 - n_{yi}^2) + (K_{32} - K_{12}) n_{xi} n_{yi} \right) - R^2 (K_{12} n_{xi} + K_{22} n_{yi}) \right] +$$

$$+ S_2 P_1 P_2 \left[g_z a n_{yi} \left(K_{21} (n_{yi}^2 - n_{xi}^2) + (K_{11} - K_{31}) n_{xi} n_{yi} \right) + R^2 (K_{11} n_{xi} + K_{21} n_{yi}) \right]$$

$$n_{3i} = S_1 P_1 P_2 \left[g_z a n_{xi} \left(K_{22} (n_{yi}^2 - n_{xi}^2) + (K_{12} - K_{32}) n_{xi} n_{yi} \right) - R^2 (K_{22} n_{xi} + K_{32} n_{yi}) \right] +$$

$$+ S_2 P_1 P_2 \left[g_z a n_{xi} \left(K_{21} (n_{xi}^2 - n_{yi}^2) + (K_{31} - K_{11}) n_{xi} n_{yi} \right) + R^2 (K_{21} n_{xi} + K_{31} n_{yi}) \right]$$

$$n_{4i} = a R^2 S_2 P_2 \left(g_z a (n_{xi}^2 + n_{yi}^2) + R^2 \right) \quad ; \quad n_{5i} = - a R^2 S_1 P_1 \left(g_z a (n_{xi}^2 + n_{yi}^2) + R^2 \right)$$

$$n_{6i} = - R S_2 P_1 P_2 \left(g_z a (n_{xi}^2 + n_{yi}^2) + R^2 \right) \quad ; \quad n_{7i} = R S_1 P_1 P_2 \left(g_z a (n_{xi}^2 + n_{yi}^2) + R^2 \right)$$

D.1

The coefficients of matrix T are

$$T_{ai} = \frac{n_{1i} + (un_{1i} - g_z n_{2i})c_{xi} + (vn_{1i} - g_z n_{3i})c_{yi}}{\sqrt{1 + c_{xi}^2 + c_{yi}^2}}$$

$$T_{ui} = \frac{n_{2i} + (an_{1i} + un_{2i} + K_{11}n_{6i} + K_{12}n_{7i})c_{xi} + (vn_{2i} + K_{21}n_{6i} + K_{22}n_{7i})c_{yi}}{\sqrt{1 + c_{xi}^2 + c_{yi}^2}}$$

$$T_{vi} = \frac{n_{3i} + (un_{3i} + K_{21}n_{6i} + K_{22}n_{7i})c_{xi} + (an_{1i} + vn_{3i} + K_{31}n_{6i} + K_{32}n_{7i})c_{yi}}{\sqrt{1 + c_{xi}^2 + c_{yi}^2}}$$

$$T_{zi} = \frac{\beta_1 n_{6i} + (1-\beta_1)n_{7i} - g_z n_{2i}c_{xi} - g_z n_{3i}c_{yi}}{\sqrt{1 + c_{xi}^2 + c_{iy}^2}}$$

$$T_{s1i} = \frac{T_{A1}n_{4i} + an_{6i} + (uan_{6i} + L_{x1}n_{4i})c_{xi} + (van_{6i} + L_{y1}n_{4i})c_{yi}}{\sqrt{1 + c_{xi}^2 + c_{yi}^2}}$$

$$T_{s2i} = \frac{T_{A2}n_{5i} + an_{7i} + (uan_{7i} + L_{x2}n_{5i})c_{xi} + (van_{7i} + L_{y2}n_{5i})c_{yi}}{\sqrt{1 + c_{xi}^2 + c_{yi}^2}}$$

$$T_{mi} = \frac{\delta_m(n_{6i}-n_{7i}) + (uc_{xi}+vc_{yi})\left(n_{6i}(K_{41}+(D_1-D_2)K_{51}) + n_{7i}(-K_{42}+(D_1-D_2)K_{52})\right)}{\sqrt{1 + c_{xi}^2 + c_{yi}^2}}$$

D.2

for i = 1,2,3 and 4. For i = 5,6 and 7, the roots of the characteristic equation are R = 0, $P_1 = 0$ and $P_2 = 0$ respectively.

For $i = 5$

$$n_{15} = 0$$

$$n_{25} = S_1P_1P_2\left[g_z a n_y\left(K_{22}(n_x^2 - n_y^2) + (K_{32} - K_{12})n_x n_y\right)\right] +$$

$$+ S_2P_1P_2\left[g_z a n_y\left(K_{21}(n_y^2 - n_x^2) + (K_{11} - K_{31})n_x n_y\right)\right] \qquad \textbf{D.3}$$

$$n_{35} = S_1P_1P_2\left[g_z a n_x\left(K_{22}(n_y^2 - n_x^2) + (K_{12} - K_{32})n_x n_y\right)\right] +$$

$$+ S_2P_1P_2\left[g_z a n_x\left(K_{21}(n_x^2 - n_y^2) + (K_{31} - K_{11})n_x n_y\right)\right]$$

$$n_{45} = 0 \;;\; n_{55} = 0 \;;\; n_{65} = 0 \;;\; n_{75} = 0$$

and the coefficients are

$$T_{a5} = \frac{-g_z n_{25} c_{x5} - g_z n_{35} c_{y5}}{\sqrt{1 + c_{x5}^2 + c_{y5}^2}} \;;\; T_{u5} = \frac{n_{25} + u n_{25} c_{x5} + v n_{25} c_{y5}}{\sqrt{1 + c_{x5}^2 + c_{y5}^2}}$$

$$T_{v5} = \frac{n_{35} + u n_{35} c_{x5} + v n_{35} c_{y5}}{\sqrt{1 + c_{x5}^2 + c_{y5}^2}} \;;\; T_{z5} = \frac{-g_z n_{25} c_{x5} - g_z n_{35} c_{y5}}{\sqrt{1 + c_{x5}^2 + c_{y5}^2}} \qquad \textbf{D.4}$$

$$T_{s15} = 0 \;;\; T_{s25} = 0 \;;\; T_{m5} = 0$$

For $i = 6$ or 7

$$n_{1i} = 0 \;;\; n_{2i} = 0 \;;\; n_{3i} = 0$$

$$n_{4i} = aR^2 S_2 P_2\left(g_z a(n_x^2 + n_y^2) + R^2\right) \;;\; n_{5i} = -aR^2 S_1 P_1\left(g_z a(n_x^2 + n_y^2) + R^2\right) \qquad \textbf{D.5}$$

$$n_{6i} = 0 \;;\; n_{7i} = 0$$

Hence the coefficients for $i = 6$ are

$$T_{a6} = 0 \;;\; T_{u6} = 0 \;;\; T_{v6} = 0 \;;\; T_{z6} = 0$$

$$T_{s16} = n_{46}\frac{T_{A1} + L_{x1}c_{x6} + L_{y1}c_{y6}}{\sqrt{1 + c_{x6}^2 + c_{y6}^2}} \;;\; T_{s26} = 0 \;;\; T_{m6} = 0 \qquad \textbf{D.6}$$

and for $i = 7$

$$T_{a7} = 0 \;;\; T_{u7} = 0 \;;\; T_{v7} = 0 \;;\; T_{z7} = 0$$

$$T_{s17} = 0 \;;\; T_{s27} = n_{57}\frac{T_{A2} + L_{x2}c_{x7} + L_{y2}c_{y7}}{\sqrt{1 + c_{x7}^2 + c_{y7}^2}} \;;\; T_{m7} = 0 \qquad \textbf{D.7}$$

For $i = 1,2,3$ and 4, the coefficients of matrix S are

$$S_{ai} = -(un_{1i} - g_z n_{2i})\sin\theta + (vn_{1i} - g_z n_{3i})\cos\theta$$

$$S_{ui} = -(an_{1i} + un_{2i} + K_{11}n_{6i} + K_{12}n_{7i})\sin\theta + (vn_{2i} + K_{21}n_{6i} + K_{22}n_{7i})\cos\theta$$

$$S_{vi} = -(un_{3i} + K_{21}n_{6i} + K_{22}n_{7i})\sin\theta + (an_{1i} + vn_{3i} + K_{31}n_{6i} + K_{32}n_{7i})\cos\theta$$

$$S_{zi} = g_z(n_{2i}\sin\theta - n_{3i}\cos\theta) \qquad \textbf{D.8}$$

$$S_{s1i} = -(uan_{6i} + L_{x1}n_{4i})\sin\theta + (van_{6i} + L_{y1}n_{4i})\cos\theta$$

$$S_{s2i} = -(uan_{7i} + L_{x2}n_{5i})\sin\theta + (van_{7i} + L_{y2}n_{5i})\cos\theta$$

$$S_{mi} = (-u\sin\theta + v\cos\theta)(n_{6i}(K_{41} + (D_1 - D_2)K_{51}) + n_{7i}(-K_{42} + (D_1 - D_2)K_{52}))$$

For $i = 5$ the coefficients are

$$S_{a5} = g_z(n_{25}\sin\theta - n_{35}\cos\theta) \;;\; S_{u5} = n_{25}(-u\sin\theta + v\cos\theta)$$

$$S_{v5} = n_{35}(-u\sin\theta + v\cos\theta) \;;\; S_{z5} = g_z(n_{25}\sin\theta - n_{35}\cos\theta) \qquad \textbf{D.9}$$

$$S_{s15} = 0 \;;\; S_{s25} = 0 \;;\; S_{m5} = 0$$

For $i = 6$ the coefficients are

$$S_{a6} = 0 \;;\; S_{u6} = 0 \;;\; S_{v6} = 0 \;;\; S_{z6} = 0$$

$$S_{s16} = n_{46}(-L_{x1}\sin\theta + L_{y1}\cos\theta) \;;\; S_{s26} = 0 \;;\; S_{m6} = 0 \qquad \textbf{D.10}$$

and for $i = 7$ the coefficients are

$$S_{a7} = 0 \;;\; S_{u7} = 0 \;;\; S_{v7} = 0 \;;\; S_{z7} = 0$$

$$S_{s17} = 0 \;;\; S_{s27} = n_{57}(-L_{x2}\sin\theta + L_{y2}\cos\theta) \;;\; S_{m7} = 0 \qquad \textbf{D.11}$$

Consequently, T and S are

$$T = \begin{bmatrix} T_{a1} & T_{u1} & T_{v1} & T_{z1} & T_{s11} & T_{s21} & T_{m1} \\ T_{a2} & T_{u2} & T_{v2} & T_{z2} & T_{s12} & T_{s22} & T_{m2} \\ T_{a3} & T_{u3} & T_{v3} & T_{z3} & T_{s13} & T_{s23} & T_{m3} \\ T_{a4} & T_{u4} & T_{v4} & T_{z4} & T_{s14} & T_{s24} & T_{m4} \\ T_{a5} & T_{u5} & T_{v5} & T_{z5} & 0 & 0 & 0 \\ 0 & 0 & 0 & 0 & T_{s16} & 0 & 0 \\ 0 & 0 & 0 & 0 & 0 & T_{s27} & 0 \end{bmatrix} \quad ; \quad S = \begin{bmatrix} S_{a1} & S_{u1} & S_{v1} & S_{z1} & S_{s11} & S_{s21} & S_{m1} \\ S_{a2} & S_{u2} & S_{v2} & S_{z2} & S_{s12} & S_{s22} & S_{m2} \\ S_{a3} & S_{u3} & S_{v3} & S_{z3} & S_{s13} & S_{s23} & S_{m3} \\ S_{a4} & S_{u4} & S_{v4} & S_{z4} & S_{s14} & S_{s24} & S_{m4} \\ S_{a5} & S_{u5} & S_{v5} & S_{z5} & 0 & 0 & 0 \\ 0 & 0 & 0 & 0 & S_{s16} & 0 & 0 \\ 0 & 0 & 0 & 0 & 0 & S_{s27} & 0 \end{bmatrix} \qquad \textbf{D.12}$$

The coefficients of the vectors K, L and M are

$$K = \begin{bmatrix} n_{21} \\ n_{22} \\ n_{23} \\ n_{24} \\ n_{25} \\ 0 \\ 0 \end{bmatrix} \quad ; \quad L = \begin{bmatrix} n_{31} \\ n_{32} \\ n_{33} \\ n_{34} \\ n_{35} \\ 0 \\ 0 \end{bmatrix} \quad ; \quad M = \begin{bmatrix} n_{41} \\ n_{42} \\ n_{43} \\ n_{44} \\ 0 \\ n_{46} \\ 0 \end{bmatrix} \quad ; \quad N = \begin{bmatrix} n_{51} \\ n_{52} \\ n_{53} \\ n_{54} \\ 0 \\ 0 \\ n_{57} \end{bmatrix} \qquad \textbf{D.13}$$

D.2. Double-layer model.

The coefficients used to summon the system of equations are

$$n_{1i} = \delta_s g_z n_t P_1 P_2 S_1 g(1+\alpha_2)\left[2g_z a n_x n_y^2((K_{32}-K_{12})n_x - K_{22}n_y) + R^2\left(K_{32}n_y^2 - K_{12}n_x^2\right)\right] +$$
$$+ \delta_p g_z \alpha_1 n_t P_1 P_2 T_1 g(1+\alpha_2)\left[2g_z a n_x n_y\left((K_{32}-K_{12})n_x n_y + K_{22}\left(n_x^2-n_y^2\right)\right) + R^2\left(K_{32}n_y^2 - K_{12}n_x^2\right)\right] +$$
$$+ g_z n_t P_1 P_2 g(1+\alpha_1)(\delta_s S_2 + \delta_p \alpha_1 T_2)\left[2g_z a n_x n_y\left((K_{11}-K_{31})n_x n_y + K_{21}\left(n_y^2-n_x^2\right)\right) + R^2\left(K_{11}n_x^2 - K_{31}n_y^2\right)\right]$$

$$n_{2i} = n_t P_1 P_2 R g(1+\alpha_2)(\delta_s S_1 + \delta_p \alpha_1 T_1)\left[g_z a n_y\left(K_{22}n_x^2 + (K_{32}-K_{12})n_x n_y - K_{22}n_y^2\right) - R^2(K_{22}n_y + K_{12}n_x)\right] +$$
$$+ n_t P_1 P_2 R g(1+\alpha_1)(\delta_s S_2 + \delta_p \alpha_1 T_2)\left[g_z a n_y\left(-K_{21}n_x^2 + (K_{11}-K_{31})n_x n_y + K_{21}n_y^2\right) + R^2(K_{21}n_y + K_{11}n_x)\right]$$

$$n_3 = n_t P_1 P_2 R g(1+\alpha_2)(\delta_s S_1 + \delta_p \alpha_1 T_1)\left[g_z a n_x\left(-K_{22}n_x^2 + (K_{12}-K_{32})n_x n_y + K_{22}n_y^2\right) - R^2(K_{32}n_y + K_{22}n_x)\right] +$$
$$+ n_t P_1 P_2 R g(1+\alpha_1)(\delta_s S_2 + \delta_p \alpha_1 T_2)\left[g_z a n_x\left(K_{21}n_x^2 + (K_{31}-K_{11})n_x n_y - K_{21}n_y^2\right) + R^2(K_{31}n_y + K_{21}n_x)\right]$$

$$n_{4i} = n_t a P_2 R^3\left(g_z a\left(n_x^2+n_y^2\right) + R^2\right)(\delta_s S_2 + \delta_p \alpha_1 T_2) \quad ; \quad n_{5i} = -n_t a P_1 R^3\left(g_z a\left(n_x^2+n_y^2\right) + R^2\right)(\delta_s S_1 + \delta_p \alpha_1 T_1)$$

$$n_{6i} = -n_t P_1 P_2 R^2\left(g_z a\left(n_x^2+n_y^2\right) + R^2\right)(\delta_s S_2 + \delta_p \alpha_1 T_2) \quad ; \quad n_{7i} = n_t P_1 P_2 R^2\left(g_z a\left(n_x^2+n_y^2\right) + R^2\right)(\delta_s S_1 + \delta_p \alpha_1 T_1)$$

$$n_{8i} = P_1 P_2 R^2\left(g_z a\left(n_x^2 + n_y^2\right) + R^2\right)(S_2 T_1 - S_1 T_2)$$

D.14